AFML-TR-67-396

FINITE ELEMENT VIBRATION ANALYSIS OF CRACKED PLATES IN TENSION

MAURICE PETYT

UNIVERSITY OF SOUTHAMPTON

TECHNICAL REPORT AFML-TR-67-396

JANUARY 1968

AIR FORCE MATERIALS LABORATORY
AIR FORCE SYSTEMS COMMAND
WRIGHT-PATTERSON AIR FORCE BASE, OHIO

FINITE ELEMENT VIBRATION ANALYSIS OF CRACKED PLATES IN TENSION

MAURICE PETYT

FOREWORD

This report was prepared by the University of Southampton, Institute of Sound and Vibration Research, Southampton, England under U.S.A.F. Contract AF 61(052)-862. The contract was initiated under project No. 7351, "Metallic Materials", Task No. 735106, "Behavior of Metals", and it was administered by the European Office, Office of Aerospace Research. The work was monitored by the Metals and Ceramics Division, Air Force Materials Laboratory, Air Force Systems Command, with Dr. D. I. G. Jones acting as project engineer.

This report covers work performed during the period January 1965 to March 1967.

The manuscript of this report was released by the author May 1967 for publication.

This technical report has been reviewed and is approved.

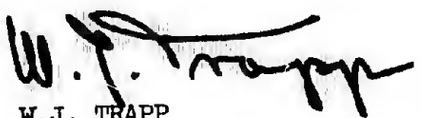

W.J. TRAPP
Chief, Strength and Dynamics Branch
Materials and Ceramics Division
Air Force Materials Laboratory

ABSTRACT

A finite element method of analysis is developed to determine the vibration characteristics of an aircraft fuselage panel, containing a fatigue crack. Experimental observations show that as the length of the crack increases, the frequency of vibration reaches a minimum when the free edge of the crack buckles. The variation in this phenomena with increasing plate width is studied both experimentally and theoretically.

The analysis is developed in a systematic manner, and calculations are performed, at each stage, on problems with known solutions, in order to determine the accuracy of the method. The problems considered include the vibrations of flat plates of varying planform, the vibrations of a cylindrical shell, the buckling of a rectangular plate, and the vibrations of a rectangular plate in compression.

The method is finally applied to the problem of a cracked plate in tension and the results compared with experimental measurements. The post buckling behaviour is calculated using a step-by-step analysis to permit linearisation of the governing equations. By considering the calculated stress distributions, the variation in buckling stress with crack length and plate width is explained.

Distribution of this abstract is unlimited.

TABLE OF CONTENTS

LIST OF ILLUSTRATIONS

LIST OF ILLUSTRATIONS

LIST OF ILLUSTRATIONS

LIST OF TABLES

LIST OF SYMBOLS

Matrix Notation

$[\ ]$	Rectangular matrix
$\{\ \}$	Column matrix
$\lfloor\ \rfloor$	Row matrix
$[\ ]^T$	Transposed matrix
$[\ ]^{-1}$	Inverse matrix

Geometry

x, y, z	Co-ordinates w.r.t. local fixed axes
x^o, y^o, z^o	Co-ordinates w.r.t. global axes
$\bar{x}, \bar{y}, \bar{z}$	Co-ordinates w.r.t. local moving axes
$\Psi_i, \Psi_i^o, \Psi_{ij}^o$	Defined in Section 5.4
$\bar{x}_{ij}$	$(\bar{x}_i - \bar{x}_j)$
Δ	Area of triangle
t	Plate thickness
$2a, 2b$	Dimensions of rectangular plate
2ℓ	Length of crack
h_x, h_y	Centroid of triangle
$\Delta r_{xx}^2, \Delta r_{yy}^2, \Delta r_{xy}^2, \Delta r_{zz}^2$	Second moments of area w.r.t. local fixed axes

Displacements and Strains

u, v, θ_z	In-plane displacements
w, θ_x, θ_y	Out of plate displacements
$\{u\}$	Displacement matrix
$\{u_i\}$	Element nodal displacements
$\{\bar{u}_i\}$	Virtual displacements
$\{U^o\}$	Displacements of complete structure
$\{A\}$	Generalized displacements
$[M]$	Assumed displacement functions

LIST OF SYMBOLS

$[C]$	Determined by evaluating $[M]$ at the nodal points
$[B]$	Defined by equation (3.4)
ε_x, ε_y, γ_{xy}	Strain components
$\{\varepsilon\}$	Matrix of strains
$\{\bar{\varepsilon}\}$	Virtual strains
$\{\delta\bar{u}\}$	Incremental displacements w.r.t. local moving axes
$[G]$	Defined by equation (6.20)
$[F]$	Defined by equations (6.7, 6.25)
Ω_1, Ω_2	Defined by equation (6.24)
$\delta\omega_x$, $\delta\omega_y$, $\delta\omega_z$	Components of the rotation of local moving axes w.r.t. local fixed axes
g_1, g_2, $\cdots$ g_6	Defined by equation (6.22)

Forces and Stresses

S^x, S^y, S^z, M^x, M^y, M^z	Element nodal forces referred to local fixed axes
$\{s_i\}$	Matrix of element nodal forces (fixed axes)
$S^{\bar{x}}$, $S^{\bar{y}}$, $S^{\bar{z}}$, $M^{\bar{x}}$, $M^{\bar{y}}$, $M^{\bar{z}}$	Element nodal forces referred to local moving axes
$\{\bar{s}\}$	Matrix of element nodal forces (moving axes)
$\{S^o\}$	Nodal forces of complete structure
σ_x, σ_y, τ_{xy}	Stress components
σ_s	Applied stress
σ_b	Buckling stress
μ	Ratio of applied stress to buckling stress
M_x, M_y, M_{xy}	Stress resultants (Plate bending)
$\{\sigma\}$	Stress matrix

LIST OF SYMBOLS

$\{f\}$	Inertia forces per unit area
F	Applied force
λ	Applied force intensity factor

Material Properties

E	Young's modulus
G	Shear modulus
ν	Poisson's ratio
E'	$E/(1 - \nu^2)$
ξ	$(1 - \nu)/2.$
D	$Et^3/12(1 - \nu^2)$
$[D]$	Matrix of material constants
ρ	Density

Inertias

$[m_p]$	Matrix of inertial constants
$[m]$	Element inertia matrix
$[\tilde{m}]$	Generalised element inertia matrix
$[m^o]$	Element inertia matrix w.r.t. global axes
$[\bar{M}^o]$	Defined by equation (3.44)
$[M^o]$	Inertia matrix of complete structure

Stiffnesses

$[k]$	Element stiffness matrix w.r.t. local fixed axes
$k^{pq}(p,q = x, y, z)$	Components of $[k_s]$ as defined by equation (5.21)
$[\tilde{k}]$	Generalised element stiffness matrix
$[\bar{k}]$	Element stiffness matrix w.r.t. local moving axes
$[k_1]$	Geometrical element stiffness matrix w.r.t. local fixed axes

LIST OF SYMBOLS

$[k_c]$	Stiffness matrix of an element in an initial state of stress
$[k_{1i}]$	Defined by equation (6.12)
$[k_{13}]$, $[k_{16}]$, $[k_{17}]$	Defined by equation (6.28)
$[k^o]$	Element stiffness matrix w.r.t. global axes
$[\bar{K}^o]$	Defined by equation (3.44)
$[K^o]$	Stiffness matrix of complete structure
$[K_1^o]$	Geometrical stiffness matrix of complete structure
$[K_c^o]$	Stiffness matrix of complete structure when in a state of initial stress

Additional Symbols

W	Virtual work
Ω	Frequency of vibration
$[a]$	Matrix relating displacements w.r.t. local fixed axes to displacements w.r.t. global axes
$[\zeta]$	Matrix of direction cosines
$[\Xi]$	Defined by equation (3.36 or 5.24)
δ	Denotes an increment of a quantity
X_i	Dimensional variables defined in 2.2
π_i	Dimensionless variables defined in 2.2
f, ϕ, ψ	Functional relationships defined in 2.2
α_i	Constants defined in 2.2
$[T]$, $[V]$, $[L]$	Defined ir 4.2

Subscripts

m	Model quantities
g	Element number

LIST OF SYMBOLS

p	In-plane effect
b	Bending effect
s	Shell effect
i, j, k	Nodal point number

Computer Variables

NE	Number of elements
NP	Number of nodal points
NPR	Number of columns
NC	Number of constraints
TH	Plate thickness
E	Young's modulus
PR	Poisson's ratio
RHŌ	Mass density
{NPC}	Number of nodal points in each column
[NGE]	Element numbering system
[G]	Coordinates of nodal points
[MCN]	Constraints

BLANK PAGE

1. INTRODUCTION

Modern aircraft structures are designed using a "fail-safe" criterion to alleviate premature failure due to metal fatigue. This criterion is based upon the concept that fatigue cracks and other forms of damage may be tolerated, provided they do not grow to a catastrophic size between major inspections. Thus, the determination of the factors which attribute to the propagation of such cracks, is of considerable importance. Many investigators have performed tests to establish the rate of propagation of a crack due to the pressurization cycle of fuselage cabins. In high speed aircraft, further propagation may take place due to pressure fluctuations associated with the turbulent boundary layer. The fact that a crack can propagate due to this effect has been established in reference 2. Some of the major factors effecting the rate of propagation were also determined.

The tests described were performed on flat plates 10 ins. wide, 13·5 ins. long and 0·064 in. thick. The specimens were subject to a constant tensile load which represented the fuselage hoop stress. A crack was initiated in the centre of each plate in a direction normal to the tensile load. When subject to pressure fluctuations in an acoustic test facility, the plate vibrated predominantly in its fundamental mode. As the length of the crack grew it was found that the frequency of this mode decreased until a point was reached when the free edge of the crack buckled outwards permanently; thereafter the frequency increased. Inthe region of minimum frequency the maximum rate of propagation occurred.

The present investigation is concerned with establishing a theoretical method of determining the vibration characteristics of this simplified model, with a view to estimating the dynamic stresses. In addition, the effect of increasing the width of the plate has been determined. This

has been done primarily by experiment, as described in Chapter 2, but some of the phenomena observed are discussed further in Chapter 7 in conjunction with the theoretical calculations.

The tests performed, determined the variation in frequency of the fundamental mode with increasing applied load, for a crack of constant length. The practical case of a constant load and a crack of increasing length was then obtained by cross plotting. These frequency stress curves may be divided up into three regions. In the first the frequency increases with increase of stress. Secondly, the frequency decreases with further increase of stress until the minimum frequency is reached, and the plate buckles permanently. Finally the frequency again increases with increase of stress, due to the increase of curvature of the free edge of the crack.

In view of the nature of the phenomenon, and the fact that the stresses at the tip of the crack are in the plastic region, it would appear that an approximate type of analysis, such as the finite element displacement method, would be the most promising method of solution. This method was first developed to determine the static stresses in aircraft structures. More recently it has been used to calculate the static stress distributions in arch dams and shell roofs.

The method assumes that the structure may be considered to be an assemblage of individual components or elements, which are interconnected at their corners or nodal points. This idealised structure is then solved by a method akin to the Rayleigh-Ritz procedure. The most common types of element used are beams and rectangular or triangular plates, but in some instances quadrilateral, trapezoidal or parallelogram elements have also been employed.

Because of the importance of the buckling region in the present problem, when part of the plate forms a doubly curved surface, it is desirable to use triangular plate elements in the idealisation, which is a convenient way of representing this shape. Consequently, only the triangular plate element is considered here. The analysis is developed

in a systematic manner, and calculations have been performed, at each stage, on problems with known solutions, either theoretical or experimental, in order to determine the order of accuracy of the method.

The general procedure for analysing flat plate vibration problems is developed in Chapter 3. It is shown later that the technique is quite general, in so far as it may be used for a number of other problems, with suitable interpretation of the matrices involved. The application of the method is dependent upon the availability of a large digital computer. The programming procedure which was adopted is described in Chapter 4. The same basic procedure was used in all the subsequent investigations reported here. The application to plates having arbitrarily shaped boundaries is demonstrated by considering rectangular, triangular and circular planforms. It is also shown that the solutions converge towards the true solutions when the number of elements is increased. The theory is extended to cover the analysis of shells having arbitrary curvature and boundary configurations in Chapter 5. The particular case of a cylindrical shell having freely supported ends is considered.

The buckling and post buckling behaviour of plates is characterised by large deflections which introduce geometrical non linearities. This type of problem is analysed in Chapter 6 by a step-by-step procedure which permits linearisation. The introduction of simplifying assumptions enables the critical buckling stress to be determined from an eigenvalue problem in an analogous form to the vibration problem. A method is given for analysing the vibration characteristics of a plate which is subject to static loads along its boundary. In general, this involves the step-by-step procedure, but this may be avoided for applied loads which are less than the buckling load of the plate, by making simplifying assumptions, as in the buckling analysis.

In Chapter 7 the problem of a rectangular plate, containing a central crack and subject to a tensile load, is considered in some detail. The ability of the method to predict static stress distributions in general, has been adequately demonstrated elsewhere [1] , and so it has not been

investigated here. The static stress distribution in the cracked plate is of some interest, however, in so far as it effects the vibration characteristics. Consequently, its ability to predict the stress distribution for this particular problem is demonstrated, and then used to explain certain phenomena which have been experimentally observed, concerning the variation in buckling stress with crack length and plate width. Support for this theory is given by the agreement obtained between measured and calculated buckling stresses. The static deflection curve in the post buckled region has been determined using the step-by-step procedure. Finally, the variation in the vibration characterisitcs with increasing applied load have been determined.

Chapter 8 contains a review of the important findings in this work. Possible methods of increasing the accuracy of the solution are discussed, and further work is suggested, which will enable investigations to be carried out on more representative structures.

2. EXPERIMENTAL STUDY OF THE VIBRATION OF A CRACKED PLATE IN TENSION

2.1 Introduction

The vibration characteristics of a rectangular plate 13·5" × 10·0" and of thickness 0·064" containing a central crack and subjected to tensile loads in a direction perpendicular to the crack, are given in reference [2]. In this chapter the effect of increasing the plate width is considered. In order to limit the magnitude of the applied load and also the size of the plate specimens, the experimental investigations were carried out on half scale models.

As described in reference [2] for a given crack length the frequency of the fundamental mode varies with overall stress in the manner shown in figure 1. This curve may be divided up into three regions. Initially the frequency increases with increase of stress. In the second region the frequency decreases with further increase of stress until the minimum frequency is reached. At this point the free edge of the crack buckles permanently due to compressive stresses which occur there. In the third region the frequency again increases with increase of stress. This is due to an increase in curvature of the buckled edge of the crack.

Any model which is tested should be capable of reproducing all these characteristics. The method of achieving this is now considered.

2.2 Model Theory

In order to simulate the physical characteristics of a vibrating cracked plate in tension by means of a model, it is essential that the significant parameters are determined. This is achieved by means of dimensional analysis. The central feature of this theory is Buckingham's π theorem [3]. Van Driest's modified form of this theorem [4] states that if, in the equation of a phenomenon, any variable X_1 depends solely

upon independent variables $X_2, X_3, \ldots, X_n$ such that

$$X_1 = f(X_2, X_3, \ldots, X_n) \tag{1}$$

or $$\phi(X_1, X_2, X_3, \ldots X_n) = 0 \tag{2}$$

then, if r is the greatest number of variables having independent dimensions, equation (2) can be expressed alternatively in terms of $(n - r)$ dimensionless quantities as

$$\psi(\pi_1, \pi_2, \ldots \pi_{n-r}) = 0 \tag{3}$$

where π_i is a dimensionless quantity taking the form of a ratio of $(r + 1)$ of the variables. In this context, independence of dimensions means that the dimensions of one quantity cannot be represented as a combination, in the form of a monomial power, of the dimensions of the other quantities. The dimensionless quantities π_i are determined from the relation

$$\pi_i = \frac{X_{r+i}}{X_1^{\alpha_1} X_2^{\alpha_2} \ldots X_r^{\alpha_r}} \tag{4}$$

where powers $\alpha_1, \ldots \alpha_r$ are chosen to render π_i dimensionless.

The deflections w of a vibrating cracked plate in tension are dependent upon the plate dimensions $2a$, $2b$, thickness t, crack length 2ℓ, the applied force F, the frequency of vibration Ω, Young's modulus E, shear modulus G, and density ρ. Thus we have the relationship

$$w = f(a, b, t, \ell, F, \Omega, E, G, \rho) \tag{5}$$

or $$\phi(w, a, b, t, \ell, F, \Omega, E, G, \rho) = 0 \tag{6}$$

The dimensions (indicated in this chapter by square brackets) of these ten parameters are

$$[\,w\,] = L \qquad [\,a\,] = L \quad [\,b\,] = L \quad [\,t\,] = L$$
$$[\,\ell\,] = L \qquad [\,F\,] = MLT^{-2} \quad [\,\Omega\,] = T^{-1}$$
$$[\,E\,] = ML^{-1}T^{-2} \quad [\,G\,] = ML^{-1}T^{-2} \quad [\,\rho\,] = ML^{-3} \tag{7}$$

where M, L, T denote mass, length and time respectively. The greatest number of variables having independent dimensions is thus three. For these variables it is convenient to choose a, E, Ω. The resulting seven independent dimensionless parameters are thus

$$\pi_1 = \frac{w}{a} \qquad \pi_2 = \frac{b}{a} \qquad \pi_3 = \frac{t}{a} \qquad \pi_4 = \frac{\ell}{a}$$
$$\pi_5 = \frac{F}{a^2E} \qquad \pi_6 = \frac{G}{E} \qquad \pi_7 = \frac{\rho}{a^{-2}E\Omega^{-2}} \tag{8}$$

giving
$$\psi(\pi_1, \pi_2, \ldots, \pi_7) = 0 \tag{9}$$

The model and full scale phenomena will be similar if all the non-dimensional variables $\pi_1, \ldots, \pi_7$ have the same numerical values. π_2, π_3, π_4 require that the model and full scale structures should be geometrically similar. Since $\frac{G}{E} = \frac{1}{2(1+\nu)}$, where ν is Poisson's ratio, π_6 requires the two materials to have the same value of Poisson's ratio. π_1, π_5, π_7 provide a means of relating the deflections, loads and frequencies respectively. If subscript m denotes model quantities we have

$$w = \left(\frac{a}{a_m}\right) w_m \tag{10}$$

$$F = \left(\frac{a}{a_m}\right)^2 \left(\frac{E}{E_m}\right) F_m \tag{11}$$

$$\Omega^2 = \left(\frac{a_m}{a}\right)^2 \left(\frac{\rho_m}{\rho}\right) \left(\frac{E}{E_m}\right) \Omega_m^2 \tag{12}$$

From (11) a relationship for stress may be deduced, namely

$$\sigma = \left(\frac{E}{E_m}\right) \sigma_m \qquad (13)$$

and so strains are given by

$$\varepsilon = \varepsilon_m \qquad (14)$$

Since there are three variables with independent dimensions, three design limitations may be imposed. By a suitable choice of material both the ratios $\frac{E_m}{E}$, $\frac{\rho_m}{\rho}$ are determined. The third choice to be made is the geometrical scaling factor $\frac{a_m}{a}$.

When choosing the material for the present application, due consideration was given to the fact that the stresses in a region around the crack tip are in the plastic range. Mansfield [5] has shown that when considering a simple deformation theory for plastic flow, the strain-stress relationships are obtained from the corresponding ones for elastic theory, by replacing Young's modulus by the secant modulus E_s and taking Poisson's ratio $\nu = \frac{1}{2}$. The secant modulus may be expressed in terms of Young's modulus and an equivalent stress σ_1 in tension. Using Ramberg and Osgood's method of representing the material's stress-strain curve in simple tension [6] a relationship for the secant modulus of the form

$$\frac{E}{E_s} = 1 + \kappa\left(\frac{\sigma_1}{E}\right)^{2n} \qquad (15)$$

is obtained where κ, n are constants which, together with E, describe the stress-strain curve.

In a region of plastic flow the non-dimensional parameters κ, n should be included in the above analysis. This would give the additional requirements that κ, n should be the same for model and full scale. This is readily satisfied by taking the model material to be the same as the material of the full scale structure.

The length scale was chosen as a compromise between the maximum load which could be applied, and also the maximum frequency it was desirable to consider. Consideration was also given to the standard thicknesses of sheet material commercially available. An upper limit of 20,000 lbs. was placed upon the loading rig for the model structure, and it was desirable to simulate a full scale value of 80,000 lbs. Thus from (11) it may be seen that $\frac{a_m}{a} = \frac{1}{2}$. This also satisfies the requirement that a full scale frequency of 500 c.p.s. be represented by a model value of no more than 1000 c.p.s. With these restrictions on the design of the model, the scaling factors for obtaining full scale parameters from model values are

$$\begin{aligned} F &= 4F_m \\ \Omega &= \tfrac{1}{2}\Omega_m \\ \sigma &= \sigma_m \\ \varepsilon &= \varepsilon_m \end{aligned} \qquad (16)$$

2.3 The Test Rig

A special loading rig, illustrated in figure 2, was constructed in order that tensile loads, up to a maximum of 20,000 lb., could be applied to specimens having widths of 5, 10, 20 ins. The specimens were clamped between half inch steel plates and the tensile load applied by means of a hydraulic jack. All the specimens in the present investigations had a depth of 6·75 ins. An increase in depth could be accommodated by re-locating the upper steel plates. This operation was simplified by using counter weights to balance the weight of the steel plates when the fixing bolts were removed.

The hydraulic system is illustrated in figure 3. Six of the seven shut-off valves and the three pressure gauges were mounted on a control panel as shown in figure 4. The system was so designed that the parts of the jack cylinder above and below the piston could be pressurised independently. Tensile loads were obtained by pressurising the part above the piston, the

pressure being measured by the 600 p.s.i. and the 2,000 p.s.i. gauges. Mounting in, and removal of the specimens from the rig, was facilitated by pressurising the part below the piston; the pressure in this case being measured by the 250 p.s.i. gauge.

The loading rig was calibrated by mounting two tensile test pieces, made of high strength steel, complete with mechanical extensometers, between the two sets of clamping plates. This gave a relationship between the extension and the gauge pressure. The relationship between the extension and the applied load was obtained by mounting the specimens in a tensile test machine, thus giving the following calibration:-

$$\text{Applied load (lbs.)} = 18{\cdot}18 \times \text{gauge pressure (p.s.i.)} \qquad (17)$$

A block diagram of the instrumentation used in the tests is shown in figure 5. The specimens were excited laterally by means of an electromagnetic exciter poisitioned centrally, just below the upper damping plates. In this way adequate response was obtained in the fundamental mode of vibration with a minimum of interference from the exciter. The displacements of the specimens were measured by means of a capacity probe. It was found that in measuring one mode shape, a far greater range of amplitudes was measured, than was possible with a single capacity probe of given sensitivity. Consequently the displacement was amplified and measured by a spectrum analyser. The displacement signal was also displayed on an oscilloscope together with a signal representing the exciter input force. In this way a check could be kept upon the phase difference between the excitation and response.

In order to demonstrate the validity of the scaling theory, the frequency of the fundamental mode of vibration of a half scale model of a 13·5" × 10·0" plate containing a 3 ins. crack, was determined for applied stresses up to 24×10^3 lb./in.^{2}. The resulting curve is compared with corresponding curves obtained from tests on full scale panels, using both discrete frequency siren excitation and electromagnetic vibrator excitation,

in figure 6. The curves show close agreement for stresses below the buckling stress. Some scatter is present in the value of the buckling stress, but this is within the accepted range of experimental scatter.

Further model tests were performed to determine the buckling stresses for 3·5 and 4·0 ins. cracks. In reference [2] it was shown that the buckling stress for a 13·5" × 10·0" plate 0·064 ins. thick could be calculated from the relation

$$\sigma_b = 1{\cdot}18\ E\left(\frac{t}{\ell}\right)^2 \qquad (18)$$

In figure 7, σ_b has been plotted against $(1/\ell^2)$ resulting in equation (18) representing a straight line. The experimental points obtained from the model tests lie close to this line.

2.4 The vibration characteristics of plates of varying width

The vibration characteristics of a 10 in., a 20 in. and a 40 in. wide plate of depth 13·5 ins. and thickness 0·064 ins. have been determined by testing half scale models as described in the previous section. The model specimens were manufactured from aluminium alloy L73. Details of the specimens are given in figure 8. The central slot, which represents a crack, is obtained by first of all drilling a 3/32" diameter hole at the centre of the plate and then making a cut to the desired length with a hacksaw blade. In the tests described here, further holes of 3/64" diameter were drilled at the ends of the slot to reduce stress concentrations there, ensuring that the crack did not propagate during the tests. On completion of the investigations for a particular crack length, the crack was extended with a hacksaw blade and a further 3/64" diameter hole drilled at each end.

The length of the central crack of the 20 ins. (full scale) wide plate was varied from 2 ins. to 6 ins. and the applied tensile stress was increased from zero to 21,000 lb./in.^{2}. Investigations on the 40 ins. wide plate covered crack lengths in the range 2 - 8 ins. and tensile stresses from zero to 26,000 lb./in.^{2}

The variation of the frequency of the fundamental mode with applied tensile stress and crack length, for these specimens, is given in

figures 10 and 11. The curves shown follow a similar pattern to the ones for a plate of dimensions 13·5" × 10·0" given in figure 9.

A comparison of the results for a given crack length, shows that there is an increase in frequency with plate width, due to an increase in plate area in direct tension. There is also a variation in the stress at which the area around the crack buckles. When this buckling occurs the frequency of vibration reaches a minimum and so the stress at buckling may be determined from these frequency curves. In figure 12 the stress at buckling σ_b has been plotted against $(1/\ell^2)$. For the 20 ins. wide plate the experimental points lie close to the line given by (18), which is the equation for the buckling stress obtained for the 10 ins. wide plate. At low stresses the experimental points for the 40 ins. plate lie close to the line

$$\sigma_b = 3{\cdot}66E\left(\frac{t}{\ell}\right)^2 \qquad (19)$$

At stresses above 17,000 lb./in.^{2} the experimental points lie below the line given by this equation. The variation in buckling coefficient and departure from a linear relationship between σ_b and $1/\ell^2$ has been caused by a variation in the stress distribution. Further discussion on this effect is deferred until Chapter 7.

The modes of vibration along the x-axis of the 20, 40 ins. plates with crack lengths of 4, 5, 6 ins. are shown in figures 13 to 18. In each case the ratio μ of applied stress to buckling stress is also varied. For a given crack length, the maximum frequency in the pre-buckled region occurs when μ lies between 0·7 and 0·75. If μ is less than this value the mode shape varies considerably with plate width and applied stress. For values of μ greater than 0·75, the predominant vibrations occur in the area around the crack. The width of this area is approximately twice the length of the crack. In the y-direction, increasing the applied stress has only a small effect on the mode shape; the predominant vibrations occuring over the full depth of the plate.

In the practical case, the crack length will be increasing and the

applied tensile stress constant. The variation of the frequency of the fundamental mode with crack length is given in figure 19 for an applied stress of 13,000 lb./in.^{2} The three curves for 10, 20, 40 ins. plates are cross plots from figures 9, 10, 11. As the crack extends the frequency is reduced until the critical buckling length, corresponding to the applied load, is reached. Further extensions in crack length result in the frequency increasing due to the increase in curvature of the free edge of the crack. Increasing the plate width produces a higher frequency and also gives a variation in the critical buckling length. For the 10 and 20 ins. plates the critical length is approximately 4 ins. whilst the 40 ins. plate buckles for a crack length of 7 ins.

The variation in frequency with crack length at an applied stress of 17,000 lb./in.^{2} is shown in figure 20 for a 40 ins. plate. The increase in stress results in a higher frequency at zero crack length and also a critical buckling length of approximately 6 ins., hence the steeper descent to the minimum frequency. The variation in mode shape as the crack extends is shown in figure 21. As the critical buckling length is approached the area of predominant vibration reduces to an area around the crack which is about twice the length of the crack in width.

These investigations have shown that increasing the plate width does have a marked effect on the dynamical characteristics under consideration. This effect is mainly due to the variation in buckling stress for a given crack length. Future investigations should consider other plate widths and also variations in the plate depth. In this way it should be possible to determine what other geometrical parameters, other than crack length and plate thickness, ought to be considered in determining the buckling stress.

3. SMALL DEFLECTION ANALYSIS

3.1 Introduction

Matrix methods of structural analysis have been developed during the last ten to fifteen years in connection with the analysis of highly complex aircraft structures. The fundamental assumption, which is common to these methods, is that the structure may be satisfactorily represented by a finite number of basic elements. In the case of an aircraft wing, the basic elements are defined by the intersections of the spars, ribs and skin. In order to utilize the facilities of an electronic digital computer, the structural analysis of the individual elements and the assembled structure is formulated in the notation of matrix algebra. These methods may also be employed to analyse two-dimensional systems such as plates and shells. The plate or shell is assumed to be represented by an assemblage of individual elements. These elements, however, are not quite so clearly defined by the geometry, as in the case of an aircraft wing. Other considerations, such as applied loading, likely stress distributions and modes of vibration, have to be taken into account in performing the idealisation.

As in the case of conventional structural analysis, matrix methods may be divided into two groups, namely, those formulated in terms of unknown forces and those formulated in terms of displacements. In reference [7], Argyris has developed the general theory with both forces and displacements as unknowns. The striking feature which emerges is that the two methods are completely analogous. Knowing the equations in either of the two procedures, we can write down, by a simple translation process, the equations in the other procedure. There does exist, however, significant differences in the detailed application of the methods.

Much of the early work on aircraft structures in this country was devoted to the first method, probably as a result of the extensive work of Argyris [7, 8]. More recently, Taig and Kerr [9] have shown that displacement techniques are particularly well suited to the analysis of low aspect ratio multicell box structures. In their application to plate and shell problems, research workers both in this country and in the United States have, in general, chosen to exploit the displacement method. It has been shown by Hessel [10], however, that linear static plate and shell problems can be analysed successfully by the force method, which is the technique adopted by Denke [11] in his analysis of non-linear static problems.

A considerable amount of development of the displacement method, as applied to static plate and shell problems, has been achieved in the field of Civil Engineering, where detailed studies of gravity dam sections [12] regarded as plane stress problems, and thin arch dams [13, 14], with either single or double curvature, have been made. These methods may be extended to analyse the vibration characteristics of plates and shells. In this chapter the procedure for analysing flat plate vibration problems is developed.

The general procedure for analysing a plate problem by the finite element displacement method may be summarised as follows:

(i) The idealisation of the plate into a finite number of individual elements, interconnected at a finite number of nodal points.

(ii) The evaluation of the element properties.

(iii) The structural analysis of the assemblage.

The idealisation process consists of approximating the plate by an assemblage of triangular, rectangular or quadrilateral elements. In what follows only the triangular element will be considered.

3.2 Element Properties

The first step in the determination of the element properties is to assume certain deformation patterns for the displacements {u} of the

element. These deformation patterns should be chosen in such a manner, that satisfaction of continuity of displacements, at the corner or nodal points, also ensures continuity along the element boundaries. It will also be advantageous to assume as many deformation patterns as there are nodal degrees of freedom. The displacements are thus written in the form

$$\{u\} = [\, M(x, y) \,] \{A\} \qquad (20)$$

where $[\, M(x, y) \,]$ is a matrix of functions defining the displacements $\{u\}$, and $\{A\}$ is a column matrix of constants. These constants may be determined by introducing the nodal co-ordinates successively into the expression (20). Thus the nodal displacements $\{u_i\}$ are given by

$$\{u_i\} = [C]\{A\} \qquad (21)$$

The matrix $[C]$ is square and so may be inverted to give

$$\{A\} = [\, C^{-1}]\{u_i\} \qquad (22)$$

The internal element "strains" $\{\varepsilon\}$ may be expressed in the form

$$\{\varepsilon\} = [\, B(x, y) \,]\{A\} \qquad (23)$$

where the matrix $[\, B(x, y) \,]$ is a differential of the matrix $[\, M(x, y) \,]$. Introducing equation (22) into (23) we obtain

$$\{\varepsilon\} = [B][C^{-1}]\{u_i\} \qquad (24)$$

The material "stress-strain" relationships may be written in the form

$$\{\sigma\} = [\, D \,] \{\varepsilon\} \qquad (25)$$

where $\{\sigma\}$ denotes the internal stresses, and $[\, D \,]$ is a matrix of material constants.

Hence $$\{\sigma\} = [\, D \,][\, B \,][\, C^{-1} \,]\{u_i\} \qquad (26)$$

Now the internal virtual work W_I associated with the virtual strains $\{\bar{\varepsilon}\}$ is

$$W_I = \int_\Delta \{\bar{\varepsilon}\}^T \{\sigma\}\, dxdy \tag{27}$$

where Δ denotes the area of the triangle. Introducing (24) and (26) into (27) we find that

$$W_I = \{\bar{u}_i\}^T [\, C^{-1}\,]^T \int_\Delta [\, B\,]^T [\, D\,][\, B] dxdy\, [C^{-1}\,]\{u_i\} \tag{28}$$

where $\{\bar{u}_i\}$ are the virtual nodal displacements associated with the virtual strains $\{\bar{\varepsilon}\}$.

The inertia forces $\{f\}$ per unit area acting on a plate element may be written in the form

$$\{f\} = \Omega^2 [m_p\,]\{u\} \tag{29}$$

where Ω is the frequency of vibration and $[\, m_p]$ is a matrix of inertial constants. The work done by these forces in the virtual displacement $\{\bar{u}\}$ is

$$W_M = \int_\Delta \{\bar{u}\}^T \{f\}\ dx\, dy \tag{30}$$

Introducing (20) and (22) we have

$$W_M = \Omega^2 \{\bar{u}_i\}^T [C^{-1}]^T \int_\Delta [M]^T [m_p] [M] dxdy [C^{-1}] \{u_i\} \tag{31}$$

If the nodal forces corresponding to the nodal displacements $\{u_i\}$ are $\{s_i\}$, then the external work done during the virtual displacement $\{\bar{u}_i\}$ is

$$W_E = \{\bar{u}_i\}^T \{s_i\} \tag{32}$$

Applying the theorem of virtual work gives

$$W_E + W_M = W_I \tag{33}$$

that is

$$\{\bar{u}_i\}^T\{s_i\} + \Omega^2\{\bar{u}_i\}^T[C^{-1}]^T \int_\Delta [M]^T[m_p][M]\,dxdy\,[C^{-1}]\,\{u_i\}$$

$$= \{\bar{u}_i\}^T[C^{-1}]^T \int_\Delta [B]^T[D][B]\,dxdy\,[C^{-1}]\{u_i\}$$

If we now apply a unit virtual displacement at each of the nodal degrees of freedom in sequence we obtain an equation of the form

$$\{s_i\} = [k]\{u_i\} - \Omega^2[m]\{u_i\} \qquad (34)$$

where

$$[k] = [C^{-1}]^T \int_\Delta [B]^T[D][B]\,dxdy\,[C^{-1}] \qquad (35)$$

is the element stiffness matrix and

$$[m] = [\,C^{-1}\,]^T \int_\Delta [M]^T[m_p][M]\,dxdy\,[C^{-1}] \qquad (36)$$

is the element inertia matrix.

Equation (34) relates the nodal forces $\{s_i\}$ to the harmonic nodal displacements $\{u_i\}$ of frequency Ω. The matrices [k], [m] represent the element structural properties. The stiffness matrix [k] is the same matrix that would have been obtained by a purely static analysis. The columns of this matrix represent the nodal forces required to produce a unit displacement at a single nodal point. The inertia matrix [m] represents the equivalent point masses and moments of inertia required at the nodal points to produce the same loading as the distributed inertias.

3.3 Assumed Displacement Functions

The critical phase in the preceding analysis is in prescribing suitable deformation patterns (equation (20) for the element. Any assumed displacement function should satisfy certain requirements in order to ensure convergence to the true solution as the size of the element is reduced. The requirements, which have been proposed by various authors, may be summarised as follows:

(i) The element should be allowed to deform similarly to the deformations developed in the corresponding region of the continuum [15].

(ii) The function must be a linear function of the generalised displacements [16].

(iii) Continuity of deflections and slopes must exist between adjacent elements [15, 16, 17].

(iv) If the nodal slopes and displacements are consistent with a state of constant curvature and twist, then the chosen displacement function should implement this state (ref. 20). In particular the complete set of rigid body displacements must be represented [16].

(v) When increasing the fineness of the network representing the structure, the displacements of a sub-element should be identical to those generated in it before sub-division [16, 18].

Most of these requirements are easily satisfied. The condition which causes most difficulty for a triangular element in bending is the third. One of the first displacement functions to be used is one proposed by Clough [15]. Taking the lateral displacement w and the rotations $\partial w/\partial y$, $-\partial w/\partial x$ as nodal degrees of freedom, he assumed the following polynomial expression for the displacement w:

$$w = A_1 + A_2x + A_3y + A_4x^2 + A_5xy + A_6y^2 + A_7x^3 + A_8(x^2y + xy^2) + A_9y^3 \qquad (37)$$

where $A_1, A_2, \ldots A_9$ are constants. This function satisfies all the above requirements except continuity of slope between adjacent elements. Only recently [19] has a function been proposed which does ensure continuity of slope. With this function, however, numerical integration becomes imperative in deriving the element characteristics.

3.4 Triangular Element in Bending

The procedure for determining the stiffness and inertia matrices of an element, as developed in section 3.2, may be applied to elements of any shape. By way of illustration a triangular element will now be considered.

If the polynomial expression (37) is used for the assumed displacement function, then equation (20) takes the form

$$\begin{bmatrix} w \\ \theta_x \\ \theta_y \end{bmatrix} = \begin{bmatrix} w \\ \frac{\partial w}{\partial y} \\ -\frac{\partial w}{\partial x} \end{bmatrix} = \begin{bmatrix} 1 & x & y & x^2 & xy & y^2 & x^3 & (x^2y + xy^2) & y^3 \\ 0 & 0 & 1 & 0 & x & 2y & 0 & (x^2 + 2xy) & 3y^2 \\ 0 & -1 & 0 & -2x & -y & 0 & -3x^2 & -(2xy + y^2) & 0 \end{bmatrix} \begin{bmatrix} A_1 \\ A_2 \\ \vdots \\ A_9 \end{bmatrix} \tag{38}$$

where the lateral displacement w and rotations θ_x, θ_y are defined in figure 22. Evaluating this equation at each of the nodal points, we see that the matrices given in equation (21) are defined by

$$\{u_i\} = \{w_1, \theta_{x1}, \theta_{y1}, w_2, \theta_{x2}, \theta_{y2}, w_3, \theta_{x3}, \theta_{y3}\}$$

$$\{A\} = \{A_1, A_2, \ldots, A_9\}$$

$$[C] = \begin{bmatrix} 1 & 0 & 0 & 0 & 0 & 0 & 0 & 0 & 0 \\ 0 & 0 & 1 & 0 & 0 & 0 & 0 & 0 & 0 \\ 0 & -1 & 0 & 0 & 0 & 0 & 0 & 0 & 0 \\ 1 & x_2 & 0 & x_2^2 & 0 & 0 & x_2^3 & 0 & 0 \\ 0 & 0 & 1 & 0 & x_2 & 0 & 0 & x_2^2 & 0 \\ 0 & -1 & 0 & -2x_2 & 0 & 0 & -3x_2^2 & 0 & 0 \\ 1 & x_3 & y_3 & x_3^2 & x_3y_3 & y_3^2 & x_3^3 & (x_3^2y_3 + x_3y_3^2) & y_3^3 \\ 0 & 0 & 1 & 0 & x_3 & 2y_3 & 0^3 & (x_3^2 + 2x_3y_3) & 3y_3^2 \\ 0 & -1 & 0 & -2x_3 & -y_3 & 0 & -3x_3^2 & -(2x_3y_3 + y_3^2) & 0 \end{bmatrix} \tag{39}$$

The columns of the inverse matrix $[\ C^{-1}\ ]$ may be obtained by taking each nodal displacement in equation (21) to be unity in sequence, whilst the others are assumed zero. Because of the large number of zeros in the matrix $[\ C\ ]$ the resulting set of equations are easily solved. It may be seen, however, that this process breaks down whenever

$$y_3 + 2x_3 - x_2 = 0 \tag{40}$$

In this case the matrix $[\ C\ ]$ is singular and therefore an inverse does not exist.

In plate bending the stress resultants are given, using the sign convention in figure 23, by

$$\begin{aligned} M_x &= +D\left(\frac{\partial^2 w}{\partial y^2} + \nu \frac{\partial^2 w}{\partial x^2}\right) \\ M_y &= -D\left(\nu \frac{\partial^2 w}{\partial y^2} + \frac{\partial^2 w}{\partial x^2}\right) \\ M_{xy} &= +D\,(1-\nu)\,\frac{\partial^2 w}{\partial x \partial y} \end{aligned} \tag{41}$$

where $D = \dfrac{Et^3}{12(1-\nu^2)}$, E being Young's modulus, ν Poisson's ratio and t the plate thickness. Defining the "stress" and "strain" matrices as

$$\{\sigma\} = \{M_x,\ M_y,\ M_{xy}\}, \quad \{\varepsilon\} = \left\{\frac{\partial^2 w}{\partial y^2},\ -\frac{\partial^2 w}{\partial x^2},\ 2\frac{\partial^2 w}{\partial x \partial y}\right\}$$

the matrix of material constants $[\ D\ ]$, as defined by equation (25) becomes

$$[\ D\ ] = D \begin{bmatrix} 1 & -\nu & 0 \\ -\nu & 1 & 0 \\ 0 & 0 & \xi \end{bmatrix} \tag{42}$$

where $\xi = \dfrac{1-\nu}{2}$.

Differentiating the displacement function yields the "strain" matrix [B] as defined by equation (23).

$$[B] = \begin{bmatrix} 0 & 0 & 0 & 0 & 0 & 2 & 0 & 2x & 6y \\ 0 & 0 & 0 & -2 & 0 & 0 & -6x & -2y & 0 \\ 0 & 0 & 0 & 0 & 2 & 0 & 0 & 4(x+y) & 0 \end{bmatrix} \qquad (43)$$

Introducing (42) and (43) into equation (35), and defining a generalised stiffness matrix

$$[\tilde{k}] = \int_{\Delta} [B]^T [D] [B] \, dxdy \qquad (44)$$

it will be seen that

$[\tilde{k}] =$

$$4D\Delta \begin{bmatrix} 0 & & & & & & & & \\ 0 & 0 & & & & & & & \\ 0 & 0 & 0 & & & & & & \\ 0 & 0 & 0 & 1 & & \text{SYMMETRIC} & & & \\ 0 & 0 & 0 & 0 & \xi & & & & \\ 0 & 0 & 0 & \nu & 0 & 1 & & & \\ 0 & 0 & 0 & 3h_x & 0 & 3\nu h_x & 9r^2_{yy} & & \\ 0 & 0 & 0 & (\nu h_x + h_y) & 2\xi(h_x+h_y) & (h_x+\nu h_y) & 3(\nu r^2_{yy}+r^2_{xy}) & \{(3-2\nu)r^2_{zz} & \\ & & & & & & & +2(2-\nu)r^2_{xy}\} & \\ 0 & 0 & 0 & 3h_y & 0 & 3h_y & 9\nu r^2_{xy} & 3(r^2_{xy}+\nu r^2_{xx}) & 9r^2_{xx} \end{bmatrix} \qquad (45)$$

where h_x, h_y = coordinates of the centroid of the triangle

Δr^2_{xx}, Δr^2_{yy}, Δr^2_{xy} = second moments of area with respect to the given axes

$$r^2_{zz} = r^2_{xx} + r^2_{yy}$$

The element stiffness matrix is then given by

$$[k] = [C^{-1}]^T [\tilde{k}] [C^{-1}] \tag{46}$$

If rotary inertia effects are neglected then the matrix of inertia constants takes the form

$$[m_p] = \begin{bmatrix} \rho t & 0 & 0 \\ 0 & 0 & 0 \\ 0 & 0 & 0 \end{bmatrix} \tag{47}$$

where ρ denotes the density of the material. Thus the integrand in equation (36) becomes

$$[M]^T [m_p] [M] =$$

$$\rho t \begin{bmatrix}
1 & & & & & & & & \\
x & x^2 & & & & & & & \\
y & xy & y^2 & & & & & & \\
x^2 & x^3 & x^2y & x^4 & & \text{SYMMETRIC} & & & \\
xy & x^2y & xy^2 & x^3y & x^2y^2 & & & & \\
y^2 & xy^2 & y^3 & x^2y^2 & xy^3 & y^4 & & & \\
x^3 & x^4 & x^3y & x^5 & x^4y & x^3y^2 & x^6 & & \\
(x^2y+xy^2) & (x^3y+x^2y^2) & (x^2y^2+xy^3) & (x^4y+x^3y^2) & (x^3y^2+x^2y^3) & (x^2y^3+xy^4) & (x^5y+x^4y^2) & (x^2y+xy^2)^2 & \\
y^3 & xy^3 & y^4 & x^2y^3 & xy^4 & y^5 & x^3y^3 & (x^2y^4+xy^5) & y^6
\end{bmatrix} \tag{48}$$

Defining a generalised inertia matrix

$$[\tilde{m}] = \int_{\Delta} [M]^T [m_p] [M] \, dxdy \tag{49}$$

it may be noted that each element of this matrix involves an integral of the form $\int_{\Delta} x^m y^n \, dxdy$.

In Appendix it is shown that the result of this integration is

$$\int_{\Delta} x^m y^n dxdy = \frac{y_3^{n+1}}{(m+1)} \left[\sum_{r=0}^{m+1} \sum_{s=0}^{r} \frac{(-1)^{r+s}(m+1)!}{(m+1-r)!(r-s)!s!(n+r+1)} x_2^{m+1-s} x_3^s - \frac{x_3^{m+1}}{(m+n+2)} \right] \qquad x_3 \neq 0, \; x_3 \neq x_2$$

$$= \frac{y_3^{n+1} x_2^{m+1}}{(m+1)} \sum_{r=0}^{m+1} \frac{(-1)^r (m+1)!}{(m+1-r)!r!(n+r+1)} \qquad x_3 = 0 \qquad (50)$$

$$= \frac{y_3^{n+1} x_2^{m+1}}{(n+1)(m+n+2)} \qquad x_3 = x_2$$

Thus it is possible to compute the elements of $[\tilde{m}]$, and hence the structural element inertia matrix which is given by

$$[m] = [c^{-1}]^T [\tilde{m}] [c^{-1}] \qquad (51)$$

3.5 Equilibrium of the Complete Structure

Having idealised the structure as an assemblage of finite elements and also having determined the element properties, the next step is to ensure equilibrium of the complete structure. This is achieved by considering the equilibrium of the internal and external applied forces at each nodal point.

The structural properties of each individual element, as represented by equations (34) - (36) , are referred to local coordinate axes. In order to simplify the equilibrium relationships, these equations are now referred to global coordinate axes, which are common to all elements.

Referring to figure 22, the coordinates in the local system are related to the ones in the global system by the equation

$$\begin{bmatrix} x \\ y \end{bmatrix} = [\zeta]\left[\begin{bmatrix} x^o \\ y^o \end{bmatrix} - \begin{bmatrix} x_o^o \\ y_o^o \end{bmatrix}\right] \tag{52}$$

where $\{x_o^o, y_o^o\}$ are the coordinates (w.r.t. axes $O^o x^o y^o$) of the point O, and $[\zeta]$ is a matrix of direction cosines, namely

$$[\zeta] = \begin{bmatrix} \cos(x, x^o) & \cos(x, y^o) \\ \cos(y, x^o) & \cos(y, y^o) \end{bmatrix} \tag{53}$$

Thus if the displacements $\{u\}$ are taken to be $\{w, \partial w/\partial y, -\partial w/\partial x\}$, then the displacements $\{u_i\}$ are related to the corresponding displacements $\{u_i^o\}$ in the global system by the equation

$$\{u_i\} = [\Xi]\{u_i^o\} \tag{54}$$

where

$$[\Xi] = \begin{bmatrix} 1 & & & & & \\ & \zeta & & & & \\ & & 1 & & & \\ & & & \zeta & & \\ & & & & 1 & \\ & & & & & \zeta \end{bmatrix} \tag{55}$$

Similarly, the nodal forces are related by

$$\{s_i^o\} = [\Xi]^T \{s_i\} \tag{56}$$

Introducing equations (54), (56) into (34) yields

$$\{s_i^o\} = [k^o]\{u_i^o\} - \Omega^2[m^o]\{u_i^o\} \tag{57}$$

where

$$[k^o] = [\Xi]^T [k] [\Xi] \tag{58}$$

and

$$[m^o] = [\Xi]^T [m] [\Xi] \tag{59}$$

Now the nodal displacements of the element g - $\{u_i^o\}_g$ may be expressed in terms of the displacements of the complete structure $\{U^o\}$ by the relation

$$\{u_i^o\}_g = [a_g] \{U^o\} \tag{60}$$

The matrix $[a_g]$ will consist of rows which are entirely zero except for one element which is unity. In formulating this matrix for the various elements, it is assumed that the elements are interconnected at their nodal points.

The internal forces for the element g are thus

$$\{s_i^o\}_g = [[k_g^o] - \Omega^2 [m_g^o]] [a_g] \{U^o\} \tag{61}$$

And so the internal forces for all the elements may be written in the form

$$\{s^o\} = [[\bar{K}^o] - \Omega^2 [\bar{M}^o]] [a] \{U^o\} \tag{62}$$

where

$$\{s^o\} = \begin{bmatrix} \{s_i^o\}_1 \\ \{s_i^o\}_2 \\ \vdots \\ \{s_i^o\}_n \end{bmatrix} \quad [\bar{K}^o] = \begin{bmatrix} k_1^o & & & \\ & k_2^o & & \\ & & \ddots & \\ & & & k_n^o \end{bmatrix}$$

$$[a] = \begin{bmatrix} a_1 \\ a_2 \\ \vdots \\ a_n \end{bmatrix} \quad [\bar{M}^o] = \begin{bmatrix} m_1^o & & & \\ & m_2^2 & & \\ & & \ddots & \\ & & & m_n^o \end{bmatrix} \tag{63}$$

If the external forces applied to the structure are denoted by $\{S^o\}$, then equilibrium of the nodal points of the complete structure is given by

$$\{S^o\} = [a]^T \{s^o\} \tag{64}$$

That is

$$\{S^o\} = [\,[K^o] - \Omega^2[M^o]\,]\,\{U^o\} \tag{65}$$

where

$$[K^o] = [a]^T\,[\bar{K}^o]\,[a] \tag{66}$$

$$[M^o] = [a]^T\,[\bar{M}^o]\,[a] \tag{67}$$

Equations (66), (67) may also be written in the form

$$[K^o] = \sum_g [a_g]^T\,[k_g^o]\,[a_g] \tag{68}$$

$$[M^o] = \sum_g [a_g]^T\,[m_g^o]\,[a_g] \tag{69}$$

The operations involved in the right hand side of equation (68) consist of adding the elements of the structural element stiffness matrix $[k_g^o]$ to the appropriate elements, depending on the ordering of the nodal displacements, of the overall stiffness matrix $[K^o]$. This process is repeated for every element of the structure. The whole operation is equivalent to adding the stiffnesses of the elements adjacent to a given nodal point. In practice, it is unnecessary to calculate the matrices $[a_g]$. The information they contain is calculated from the ordering of the nodal points and the ordering of the structural elements. Similar arguments also hold for equation (69).

3.6 Boundary Conditions

The final stage of the analysis is to find solutions of equation (65) which satisfy the conditions which exist at the boundaries of the structure. These conditions consist of the so-called "artificial" and "natural" boundary conditions. For plate and shell type structures part or whole of the boundary will be either clamped or freely supported. This gives rise to the artificial boundary conditions that either the displacements and/or the rotations are zero. The natural boundary conditions arise from free boundaries along which the shear forces and bending moments,

vanish. Therefore the nodal forces and moments, collectively referred to as forces, will be zero along this part of the boundary. It may be noted that flexible supports do not constitute either artificial or natural boundary conditions. The known stiffnesses of the supports are added into the appropriate locations of the stiffness matrix $[K^o]$. If the natural modes of vibration of the structure are required then the nodal forces at the interior points are also taken to be zero.

If the nodal forces and displacements are re-ordered such that the known displacements and the corresponding forces appear together in $\{U^o\}$, $\{S^o\}$ then equation (66) may be written in the form

$$\begin{bmatrix} S_1^o \\ S_2^o \end{bmatrix} = \left[\begin{bmatrix} K_{11}^o & K_{12}^o \\ K_{21}^o & K_{22}^o \end{bmatrix} - \Omega^2 \begin{bmatrix} M_{11}^o & M_{12}^o \\ M_{21}^o & M_{22}^o \end{bmatrix} \right] \begin{bmatrix} U_1^o \\ U_2^o \end{bmatrix} \qquad (70)$$

where $\{U_2^o\}$ are the known displacements. The boundary conditions may now be written as

$$\{U_2^o\} = 0, \quad \{S_1^o\} = 0 \qquad (71)$$

Introducing them into equation (71) yields the following equations

$$\left[[K_{11}^o] - \Omega^2 [M_{11}^o] \right] \{U_1^o\} = 0 \qquad (72)$$

$$\{S_2^o\} = \left[[K_{21}^o] - \Omega^2 [M_{21}^o] \right] \{U_1^o\} \qquad (73)$$

The first of these equations (72), is in the form of an eigenvalue problem, the solution of which gives the natural frequencies and the corresponding modes of vibration of the structure. In practice the matrices $[K_{11}^o]$, $[M_{11}^o]$ in equation (72) are obtained by deleting the rows and columns of $[K^o]$, $[M^o]$, respectively, which correspond to the zero displacements. Having obtained Ω, $\{U_1^o\}$, equation (73) may then be used to calculate the forces on the part of the boundary along which the displacements have been prescribed.

4. THE VIBRATION OF FLAT PLATES

4.1 Introduction

Finite element techniques may be used to determine the vibration characteristics of flat plates having arbitrarily shaped boundaries. To demonstrate this, and also to illustrate the accuracy which can be expected, three plates having different shaped boundaries are considered. The first is a simply supported rectangular plate whose sides are in the ratio 1·48 : 1, the results of which are compared with an exact solution. The second is a cantilevered triangular plate of aspect ratio 6·7, and the results are compared with experimental data. Finally, a clamped circular plate is considered and the results compared with a Rayleigh-Ritz type solution.

The method used is given in chapter 3. The assumed displacement function used is the cubic polynomial

$$w = A_1 + A_2x + A_3y + A_4x^2 + A_5xy + A_6y^2 + A_7x^3 + A_8(x^2y + xy^2) + A_9y^3 \qquad (74)$$

This function is not invariant with respect to the choice of coordinate axes, and so the positions of the local axes have been varied in the rectangular and triangular plates and the resulting solutions compared. Finally, the number of elements used has been varied to illustrate the convergence characteristics of the solution as the size of element is decreased.

4.2 Computer Programme

Finite element techniques are computer orientated methods of analysing structures. Any discussion of a particular application would not be complete, therefore, without a description of the programming procedure adopted. The sequence of calculations which are necessary for the solution of flat plate vibration problems are indicated in the flow

diagram in figure 24. It may be seen that the programme is composed of four main stages, namely:

(i) The input of data

(ii) The formation of the stiffness matrix of the assembled structure $[K^{o}_{11}]$

(iii) The formation of the inertia matrix of the assembled structure $[M^{o}_{11}]$

(iv) The calculation of the characteristic roots and vectors of the equation

$$\left[[K^{o}_{11}] - \lambda [M^{o}_{11}] \right] \{U^{o}_{1}\} = 0 \qquad (75)$$

where $\lambda = \Omega^2$, to give the natural frequencies and normal modes of vibration of the structure.

In calculating the input data it is assumed that a plate is divided up into NE triangular elements in such a way that there are NPR columns, the I'th column of which contains NPC(I) nodal points, giving a total of NP. An example of how this is done is given in figure 25. The data required by the programme is as follows.

NE, NP, NPR - as defined

{NPC} - a matrix of order (NPR,1) as defined

[NGE] - a matrix of order (NE,3) whose I'th row gives the nodal point numbers of element number I.

[G] - a matrix of order (NP, 2) whose I'th row gives the global coordinates of nodal point number I.

TH, E, PR, RHŌ - plate thickness, Young's modulus, Poisson's ratio, mass density.

NC - number of constraints

[MCN] - a matrix of order (NC,2). The first number of any row specifies the row and/or column to be eliminated from the diagonal submatrix, indicated by the second number in the row, and its neighbours.

The stiffness matrix $[K^o]$ is formed by, first of all, calculating the nodal coordinates of element number one referred to local axes specified by the matrix [NGE]. This information, together with the plate thickness, Young's modulus and Poisson's ratio, is used to calculate the element stiffness matrix $[k^o]$ referred to global axes, which is defined (see chapter 3) by

$$[k^o] = [\Xi]^T[C^{-1}]^T \int_\Delta [B]^T [D] [B] dS [C^{-1}] [\Xi] \qquad (76)$$

The elements of $[k^o]$ are finally added to the appropriate elements of $[K^o]$. If the nodal points of the element are numbered n_1, n_2, n_3 and $[k^o]$ is partitioned into nine submatrices $[k^o_a]_{ij}$ of order (3, 3), then the submatrix $[k^o_a]_{ij}$ will be added to the (3, 3) submatrix of $[K^o]$ whose leading element occupies the position $(3n_i - 2, 3n_j - 2)$, for i, j = 1,2,3. This process is repeated for each of the NE elements. It is interesting to note here, that by suitable ordering of the nodal displacements the matrix $[K^o]$ takes the form of a band matrix as indicated in figure 26. All the non zero elements lie in a triple band of (3NPR - 2) submatrices about the main diagonal, the diagonal submatrices being of order 3NPC(I) for I = 1, 2, .., NPR. There are a number of ways of achieving this, as described by Argyris in reference [8]. The method adopted here is to keep the displacements at each nodal point adjacent to one another. Finally, the matrix $[K^o_{11}]$ is obtained from $[K^o]$ by deleting the NC rows and columns specified by the matrix [MCN]. The inertia matrix $[M^o_{11}]$ is obtained using a like procedure.

In the investigations described in this chapter, two methods of determining the characteristic roots and vectors of equation (75) have been used. When the order of the matrices $[K^o_{11}]$, $[M^o_{11}]$ was less than 50 a method was adopted which made use of existing methods of finding the roots and vectors of a single matrix. Equation (75) may be transformed into the more usual characteristic value problem

$$[\,[T] - \lambda[I]\,]\,\{V\} = 0 \qquad (77)$$

where $[I]$ denotes the unit matrix, by expressing $[M^{o}_{11}]$ in the form

$$[M^{o}_{11}] = [L]\,[L]^{T} \tag{78}$$

where $[L]$ is a lower triangular matrix. This is obtained by using a symmetric Cholesky decomposition [20] . Premultiplying equation (75) by $[L^{-1}]$ yields equation (77) where

$$[T] = [L^{-1}][K^{o}_{11}]\,[L^{-1}]^{T} \tag{79}$$

and

$$\{V\} = [L]^{T}\,\{U^{o}_{1}\} \tag{80}$$

Equation (77) may now be solved by Householder's method [21] . It may be noted that the matrix $[T]$ is a fully populated matrix, and so, if its order is large the method is inefficient with regard to storage requirements. On the other hand, the Householder method of solving equation (77) is a very efficient method indeed.

For larger order matrices the method used was to evaluate the determinant $DET(\lambda) = [[K^{o}_{11}] - \lambda[M^{o}_{11}]]$ for a range of values of λ until a change in sign of the determinant was found, indicating a root of the equation $DET(\lambda) = 0$. The rule of false position [22] was then used to iterate to the root, correct to a specified number of significant figures. If the determinant is evaluated by means of the Gauss elimination procedure [20] then very little working space is required, additional to the space required to store the non zero submatrices of $[[K^{o}_{11}] - \lambda[M^{o}_{11}]]$. Thus for large order matrices the method is more efficient with regard to storage requirements than the previous method. In comparison with the Householder technique, however, the method of obtaining the roots is very slow.

4.3 Simply Supported Rectangular Plate

The simplest problem one could use to demonstrate the finite element method is a simply supported rectangular plate. The exact solution to this problem [23] gives a frequency

$$f = \frac{\pi}{2}\left(\frac{D}{\rho t}\right)^{\frac{1}{2}}\left[\frac{(m-1)^2}{a^2} + \frac{(n-1)^2}{b^2}\right] \tag{81}$$

where the plate has dimensions a and b, m and n are the number of node lines, including boundaries, in the directions of a and b, and other notation as in chapter 3. In the case considered here, the plate has dimensions 13·5 x 20·0 ins.

Initially the plate was idealised into 8, 16 and 40 elements as shown in figure 27 and the local axes taken parallel to global axes as shown in figure 28 (a). The error in frequency, when compared with the exact solution, is given in table 1. Two factors emerge from this analysis. Firstly, all the frequencies are underestimated. Secondly, as the grid is made successively finer, an increased number of modes appear and the accuracy of each increases. The overestimate of 7·37% for mode 3, case 27 (b) may be accounted for by the fact that too few nodal points have been used to represent the mode shape in the direction having three nodal lines.

The local axes were then taken as indicated in 28 (b) and the idealisations as shown in figure 29. In order to minimize computer storage requirements only one quarter of the plate was considered. The boundary conditions along the plate centre lines are obtained by considering symmetrical and antisymmetrical modes of vibration. When one of the plate centre lines is a line of symmetry then the slope and shear force along this line are zero. On the other hand, if it is a line of antisymmetry, then the displacement and bending moment are zero. The error in frequency obtained on comparison with the exact solution for the first ten modes are plotted in figures 30, 31. The number of nodal lines, including boundaries, in the directions of the sides are given in table 2 for each mode. The first five calculated frequencies converge towards the exact solution for mesh sizes greater than 3, whilst the next five converge for mesh sizes greater than 4.

Finally the local axes were taken as indicated in figure 28 (c) for a mesh size of 5. The results are compared with the corresponding results from figures 30, 31 in table 3. It will be seen that on the whole the errors in frequency are much greater, and also that some of the errors are also over-estimates.

4.4 Cantilevered Triangle

A general solution for the vibrations of triangular plates has not yet been found. A survey of the particular cases for which exact or approximate solutions do exist is given in reference [24]. Gustafson, Stokey and Zorowski have presented experimental results for cantilevered triangular plates of varying aspect ratio in reference [25].

A finite element solution has been obtained for a cantilevered triangular plate of aspect ratio 6.7. Solutions were obtained for mesh sizes 5 and 10 as shown in figure 32. For a mesh size of 5 local axes were chosen as in 28 (a) and 28 (b), and for the mesh size of 10 type 28 (b) were chosen. The frequencies obtained are compared in table 4. When the mesh size is 5 and type 28 (a) axes used, the error in frequency is less than 2·5% for the first six modes. The nodal patterns for this case are compared in figure 33 and show excellent agreement. The first mode is the fundamental bending with the node line at the root. Changing to type 28 (b) local axes shows a marked deterioration in the accuracy. The first two frequencies are still within 2·5% of the measured values but the error of the next four varies from 5·76% to 18·98%. However, increasing the mesh size to 10 yields all six frequencies within 3·26% The nodal pattern for the last two cases are very similar to the first and so have not been presented.

4.5 Clamped Circular Plate

Plates with curved boundaries may be solved by finite element techniques by approximating the boundary to a series of straight lines. In order to determine the accuracy of this method a circular plate with a clamped boundary was analysed and the solution compared with a Rayleigh-Ritz type solution [23] . A quarter of the plate was idealised as shown in figure 34, the mesh sizes being denoted by 5 and 8. The results obtained are presented in table 5. Modes 1 and 4 were obtained by assuming the normal slope along AB and BC to be zero. For mode 2 the assumption was made that the normal slope along AB was zero and that BC was simply supported, and for mode 3 both AB and BC were assumed to be simply supported. For a mesh size of 5 all of these four modes were underestimated, the variation ranging

from 5·72% to 12·26%. Increasing the mesh size to 8, all four are estimated to within 6%.

4.6 Discussion

A finite element solution of the vibration characteristics of three flat plates with different shaped boundaries has been presented. These solutions have been compared with either analytic solutions or experimental results.

Considering the type of axes illustrated in figure 28 (b), the method underestimates the frequencies. When the number of elements is increased, it is found that after, possibly, an initial deterioration in accuracy, the solution then converges towards the true solution. This behaviour may be explained by the fact that the lack of slope continuity between elements induces excessive flexibility of the assembled structure. However, as the number of elements increases, the number of nodal points, at which compatibility of slope exists, also increases. This effect seems to have had a far greater influence on the results than the excessive stiffness of the individual elements.

Using type 28(a) local axes has produced good results for only a small number of elements. This is probably due to a balance between the excessive stiffness of the individual elements and the excessive flexibility of the assemblage. In general, this type of local axis is not convenient to use.

The one case in which axes of type 28 (c) were used (table 3) produced very erratic results. The lower modes were very greatly underestimated whilst some of the higher modes were overestimated.

This investigation has shown that the method of finite elements may be used to calculate the vibration characteristics of flat plates of arbitrary shape. Also, if the number of elements used in the idealisation is increased then the solution converges towards the true solution.

5. THE VIBRATION OF SHELLS

5.1 Introduction

The vibration characteristics of shells may be determined using finite element techniques, if the continuously curved surface is approximated by an assemblage of flat plate elements joined together at their edges. Rectangular elements may be used to approximate cylindrical shells [26] whilst shells of double curvature are conveniently represented by an assemblage of triangular elements. These techniques are illustrated in figure 35.

Each of the elements is subject to flexure and stresses within its plane. If the stiffness and inertia matrices of an element are first of all calculated in the Oxyz axes (fig. 36), then they may be obtained by combining the plate bending matrices, derived in chapter 3, and 'in-plane' matrices, which will be derived in the next section. After transforming to global axes, the final stiffness and inertia matrices are assembled in a manner similar to the one described for flat plate problems in chapter 3.

5.2 In-plane Analysis of a Triangular Element

The static analysis of two dimensional systems using triangular elements was first proposed by Clough in reference [12]. This work will now be extended to the dynamic analysis of such systems.

Taking the displacements u, v as modal degrees of freedom, Clough assumed the following displacement functions

$$u = A_1 + A_2x + A_3y$$
$$v = A_4 + A_5x + A_6y \qquad (82)$$

These functions satisfy all the requirements for convergence of the solution on reduction of the size of the element, as stated in chapter 3, provided the fourth condition is now taken to refer to a state of constant strain.

The in-plane analysis of a triangular element may be obtained from the bending analysis presented in chapter 3 by suitable interpretation of the basic matrices involved. The notation used will be the same except where stated.

Writing equation (82) in matrix form gives

$$\begin{bmatrix} u \\ v \end{bmatrix} = \begin{bmatrix} 1 & x & y & 0 & 0 & 0 \\ 0 & 0 & 0 & 1 & x & y \end{bmatrix} \begin{bmatrix} A_1 \\ \vdots \\ A_6 \end{bmatrix} \qquad (83)$$

$$= [M]\{A\}$$

Evaluating $[M]$ at each of the nodal points yields the matrix $[C]$ which may be invert d to give

$$[C^{-1}] = \begin{bmatrix} 1 & 0 & 0 & 0 & 0 & 0 \\ -\frac{1}{x_2} & 0 & \frac{1}{x_2} & 0 & 0 & 0 \\ \frac{1}{y_3}\left(\frac{x_3}{x_2} - 1\right) & 0 & \frac{-x_3}{x_2 y_3} & 0 & \frac{1}{y_3} & 0 \\ 0 & 1 & 0 & 0 & 0 & 0 \\ 0 & -\frac{1}{x_2} & 0 & \frac{1}{x_2} & 0 & 0 \\ 0 & \frac{1}{y_3}\left(\frac{x_3}{x_2} - 1\right) & 0 & \frac{-x_3}{x_2 y_2} & 0 & \frac{1}{y_3} \end{bmatrix} \qquad (84)$$

The stress-strain relations for plane stress are

$$\begin{aligned} \sigma_x &= \frac{E}{(1 - \nu^2)} (\varepsilon_x + \nu\varepsilon_y) \\ \sigma_y &= \frac{E}{(1 - \nu^2)} (\nu\varepsilon_x + \varepsilon_y) \qquad (85) \\ \tau_{xy} &= \frac{E}{2(1 + \nu)} \gamma_{xy} \end{aligned}$$

Taking the stress and strain matrices as

$$\{\sigma\} = \{\sigma_x, \sigma_y, \tau_{xy}\} \qquad \{\varepsilon\} = \{\varepsilon_x, \varepsilon_y, \gamma_{xy}\} \tag{86}$$

the matrix of material constants $[D]$ becomes

$$[D] = E' \begin{bmatrix} 1 & \nu & 0 \\ \nu & 1 & 0 \\ 0 & 0 & \xi \end{bmatrix} \tag{87}$$

where $E' = E/(1 - \nu^2)$, and $\xi = (1 - \nu)/2$.

The strain-displacement relations are

$$\{\varepsilon\} = \begin{bmatrix} \frac{\partial}{\partial x} & 0 \\ 0 & \frac{\partial}{\partial y} \\ \frac{\partial}{\partial y} & \frac{\partial}{\partial x} \end{bmatrix} \begin{bmatrix} u \\ v \end{bmatrix} \tag{88}$$

Thus the matrix $[B]$ is defined by

$$[B] = \begin{bmatrix} 0 & 1 & 0 & 0 & 0 & 0 \\ 0 & 0 & 0 & 0 & 0 & 1 \\ 0 & 0 & 1 & 0 & 1 & 0 \end{bmatrix} \tag{89}$$

Calculating the generalised stiffness matrix

$$[\tilde{k}] = t \int_{\Delta} [B]^T [D][B] \, dxdy \tag{90}$$

we obtain

$$[\tilde{k}] = \tfrac{1}{2}x_2y_3tE' \begin{bmatrix} 0 & 0 & 0 & 0 & 0 & 0 \\ 0 & 1 & 0 & 0 & 0 & \nu \\ 0 & 0 & \xi & 0 & \xi & 0 \\ 0 & 0 & 0 & 0 & 0 & 0 \\ 0 & 0 & \xi & 0 & \xi & 0 \\ 0 & \nu & 0 & 0 & 0 & 1 \end{bmatrix} \tag{91}$$

Finally, the element stiffness matrix with respect to local axes is given by

$$[k] = [C^{-1}]^T [\tilde{k}] [C^{-1}] \tag{92}$$

The generalised inertia matrix $[\tilde{m}]$ is defined by

$$[\tilde{m}] = \int_{\Delta} [M]^T [m_p] [M] \, dxdy \tag{93}$$

where $[M]$ is defined by equation (83) and

$$[m_p] = \begin{bmatrix} \rho t & 0 \\ 0 & \rho t \end{bmatrix} \tag{94}$$

which results in

$$[\tilde{m}] = \tfrac{1}{2}x_2y_3t\rho \begin{bmatrix} 1 & & & & & \\ h_x & r_{yy}^2 & & \text{SYMMETRIC} & & \\ h_y & r_{xy}^2 & r_{xx}^2 & & & \\ 0 & 0 & 0 & 1 & & \\ 0 & 0 & 0 & h_x & r_{yy}^2 & \\ 0 & 0 & 0 & h_y & r_{xy}^2 & r_{xx}^2 \end{bmatrix} \tag{95}$$

the notation being the same as in chapter 3. The element inertia matrix referred to local axes is then given by

$$[m] = [C^{-1}]^T [\tilde{m}] [C^{-1}] \tag{96}$$

As shown in chapter 3 the nodal forces and displacements are related by the equation

$$\{s_i\} = [k]\{u_i\} - \Omega^2[m]\{u_i\} \qquad (97)$$

5.3 Analysis of a Shell Element

The stiffness and inertia matrices of a shell element referred to local axes Oxyz (figure 36) are obtained by combining the in-plane matrices given in the previous section, and the plate bending matrices derived in chapter 3.

The in-plane forces at point j are related to the in-plane displacements at point k as follows (see equation (97).

$$\begin{bmatrix} S^x \\ S^y \\ M^z \end{bmatrix}_j = \left[[k_p]_{jk} - \Omega^2[m_p]_{jk} \right] \begin{bmatrix} u \\ v \\ \theta_z \end{bmatrix}_k \qquad (98)$$

where

$$[k_p]_{jk} = \begin{bmatrix} k_p^{xx} & k_p^{xy} & 0 \\ k_p^{yx} & k_p^{yy} & 0 \\ 0 & 0 & 0 \end{bmatrix}_{jk}$$

and

$$[m_p]_{jk} = \begin{bmatrix} m_p^{xx} & m_p^{xy} & 0 \\ m_p^{yx} & m_p^{yy} & 0 \\ 0 & 0 & 0 \end{bmatrix}_{jk}$$

subscript p denoting in-plane effects. The rotation θ_z and the associated moment M^z have been introduced for convenience. The stiffness and inertia elements associated with θ_z have been neglected. In reference[13]it is

suggested that this is justifiable when considering smoothly curving shell surfaces, since these terms will then have little influence on the bending forces in neighbouring elements.

The bending equation (chapter 3, equation (34)) may be rewritten in a similar form, namely

$$\begin{bmatrix} S^z \\ M^x \\ M^y \end{bmatrix}_j = \left[[k_b]_{jk} - \Omega^2 [m_b]_{jk} \right] \begin{bmatrix} w \\ \theta_x \\ \theta_y \end{bmatrix}_k \qquad (99)$$

where $$[k_b]_{jk} = \begin{bmatrix} k_b^{zz} & k_b^{zx} & k_b^{zy} \\ k_b^{xz} & k_b^{xx} & k_b^{xy} \\ k_b^{yz} & k_b^{yx} & k_b^{yy} \end{bmatrix}_{jk}$$

the subscript b denoting bending effects. The submatrix $[m_b]_{jk}$ is defined in a similar manner.

Combining equations (98), (99) yields the following relationship between all the forces at point j and all the displacements at point k.

$$\{s_j\} = \left[[k_S]_{jk} - \Omega^2 [m_S]_{jk} \right] \{u_k\} \qquad (100)$$

where

$$\{s_j\} = \{S^x, S^y, S^z, M^x, M^y, M^z\}_j$$

$$\{u_k\} = \{u, v, w, \theta_x, \theta_y, \theta_z\}_k \qquad (101)$$

and $[k_S]_{jk} =$

$$\begin{bmatrix} k_p^{xx} & k_p^{xy} & 0 & 0 & 0 & 0 \\ k_p^{yx} & k_p^{yy} & 0 & 0 & 0 & 0 \\ 0 & 0 & k_b^{zz} & k_b^{zx} & k_b^{zy} & 0 \\ 0 & 0 & k_b^{xz} & k_b^{xx} & k_b^{xy} & 0 \\ 0 & 0 & k_b^{yz} & k_b^{yx} & k_b^{yy} & 0 \\ 0 & 0 & 0 & 0 & 0 & 0 \end{bmatrix}_{jk} \qquad (102)$$

The submatrix $[m_S]_{jk}$ is similarly defined. Thus for a shell element the complete relationship is

$$\{s_i\} = [k_S]\{u_i\} - \Omega^2[m_S]\{u_i\} \qquad (103)$$

The matrices $[k_S]$, $[m_S]$ are of the order (18 x 18), each (6 x 6) submatrix being of the form illustrated in equation (102).

In order to transform this equation to the global system of coordinates, we first note that the displacements in the two systems are related by the equation

$$\{u_i\} = [\Xi]\{u_i^o\} \qquad (104)$$

where

$$[\Xi] = \begin{bmatrix} \zeta & & & & & \\ & \zeta & & & & \\ & & \zeta & & & \\ & & & \zeta & & \\ & & & & \zeta & \\ & & & & & \zeta \end{bmatrix} \qquad (105)$$

and $[\zeta]$ is a matrix of direction cosines, namely

$$[\zeta] = \begin{bmatrix} \cos(x,x^o) & \cos(x,y^o) & \cos(x,z^o) \\ \cos(y,x^o) & \cos(y,y^o) & \cos(y,z^o) \\ \cos(z,x^o) & \cos(z,y^o) & \cos(z,z^o) \end{bmatrix} \tag{106}$$

Similarly the corresponding nodal forces in the two systems are related by

$$\{s_i^o\} = [\Xi]^T \{s_i\} \tag{107}$$

Introducing equations (104) , (107) into (103) yields the following equation referred to global axes

$$\{s_i^o\} = [k_s^o]\{u_i^o\} - \Omega^2[m_s^o]\{u_i^o\} \tag{108}$$

where $$[k_s^o] = [\Xi]^T \ [k_s][\Xi] \tag{109}$$

and $$[m_s^o] = [\Xi]^T \ [m_s][\Xi] \tag{110}$$

These are the stiffness and inertia matrices respectvely of a shell element referred to global axes. The problem of determining the matrix of direction cosines $[\zeta]$ will now be considered.

5.4 Rotation of Axes

From a computational viewpoint, the most convenient method of calculating the matrix of direction cosines $[\zeta]$ is the one suggested by Argyris [8].

Define $$\psi_i^o = \{x_i^o, y_i^o, z_i^o\} \tag{111}$$

and

$$\psi_{ij}^o = \psi_i^o - \psi_j^o$$

$$= \{(x_i^o - x_j^o), (y_i^o - y_j^o), (z_i^o - z_j^o)\} \tag{112}$$

where (x_i^o, y_i^o, z_i^o) defines the coordinates of the point i in the global system.

If we denote the rows of $[\zeta]$ by $|\zeta_1|$, $|\zeta_2|$ and $|\zeta_3|$ then we can

determine $\lfloor \zeta_1 \rfloor$, the direction cosines of Ox (see fig. 36), immediately from

$$\lfloor \zeta_1 \rfloor = \frac{1}{\ell^o_{21}} \{\psi^o_{21}\}^T = \frac{1}{\ell^o_{21}} \lfloor (x^o_2 - x^o_1), (y^o_2 - y^o_1), (z^o_2 - z^o_1) \rfloor \qquad (113)$$

where $(\ell^o_{21})^2 = \{\psi^o_{21}\}^T \{\psi^o_{21}\}$

$$= (x^o_2 - x^o_1)^2 + (y^o_2 - y^o_1)^2 + (y^o_3 - y^o_1)^2 \qquad (114)$$

Hence $\lfloor \zeta_1 \rfloor$ is merely a (mathematical) normalisation of the row matrix $\{\psi^o_{21}\}^T$.

$\lfloor \zeta_2 \rfloor$ represents the direction cosines of Oy. If we draw the line 34 perpendicular to 12, and meeting 12 at the point 4, then $\lfloor \zeta_2 \rfloor$ also represents the direction cosines of the line 34.

Defining $\psi_i = \{x_i, y_i, z_i\}$ (115)

where (x_i, y_i, z_i) are the coordinates of the point i referred to local axes, then

$$\psi_3 = \{x_3, y_3, 0\} \quad \text{and} \quad \psi_4 = \{x_3, 0, 0\} \qquad (116)$$

The two coordinate systems are related by

$$\psi = [\zeta]\{\psi^o - \psi^o_1\} \qquad (117)$$

Hence $$\psi_3 = [\zeta]\{\psi^o_{31}\} \qquad (118)$$

Comparing (116), (118) we see that

$$x_3 = \lfloor \zeta_1 \rfloor \{\psi^o_{31}\} \qquad (119)$$

Now $$\{\psi^o_{34}\} = \{\psi^o_3\} - \{\psi^o_4\}$$

$$= [\zeta]^T \{\psi_3 - \psi_4\}$$

$$= \{\psi^o_{31}\} - \lfloor \zeta_1 \rfloor^T x_3$$

$$= \{\psi^o_{31}\} - \lfloor \zeta_1 \rfloor^T \lfloor \zeta_1 \rfloor \{\psi^o_{31}\}$$

That is $\{\psi^o_{34}\} = [I - [\zeta_1]^T[\zeta_1]]\{\psi^o_{31}\}$ (120)

where $[I]$ denotes the unit matrix. $[\zeta_2]$ may now be obtained by normalising the row matrix $\{\psi^o_{34}\}^T$.

In order to determine $[\zeta_3]$ we depart from Argyris' analysis. Denoting unit vectors in the directions of the axes x, y and z by $\hat{x}$, $\hat{y}$ and $\hat{z}$, then $\hat{z}$ is equal to the vector product of $\hat{x}$ and $\hat{y}$; that is

$$\hat{z} = \hat{x} \wedge \hat{y} \tag{121}$$

Since $[\zeta_1]$, $[\zeta_2]$ and $[\zeta_3]$ represent the components of $\hat{x}$, $\hat{y}$ and $\hat{z}$ referred to axes $O^o x^o y^o z^o$, then $[\zeta_3]$ will be given by the components of $\hat{x} \wedge \hat{y}$, namely

$$\begin{aligned} \zeta_{31} &= \zeta_{12}\zeta_{23} - \zeta_{22}\zeta_{13} \\ \zeta_{32} &= \zeta_{13}\zeta_{21} - \zeta_{23}\zeta_{11} \\ \zeta_{33} &= \zeta_{11}\zeta_{22} - \zeta_{21}\zeta_{12} \end{aligned} \tag{122}$$

5.5 The Complete Shell

By considering the equilibrium of each nodal point, as in chapter 3, we obtain the equilibrium relationship for the complete shell, namely

$$\{S^o\} = [\,[K^o_S] - \Omega^2[M^o_S]\,]\,\{U^o\} \tag{123}$$

where $\{S^o\}$ are the external forces applied to the shell and $\{U^o\}$ are the global displacements. The assembled stiffness and inertia matrices $[K^o_S]$ and $[M^o_S]$ are defined by

$$[K^o_S] = \sum_g [a_g]^T [k^o_{Sg}] [a_g] \tag{124}$$

$$[M^o_S] = \sum_g [a_g]^T [M^o_{Sg}] [a_g] \tag{125}$$

where the matrix $[a_g]$ is a matrix of ones and zeros as defined in chapter 3. The operation defined by equation (124) is equivalent to adding the stiffnesses of the elements adjacent to a given nodal point. In practice, if the nodal points of an element are numbered n_1, n_2, n_3 and

determine $[\zeta_1]$, the direction cosines of Ox (see fig. 36), immediately from

$$[\zeta_1] = \frac{1}{\ell^o_{21}} \{\psi^o_{21}\}^T = \frac{1}{\ell^o_{21}} [(x^o_2 - x^o_1), (y^o_2 - y^o_1), (z^o_2 - z^o_1)] \qquad (113)$$

where $(\ell^o_{21})^2 = \{\psi^o_{21}\}^T \{\psi^o_{21}\}$

$$= (x^o_2 - x^o_1)^2 + (y^o_2 - y^o_1)^2 + (y^o_3 - y^o_1)^2 \qquad (114)$$

Hence $[\zeta_1]$ is merely a (mathematical) normalisation of the row matrix $\{\psi^o_{21}\}^T$.

$[\zeta_2]$ represents the direction cosines of Oy. If we draw the line 34 perpendicular to 12, and meeting 12 at the point 4, then $[\zeta_2]$ also represents the direction cosines of the line 34.

Defining $\psi_i = \{x_i, y_i, z_i\}$ (115)

where (x_i, y_i, z_i) are the coordinates of the point i referred to local axes, then

$$\psi_3 = \{x_3, y_3, 0\} \quad \text{and} \quad \psi_4 = \{x_3, 0, 0\} \qquad (116)$$

The two coordinate systems are related by

$$\psi = [\zeta]\{\psi^o - \psi^o_1\} \qquad (117)$$

Hence $$\psi_3 = [\zeta]\{\psi^o_{31}\} \qquad (118)$$

Comparing (116), (118) we see that

$$x_3 = [\zeta_1]\{\psi^o_{31}\} \qquad (119)$$

Now $$\{\psi^o_{34}\} = \{\psi^o_3\} - \{\psi^o_4\}$$

$$= [\zeta]^T \{\psi_3 - \psi_4\}$$

$$= \{\psi^o_{31}\} - [\zeta_1]^T x_3$$

$$= \{\psi^o_{31}\} - [\zeta_1]^T [\zeta_1]\{\psi^o_{31}\}$$

That is $\{\psi^o_{34}\} = [I - [\zeta_1]^T[\zeta_1]]\{\psi^o_{31}\}$ (120)

where $[I]$ denotes the unit matrix. $[\zeta_2]$ may now be obtained by normalising the row matrix $\{\psi^o_{34}\}^T$.

In order to determine $[\zeta_3]$ we depart from Argyris' analysis. Denoting unit vectors in the directions of the axes x, y and z by $\hat{\underline{x}}$, $\hat{\underline{y}}$ and $\hat{\underline{z}}$, then $\hat{\underline{z}}$ is equal to the vector product of $\hat{\underline{x}}$ and $\hat{\underline{y}}$; that is

$$\hat{\underline{z}} = \hat{\underline{x}} \wedge \hat{\underline{y}} \tag{121}$$

Since $[\zeta_1]$, $[\zeta_2]$ and $[\zeta_3]$ represent the components of $\hat{\underline{x}}$, $\hat{\underline{y}}$ and $\hat{\underline{z}}$ referred to axes $O^o x^o y^o z^o$, then $[\zeta_3]$ will be given by the components of $\hat{\underline{x}} \wedge \hat{\underline{y}}$, namely

$$\begin{aligned} \zeta_{31} &= \zeta_{12}\zeta_{23} - \zeta_{22}\zeta_{13} \\ \zeta_{32} &= \zeta_{13}\zeta_{21} - \zeta_{23}\zeta_{11} \\ \zeta_{33} &= \zeta_{11}\zeta_{22} - \zeta_{21}\zeta_{12} \end{aligned} \tag{122}$$

5.5 The Complete Shell

By considering the equilibrium of each nodal point, as in chapter 3, we obtain the equilibrium relationship for the complete shell, namely

$$\{S^o\} = [\,[K^o_S] - \Omega^2[M^o_S]\,]\,\{U^o\} \tag{123}$$

where $\{S^o\}$ are the external forces applied to the shell and $\{U^o\}$ are the global displacements. The assembled stiffness and inertia matrices $[K^o_S]$ and $[M^o_S]$ are defined by

$$[K^o_S] = \sum_g [a_g]^T [k^o_{Sg}] [a_g] \tag{124}$$

$$[M^o_S] = \sum_g [a_g]^T [M^o_{Sg}] [a_g] \tag{125}$$

where the matrix $[a_g]$ is a matrix of ones and zeros as defined in chapter 3. The operation defined by equation (124) is equivalent to adding the stiffnesses of the elements adjacent to a given nodal point. In practice, if the nodal points of an element are numbered n_1, n_2, n_3 and

$[k_s^o]$ is partitioned into nine submatrices $[k_{sa}^o]_{ij}$ of order (6,6) then the submatrix $|k_{sa}^o|_{ij}$ is added to the (6,6) submatrix of $|K_S^o|$ whose leading element occupies the position $(6n_i - 5, 6n_j - 5)$, for i, j = 1, 2, 3. The inertia matrix is assembled in a similar manner.

As in the case of a flat plate the next step in the analysis is to apply the boundary conditions. Again this is achieved by deleting the rows and columns of $[K_S^o]$ and $[M_S^o]$ which correspond to zero displacements and prescribing zero external forces elsewhere. This results in the following eigenvalue problem

$$\left[[K_{S11}^o] - \Omega^2 [M_{S11}^o] \right] \{U_1^o\} = 0 \qquad (126)$$

In the applications described in the next section the eigenvalues of equation (126) were obtained by the method of determinant evaluation as described in chapter 4.

The computer programme used for solving shell problems follows a similar pattern to the one described for flat plates in chapter 4.

5.6 Vibration of a Cylindrical Shell

The analysis described in the previous sections has been used to determine the vibration characteristics of a cylindrical shell of length 7·7 ins., mean radius 1·925 ins. and thickness 0·101 ins. The ends of the cylinder were taken to be freely supported. One quarter of the shell was represented by 72 elements as shown in figure 37. The frequencies obtained have been compared with the experimental results of Arnold and Warburton [27].

The modes of vibration considered were those which gave the four lowest natural frequencies. The waveforms of these modes are illustrated in figure 38. When there is an even number of circumferential waves n, then the waveform is antisymmetric with respect to both the axes Ox and Oz. An odd number of waves produces a pattern which is antisymmetric with respect to Ox and symmetric with respect to Oz. Thus in both cases AB may be considered to be freely supported. When n is even CD is freely supported and when n is odd it is assumed to be a sliding support.

Along a freely supported boundary the transverse and tangential displacements are zero, whilst along a sliding support the normal slope is zero. Thus in all the cases considered we have the following boundary conditions.

(i) along DA u^o, w^o, θ_y^o are zero

(ii) along AB u^o, v^o, θ_z^o are zero

(iii) along BC u^o, w^o, θ_y^o are zero

(iv) along CD

either v^o, w^o, θ_x^o are zero when n is even

or θ_y^o is zero when n is odd.

In addition we have assumed the in-plane rotations to be negligible, and so we must specify these to be zero along the boundary giving

(v) along AB θ_x^o is zero

and along CD θ_z^o is zero.

The results obtained are compared with the experimental results of reference [27] in table 6, where m denotes the number of axial half waves and n the number of circumferential waves. Considering the modes with only one axial half wave, that is 1, 2 and 4, then it may be seen that the first frequency has been overestimated. As the number of circumferential waves increase the error reduces. Figure 6 of reference [27] shows that the strain energy in mode one is predominately due to stretching, whilst in mode four it is entirely due to bending. The in-plane displacement functions used in the analysis assume a linear variation of displacement. This produces an excessive stiffness when stretching of the middle plane takes place, thus accounting for the overestimate in frequency for mode one. On the other hand, the in-plane and bending displacements together do not give continuity between elements. This has the effect of producing excessive flexibility at the joins, and so has more effect when the bending energy predominates. In the case considered here the excessive stiffness of the individual elements and the excessive flexibility of the joins between the elements, has had approximately equal effect producing good results for

modes two and four. Mode three has two axial half waves which produces an increase in the bending energy. Thus the excessive flexibility of the joins predominates more producing an underestimate in frequency as shown.

5.7 Discussion

A method has been given whereby shell vibration problems may be analysed using finite element techniques. Application of the method to a freely supported cylindrical shell has shown that fairly accurate results may be obtained for the lower frequency modes when a balance between the overstiffness of elements and overflexibility of joins exists. This balance does not exist for higher frequency modes, and so good estimates of frequency cannot be obtained. The overflexibility of the joins predominate, and so the accuracy of the method may be improved by using in-plane and bending displacements functions which together ensure continuity of displacement between elements.

6. LARGE DEFLECTION ANALYSIS

6.1 Introduction

If a plate is loaded in such a manner that the lateral deflections are large in comparison with the thickness of the plate, but small when compared with the other dimensions, then the problem is geometrically non linear, as defined by Novozhilov [28] . In this type of problem the strains are small compared with unity, but the rotations may be large in comparison to the strain.

Problems involving geometrical non linearities may be analysed by finite element techniques using a step-by-step procedure. It is assumed that the loading process is divided into a series of small steps, each incremental load being small enough to permit linearization. After the application of 'n' incremental loads a typical structural element will be in a state of stress. If a further incremental load is applied the element will deform, and so there will be a change in the nodal forces with respect to fixed axes. It will be shown that the stiffness matrix $[k_c]$ for an element in an initial state of stress takes the form

$$[k_c] = [k] + [k_1] \qquad (127)$$

This corresponds to the segregation of nodal force increments, resulting from nodal displacements $\{\delta u\}$, into a set $[k]\{\delta u\}$, which are generated by incremental strains, and the remainder $[k_1]\{\delta u\}$, which are of geometric origin, resulting from angular displacement of the initial nodal forces.

6.2 Determination of the Stiffness Matrix of an Element in an Initial State of Stress

In developing the stiffness matrix of an element in an initial state of stress we shall consider a triangular element subjected to both bending and in-plane forces. The analysis will be based upon that given by

Turner, Martin and Weikel [29] for a triangular element subjected to in-plane forces only.

It is convenient to consider axes $\bar{o}\ \bar{x}\ \bar{y}\ \bar{z}$ which move with the element and local fixed axes $o\ x\ y\ z$ which coincide with the moving axes in their initial position, as shown in figure 39. The plane $\bar{o}\ \bar{x}\ \bar{y}$ is defined by the plane of the element.

Defining $\{\delta\bar{u}\}$ and $\{\delta u\}$ as incremental displacements with respect to moving and fixed axes respectively, we have

$$\{\delta\bar{u}\} = \{\delta\bar{\theta}_{x1}, \delta\bar{\theta}_{y1}, \delta\bar{u}_2, \delta\bar{\theta}_{x2}, \delta\bar{\theta}_{y2}, \delta\bar{u}_3, \delta\bar{v}_3, \delta\bar{\theta}_{x3}, \delta\bar{\theta}_{y3}\}$$

$$\{\delta u\} = \{\delta u_1, \delta v_1, \delta w_1, \delta\theta x_1, \delta\theta y_1, \delta u_2, \delta v_2, \delta w_2, \delta\theta_{x2}, \delta\theta_{y2}, \delta u_3, \delta v_3, \delta w_3, \delta\theta_{x3}\ \delta\theta_{y3}\} \tag{128}$$

Assuming the rotation of axes to be small, we may write the transformation

$$\{\delta\bar{u}\} = [G]\{\delta u\} \tag{129}$$

where the matrix $[G]$ is a function of the element geometry. Considering equilibrium in the initial position we have

$$\{s\} = [G]^T \{\bar{s}\} \tag{130}$$

where

$$\{\bar{s}\} = \{M^{\bar{x}1}, M^{\bar{y}1}, S^{\bar{x}2}, M^{\bar{x}2}, M^{\bar{y}2}, S^{\bar{x}3}, S^{\bar{y}3}, M^{\bar{x}3}, M^{\bar{y}3}\}$$

$$\{s\} = \{S^{x1}, S^{y1}, S^{z1}, M^{x1}, M^{y1}, S^{x2}, S^{y2}, S^{z2},$$
$$M^{x2}, M^{y2}, S^{x3}, S^{y3}, S^{z3}, M^{x3}, M^{y3}\} \tag{131}$$

Thus, in the displaced position, the equilibrium conditions referred to fixed axes are

$$\{s\} + \{\delta s\} = [F][G + \delta G]^T \{\bar{s} + \delta\bar{s}\} \tag{132}$$

The increment $[\delta G]$ to the matrix $[G]$ is due to the deformation of the element introduced by the incremental load $\{\delta\bar{s}\}$. The matrix $[F]$ is introduced to account for the rotation of the axes $\bar{O}\ \bar{x}\ \bar{y}\ \bar{z}$. It is shown in the next section that $[F]$, which is a function of the displacements in the unbarred system, may be written in the form

$$[F] = [I] + [\delta F] \tag{133}$$

where $[I]$ denotes the unit matrix.

Expanding (132), introducing (130) and (133) and neglecting second order terms gives the following equation

$$\{\delta s\} = [\,[\delta F][G]^T + [\delta G]^T]\{\bar{s}\} + [G]^T\{\delta\bar{s}\} \tag{134}$$

Now, if we assume that the strains and fibre rotations with respect to the moving axes are small, then we may write

$$\{\delta\bar{s}\} = [\bar{k}]\{\delta\bar{u}\} = [\bar{k}][G]\{\delta u\} \tag{135}$$

Thus we have

$$[G]^T\{\delta\bar{s}\} = [G]^T[\bar{k}][G]\{\delta u\} = [k]\{\delta u\} \tag{136}$$

where $[\bar{k}]$ and $[k]$ are the element stiffness matrices referred to moving and fixed axes respectively.

It is shown in the next section that we may write

$$[\,[\delta F][G]^T + [\delta G]^T]\{\bar{s}\} = [k_1]\{\delta u\} \tag{137}$$

where

$$[k_1] = \sum_i [k_{1i}]\bar{s}_i \tag{138}$$

$\bar{s}_i$ are the elements of $\{\bar{s}\}$ and $[k_{1i}]$ are matrices which are functions of element geometry only.

Introducing (136) and (137) into (134) gives

$$\{\delta s\} = [k]\{\delta u\} + [k_1]\{\delta u\} \tag{139}$$

The matrix $[k_1]$ is referred to as the geometrical stiffness matrix of the

element.

6.3 The geometrical stiffness matrix

In order to obtain the geometrical stiffness matrix of a triangular element, it is essential that we first of all determine the orientation of the axes $\bar{O}\ \bar{x}\ \bar{y}\ \bar{z}$ with respect to the axes O x y z and hence the matrix [G]. By restricting displacement components to sufficiently small values, the orientation of the displaced axes may be attained by a sequence of three small rotations $\delta\omega_x$, $\delta\omega_y$, $\delta\omega_z$ about Ox, Oy, Oz respectively, the order in which they occur being immaterial.

The displacement of an element consists of an elastic strain, a rigid body rotation and a rigid body translation. Thus, if we consider the point 2 (fig. 39), we have in the notation of vector analysis

$$\begin{aligned}(\bar{x}_2 + \delta u_2,\ \delta v_2,\ \delta w_2) &= (\bar{x}_2 + \delta\bar{u}_2,\ 0,\ 0) \\ &\quad + (\delta\omega_x,\ \delta\omega_y,\ \delta\omega_z) \wedge (\bar{x}_2 + \delta\bar{u}_2,\ 0,\ 0) \\ &\quad + (\delta u_1,\ \delta v_1,\ \delta w_1) \qquad (140)\end{aligned}$$

Equating components and neglecting second order terms yields

$$\begin{aligned}\delta\bar{u}_2 &= \delta u_2 - \delta u_1 \\ \delta\omega_z &= \frac{\delta v_2 - \delta v_1}{\bar{x}_2} \qquad (141) \\ \delta\omega_y &= \frac{-(\delta w_2 - \delta w_1)}{\bar{x}_2}\end{aligned}$$

Considering point 3 in a similar manner we have

$$(\bar{x}_3 + \delta u_3, \bar{y}_3 + \delta v_3, \delta w_3) = (\bar{x}_3 + \delta\bar{u}_3, \bar{y}_3 + \delta\bar{v}_3, 0)$$

$$+ (\delta\omega_x, \delta\omega_y, \delta\omega_z) \wedge (\bar{x}_3 + \delta\bar{u}_3, \bar{y}_3 + \delta\bar{v}_3, 0)$$

$$+ (\delta u_1, \delta v_1, \delta w_1) \qquad (142)$$

Introducing (141) into this equation we obtain

$$\delta\bar{u}_3 = \delta u_3 - \delta u_1 + \frac{\bar{y}_3}{\bar{x}_2}(\delta v_2 - \delta v_1)$$

$$\delta\bar{v}_3 = \frac{-\bar{x}_{23}}{\bar{x}_2}\delta v_1 - \frac{\bar{x}_3}{x_2}\delta v_2 + \delta v_3 \qquad (143)$$

$$\delta\omega_x = \frac{-\bar{x}_{23}}{\bar{x}_2\bar{y}_3}\delta w_1 - \frac{\bar{x}_3}{\bar{x}_2\bar{y}_3}\delta w_2 + \frac{1}{\bar{y}_3}\delta w_3$$

where $\bar{x}_{23} = \bar{x}_2 - \bar{x}_3$.

Considering the rotations at any one of the vertices of the triangle we have

$$(\delta\theta_x, \delta\theta_y, \delta\theta_z) = (\delta\bar{\theta}_x, \delta\bar{\theta}_y, 0) + (\delta\omega_x, \delta\omega_y, \delta\omega_z) \qquad (144)$$

That is

$$\delta\bar{\theta}_x = \delta\theta_x - \delta\omega_x$$

$$\delta\bar{\theta}_y = \delta\theta_y - \delta\omega_y \qquad (145)$$

From equations (141), (143) and (145) we can determine the matrix [G] giving

$$[G] = \begin{bmatrix}
0 & 0 & \frac{\bar{x}_{23}}{\bar{x}_2\bar{y}_3} & 1 & 0 & 0 & 0 & \frac{\bar{x}_3}{\bar{x}_2\bar{y}_3} & 0 & 0 & 0 & 0 & -\frac{1}{\bar{y}_3} & 0 & 0 \\
0 & 0 & -\frac{1}{\bar{x}_2} & 0 & 1 & 0 & 0 & \frac{1}{\bar{x}_2} & 0 & 0 & 0 & 0 & 0 & 0 & 0 \\
-1 & 0 & 0 & 0 & 0 & 1 & 0 & 0 & 0 & 0 & 0 & 0 & 0 & 0 & 0 \\
0 & 0 & \frac{\bar{x}_{23}}{\bar{x}_2\bar{y}_3} & 0 & 0 & 0 & 0 & \frac{\bar{x}_3}{\bar{x}_2\bar{y}_3} & 1 & 0 & 0 & 0 & -\frac{1}{\bar{y}_3} & 0 & 0 \\
0 & 0 & -\frac{1}{\bar{x}_2} & 0 & 0 & 0 & 0 & \frac{1}{\bar{x}_2} & 0 & 1 & 0 & 0 & 0 & 0 & 0 \\
-1 & -\frac{\bar{y}_3}{\bar{x}_2} & 0 & 0 & 0 & 0 & \frac{\bar{y}_3}{\bar{x}_2} & 0 & 0 & 0 & 1 & 0 & 0 & 0 & 0 \\
0 & -\frac{\bar{x}_{23}}{\bar{x}_2} & 0 & 0 & 0 & 0 & -\frac{\bar{x}_3}{\bar{x}_2} & 0 & 0 & 0 & 0 & 1 & 0 & 0 & 0 \\
0 & 0 & \frac{\bar{x}_{23}}{\bar{x}_2\bar{y}_3} & 0 & 0 & 0 & 0 & \frac{\bar{x}_3}{\bar{x}_2\bar{y}_3} & 0 & 0 & 0 & 0 & -\frac{1}{\bar{y}_3} & 1 & 0 \\
0 & 0 & -\frac{1}{\bar{x}_2} & 0 & 0 & 0 & 0 & \frac{1}{\bar{x}_2} & 0 & 0 & 0 & 0 & 0 & 0 & 1
\end{bmatrix} \qquad (146)$$

As a result of elastic strain $\bar{x}_2$, $\bar{x}_3$, $\bar{y}_3$ become $(\bar{x}_2 + \delta\bar{u}_2)$, $(\bar{x}_3 + \delta\bar{u}_3)$ and $(\bar{y}_3 + \delta\bar{v}_3)$ respectively. We can thus calculate the matrix $[G + \delta G]$. Neglecting second order terms we obtain

$$[\delta G] = \begin{bmatrix}
0 & 0 & \varepsilon_6 & 0 & 0 & 0 & 0 & \varepsilon_4 & 0 & 0 & 0 & 0 & -\varepsilon_2 & 0 & 0 \\
0 & 0 & -\varepsilon_1 & 0 & 0 & 0 & 0 & \varepsilon_1 & 0 & 0 & 0 & 0 & 0 & 0 & 0 \\
0 & 0 & 0 & 0 & 0 & 0 & 0 & 0 & 0 & 0 & 0 & 0 & 0 & 0 & 0 \\
0 & 0 & \varepsilon_6 & 0 & 0 & 0 & 0 & \varepsilon_4 & 0 & 0 & 0 & 0 & -\varepsilon_2 & 0 & 0 \\
0 & 0 & -\varepsilon_1 & 0 & 0 & 0 & 0 & \varepsilon_1 & 0 & 0 & 0 & 0 & 0 & 0 & 0 \\
0 & -\varepsilon_3 & 0 & 0 & 0 & 0 & \varepsilon_3 & 0 & 0 & 0 & 0 & 0 & 0 & 0 & 0 \\
0 & -\varepsilon_5 & 0 & 0 & 0 & 0 & \varepsilon_5 & 0 & 0 & 0 & 0 & 0 & 0 & 0 & 0 \\
0 & 0 & \varepsilon_6 & 0 & 0 & 0 & 0 & \varepsilon_4 & 0 & 0 & 0 & 0 & -\varepsilon_2 & 0 & 0 \\
0 & 0 & -\varepsilon_1 & 0 & 0 & 0 & 0 & \varepsilon_1 & 0 & 0 & 0 & 0 & 0 & 0 & 0
\end{bmatrix} \qquad (147)$$

where

$$g_1 = -\frac{\delta\bar{u}_2}{\bar{x}_2^2}$$

$$g_2 = -\frac{\delta\bar{v}_3}{\bar{y}_3^2}$$

$$g_3 = -\frac{\bar{y}_3}{\bar{x}_2}\left(\frac{\delta\bar{u}_2}{\bar{x}_2} - \frac{\delta\bar{v}_3}{\bar{y}_3}\right) \tag{148}$$

$$g_4 = -\frac{\bar{x}_3}{\bar{x}_2\bar{y}_3}\left(\frac{\delta\bar{u}_2}{\bar{x}_2} - \frac{\delta\bar{u}_3}{\bar{x}_3} + \frac{\delta\bar{v}_3}{\bar{y}_3}\right)$$

$$g_5 = +\frac{\bar{x}_3}{\bar{x}_2}\left(\frac{\delta\bar{u}_2}{\bar{x}_2} - \frac{\delta\bar{u}_3}{\bar{x}_3}\right)$$

$$g_6 = +\frac{\bar{x}_3}{\bar{x}_2\bar{y}_3}\left(\frac{\delta\bar{u}_2}{\bar{x}_2} - \frac{\delta\bar{u}_3}{\bar{x}_3}\right) - \frac{\bar{x}_{23}\,\delta\bar{v}_3}{\bar{x}_2\bar{y}_3^2}$$

Now the transformation between coordinates in the two systems can be written as

$$\begin{bmatrix} x \\ y \\ z \end{bmatrix} = \begin{bmatrix} \delta u_1 \\ \delta v_1 \\ \delta w_1 \end{bmatrix} + \begin{bmatrix} 1 & -\delta\omega_z & \delta\omega_y \\ \delta\omega_z & 1 & -\delta\omega_x \\ -\delta\omega_y & \delta\omega_x & 1 \end{bmatrix} \begin{bmatrix} \bar{x} \\ \bar{y} \\ \bar{z} \end{bmatrix} \tag{149}$$

and so defining

$$[\Omega_1] = \begin{bmatrix} 0 & -\delta\omega_z & \delta\omega_y \\ \delta\omega_z & 0 & -\delta\omega_x \\ -\delta\omega_y & \delta\omega_x & 0 \end{bmatrix} \tag{150}$$

and

$$[\Omega_2] = \begin{bmatrix} 0 & -\delta\omega_z \\ \delta\omega_z & 0 \end{bmatrix} \tag{151}$$

we can write $[\delta F]$ in the form

$$[\delta F] = \begin{bmatrix} \Omega_1 & & & & \\ & \Omega_2 & & 0 & \\ & & \Omega_1 & & \\ & 0 & & \Omega_2 & \\ & & & & \Omega_1 \\ & & & & & \Omega_2 \end{bmatrix} \tag{152}$$

Using equations (146) to (152) inclusive, we find that

$$[\,[\delta F][G]^T + [\delta G]^T\,] =$$

$$\begin{bmatrix}
\frac{\bar{x}_{23}\delta\omega_y}{\bar{x}_2\bar{y}_3} & -\frac{\delta\omega_y}{\bar{x}_2} & 0 & \frac{\bar{x}_{23}\delta\omega_y}{\bar{x}_2\bar{y}_3} & -\frac{\delta\omega_y}{\bar{x}_2} & \frac{\bar{y}_3\delta\omega_z}{\bar{x}_2} & \frac{\bar{x}_{23}\delta\omega_z}{\bar{x}_2} & \frac{\bar{x}_{23}\delta\omega_y}{\bar{x}_2\bar{y}_3} & -\frac{\delta\omega_y}{\bar{x}_2} \\
\frac{\bar{x}_{23}\delta\omega_x}{\bar{x}_2\bar{y}_3} & \frac{\delta\omega_x}{\bar{x}_2} & -\delta\omega_z & -\frac{\bar{x}_{23}\delta\omega_x}{\bar{x}_2\bar{y}_3} & \frac{\delta\omega_x}{\bar{x}_2} & -(\delta\omega_z + g_3) & -g_5 & -\frac{\bar{x}_{23}\delta\omega_x}{\bar{x}_2\bar{y}_3} & \frac{\delta\omega_x}{\bar{x}_2} \\
g_6 & -g_1 & \delta\omega_y & g_6 & -g_1 & (\delta\omega_y - \frac{\bar{y}_3\delta\omega_x}{\bar{x}_2}) & \frac{-\bar{x}_{23}\delta\omega_x}{\bar{x}_2} & g_6 & -g_1 \\
0 & -\delta\omega_z & 0 & 0 & 0 & 0 & 0 & 0 & 0 \\
\delta\omega_z & 0 & 0 & 0 & 0 & 0 & 0 & 0 & 0 \\
\frac{\bar{x}_3\delta\omega_y}{\bar{x}_2\bar{y}_3} & \frac{\delta\omega_y}{\bar{x}_2} & 0 & \frac{\bar{x}_3\delta\omega_y}{\bar{x}_2\bar{y}_3} & \frac{\delta\omega_y}{\bar{x}_2} & \frac{-\bar{y}_3\delta\omega_z}{\bar{x}_2} & \frac{\bar{x}_3\delta\omega_y}{\bar{x}_2} & \frac{\bar{x}_3\delta\omega_y}{\bar{x}_2\bar{y}_3} & \frac{\delta\omega_y}{\bar{x}_2} \\
\frac{\bar{x}_3\delta\omega_x}{\bar{x}_2\bar{y}_3} & \frac{\delta\omega_x}{\bar{x}_2} & \delta\omega_z & \frac{-\bar{x}_3\delta\omega_x}{\bar{x}_2\bar{y}_3} & \frac{-\delta\omega_x}{\bar{x}_2} & g_3 & g_5 & \frac{-\bar{x}_3\delta\omega_x}{\bar{x}_2\bar{y}_3} & \frac{-\delta\omega_x}{\bar{x}_2} \\
g_4 & g_1 & -\delta\omega_y & g_4 & g_1 & \frac{\bar{y}_3\delta\omega_x}{\bar{x}_2} & \frac{-\bar{x}_3\delta\omega_x}{\bar{x}_2} & g_4 & g_1 \\
0 & 0 & 0 & 0 & -\delta\omega_z & 0 & 0 & 0 & 0 \\
0 & 0 & 0 & \delta\omega_z & 0 & 0 & 0 & 0 & 0 \\
\frac{-\delta\omega_y}{\bar{y}_3} & 0 & 0 & \frac{-\delta\omega_y}{\bar{y}_3} & 0 & 0 & -\delta\omega_z & \frac{-\delta\omega_y}{\bar{y}_3} & 0 \\
\frac{\delta\omega_x}{\bar{y}_3} & 0 & 0 & \frac{\delta\omega_x}{\bar{y}_3} & 0 & \delta\omega_z & 0 & \frac{\delta\omega_x}{\bar{y}_3} & 0 \\
-g_2 & 0 & 0 & -g_2 & 0 & -\delta\omega_y & \delta\omega_x & -g_2 & 0 \\
0 & 0 & 0 & 0 & 0 & 0 & 0 & 0 & -\delta\omega_z \\
0 & 0 & 0 & 0 & 0 & 0 & 0 & \delta\omega_z & 0
\end{bmatrix} \qquad (153)$$

If the size of the element is taken sufficiently small, then we may assume that the in-plane forces are small relative to the buckling load of the element. In this case we may neglect the bending moments in the barred system giving

$$\{\bar{s}\} = \{0,\ 0,\ s^{\bar{x}2},\ 0,\ 0,\ s^{\bar{x}3},\ s^{\bar{y}3},\ 0,\ 0\} \qquad (154)$$

Substituting (153), (154) into (137) gives the following form for the geometrical stiffness matrix

$$[k_1] = [k_{13}]c^{\bar{x}2} + [k_{16}]s^{\bar{x}3} + [k_{17}]s^{\bar{y}3} \qquad (155)$$

where $[k_{13}] =$

$$\begin{bmatrix}
0 & & & & & & & & & & & & & & \\
0 & \frac{1}{\bar{x}_2} & & & & & & & & & & & & & \\
0 & 0 & \frac{1}{\bar{x}_2} & & & & & & & & & & & & \\
0 & 0 & 0 & 0 & & & & & & & \text{SYMMETRIC} & & & & \\
0 & 0 & 0 & 0 & 0 & & & & & & & & & & \\
0 & 0 & 0 & 0 & 0 & 0 & & & & & & & & & \\
0 & \frac{-1}{\bar{x}_2} & 0 & 0 & 0 & 0 & \frac{1}{\bar{x}_2} & & & & & & & & \\
0 & 0 & \frac{-1}{\bar{x}_2} & 0 & 0 & 0 & 0 & \frac{1}{\bar{x}_2} & & & & & & & \\
0 & 0 & 0 & 0 & 0 & 0 & 0 & 0 & 0 & & & & & & \\
0 & 0 & 0 & 0 & 0 & 0 & 0 & 0 & 0 & 0 & & & & & \\
0 & 0 & 0 & 0 & 0 & 0 & 0 & 0 & 0 & 0 & 0 & & & & \\
0 & 0 & 0 & 0 & 0 & 0 & 0 & 0 & 0 & 0 & 0 & 0 & & & \\
0 & 0 & 0 & 0 & 0 & 0 & 0 & 0 & 0 & 0 & 0 & 0 & 0 & & \\
0 & 0 & 0 & 0 & 0 & 0 & 0 & 0 & 0 & 0 & 0 & 0 & 0 & 0 & 0
\end{bmatrix} \qquad (156)$$

$$[k_{16}] =$$

$$\begin{bmatrix}
0 & & & & & & & & & & & & & & \\
\frac{\bar{y}_3}{\bar{x}_2^2} & \frac{2\bar{x}_2-\bar{x}_3}{\bar{x}_2^2} & & & & & & & & & & & & & \\
0 & 0 & \frac{2\bar{x}_2-\bar{x}_3}{\bar{x}_2^2} & & & & & & & & & & & & \\
0 & 0 & 0 & 0 & & & & \text{SYMMETRIC} & & & & & & & \\
0 & 0 & 0 & 0 & 0 & & & & & & & & & & \\
0 & \frac{\bar{y}_3}{\bar{x}_2^2} & 0 & 0 & 0 & 0 & & & & & & & & & \\
\frac{\bar{y}_3}{\bar{x}_2^2} & \frac{-\bar{x}_{23}}{\bar{x}_2^2} & 0 & 0 & 0 & \frac{-\bar{y}_3}{\bar{x}_2^2} & \frac{-\bar{x}_3}{\bar{x}_2^2} & & & & & & & & \\
0 & 0 & \frac{-\bar{x}_{23}}{\bar{x}_2^2} & 0 & 0 & 0 & 0 & \frac{-\bar{x}_3}{\bar{x}_2^2} & & & & & & & \\
0 & 0 & 0 & 0 & 0 & 0 & 0 & 0 & 0 & & & & & & \\
0 & 0 & 0 & 0 & 0 & 0 & 0 & 0 & 0 & 0 & & & & & \\
0 & 0 & 0 & 0 & 0 & 0 & 0 & 0 & 0 & 0 & 0 & & & & \\
0 & \frac{-1}{\bar{x}_2} & 0 & 0 & 0 & 0 & \frac{1}{\bar{x}_2} & 0 & 0 & 0 & 0 & 0 & & & \\
0 & 0 & \frac{-1}{\bar{x}_2} & 0 & 0 & 0 & 0 & \frac{1}{\bar{x}_2} & 0 & 0 & 0 & 0 & 0 & & \\
0 & 0 & 0 & 0 & 0 & 0 & 0 & 0 & 0 & 0 & 0 & 0 & 0 & 0 & \\
0 & 0 & 0 & 0 & 0 & 0 & 0 & 0 & 0 & 0 & 0 & 0 & 0 & 0 & 0
\end{bmatrix} \tag{157}$$

$$[k_{17}] =$$

$$\begin{bmatrix}
0 & & & & & & & & & & & & & & \\
\frac{-\bar{x}_{23}}{\bar{x}_2^2} & \frac{-\bar{y}_3}{\bar{x}_2^2} & & & & & & & & & & & & & \\
0 & 0 & \frac{\bar{x}_{23}^2}{\bar{x}_2^2\bar{y}_3} & & & & & & & & & & & & \\
0 & 0 & 0 & 0 & & & & & & & & & & & \\
0 & 0 & 0 & 0 & 0 & & & & & & & & & & \\
0 & \frac{-\bar{x}_3}{\bar{x}_2^2} & 0 & 0 & 0 & 0 & & & & & & & & & \\
\frac{\bar{x}_{23}}{\bar{x}_2^2} & \frac{\bar{y}_3}{\bar{x}_2^2} & 0 & 0 & 0 & \frac{-\bar{x}_3}{\bar{x}_2^2} & \frac{-\bar{y}_3}{\bar{x}_2^2} & & & & & & & & \\
0 & 0 & \frac{\bar{x}_3\bar{x}_{23}}{\bar{x}_2^2\bar{y}_3} & 0 & 0 & 0 & 0 & \frac{\bar{x}_3^2}{\bar{x}_2^2\bar{y}_3} & & & & & & & \\
0 & 0 & 0 & 0 & 0 & 0 & 0 & 0 & 0 & & & & & & \\
0 & 0 & 0 & 0 & 0 & 0 & 0 & 0 & 0 & 0 & & & & & \\
0 & \frac{1}{\bar{x}_2} & 0 & 0 & 0 & 0 & \frac{1}{\bar{x}_2} & 0 & 0 & 0 & 0 & & & & \\
0 & 0 & 0 & 0 & 0 & 0 & 0 & 0 & 0 & 0 & 0 & & & & \\
0 & 0 & \frac{-\bar{x}_{23}}{\bar{x}_2\bar{y}_3} & 0 & 0 & 0 & 0 & \frac{-\bar{x}_3}{\bar{x}_2\bar{y}_3} & 0 & 0 & 0 & 0 & \frac{1}{\bar{y}_3} & & \\
0 & 0 & 0 & 0 & 0 & 0 & 0 & 0 & 0 & 0 & 0 & 0 & 0 & 0 & \\
0 & 0 & 0 & 0 & 0 & 0 & 0 & 0 & 0 & 0 & 0 & 0 & 0 & 0 & 0
\end{bmatrix} \qquad \text{SYMMETRIC} \qquad (158)$$

6.4 The Complete Structure

The next stage in the analysis is to calculate the stiffness matrix of the complete structure when in an initial state of stress. Transforming to global axes we have

$$[k_c^o] = [\Xi]^T[k_c][\Xi] \tag{159}$$

where $[\Xi]$ is a matrix of direction cosines as defined in chapter 5. Before calculating this matrix product it is convenient to introduce the rotation θ_z at each nodal point when defining $[k_c]$, which will now be of order (18 x 18). Considering equilibrium at each nodal point we obtain

$$\{\delta S^o\} = [K_c^o]\{\delta U^o\} = [K^o]\{\delta U^o\} + [K_1^o]\{\delta U^o\} \tag{160}$$

where $\{\delta S^o\}$ are the incremental external forces and $\{\delta U^o\}$ the corresponding global displacements. The matrices $[K^o]$ and $[K_1^o]$ are defined by

$$[K^o] = \sum_g [a_g]^T[k_g^o][a_g] \tag{161}$$

$$[K_1^o] = \sum_g [a_g]^T[k_{1g}^o][a_g] \tag{162}$$

the matrix $[a_g]$ being defined as in chapters 3 and 5. The computational procedure for the matrices $[K^o]$ and $[K_1^o]$ is exactly the same as that described for the stiffness and inertia matrices of a shell element in chapter 5. Application of zero displacement boundary conditions again results in the appropriate rows and columns of $[K_c^o]$ being deleted.

Equation (160), in its reduced form, may now be solved for the incremental displacements $\{\delta U^o\}$ corresponding to a given set of incremental applied loads $\{\delta S^o\}$. Since the matrix $[K_c^o]$ takes the form of a triple band matrix, the most convenient method of solving this equation is the tri-diagonalisation method used by Clough, Wilson and King in their analysis of multistory building frames [30] . The advantages of this method are that only the non-zero submatrices of $[K_c^o]$ need be stored and that very little extra working space is required.

6.5 The Step-by-Step Procedure

The procedure for applying the total load by means of the step-by-step method is as follows.

(a) Calculate the stiffness matrix $[K_c^o]_1 = [K^o(0)]$, since the combined stiffness matrix is, initially, equal to the incremental strain stiffness matrix for the undeflected state. Apply an incremental load and solve for the nodal displacements $\underline{U}_1 = \{\delta U^o\}_1$, and hence the nodal forces $\{\delta \bar{s}\}_1$.

(b) Calculate the matrix $[K_c^o]_2 = [K^o(\underline{U}_1)] + [K_1^o(\underline{U}_1)]$. The combined stiffness matrix is now the sum of the incremental strain and geometrical matrices. Both these are calculated in the deformed state and are thus functions of the displacements previously calculated, which in turn are dependent upon the applied loads. Apply a second incremental load, solve for the displacements $\{\delta U^o\}_2$, giving $\underline{U}_2 = \underline{U}_1 + \{\delta U^o\}_2$, and also the incremental nodal forces $\{\delta \bar{s}\}_2$.

(c) Continue the process until the required number of incremental loads, NL, has been applied.

The above procedure is shown in flow diagram form in figure 40.

6.6 Stability Analysis

The determination of the critical load intensity at the onset of buckling of a flat plate subject to in-plane loads may be formulated as an eigenvalue problem. From equation (160) we have

$$[\,[K^o] + [K_1^o]\,]\{\delta U^o\} = \{\delta S^o\} \qquad (163)$$

Below the buckling load we may assume that the distribution of in-plane forces is fixed and so write

$$[K_1^o] = \lambda [K_2^o] \qquad (164)$$

where $[K_2^o]$ is a constant matrix and λ a load intensity factor. In addition, $[K^o]$ may be assumed constant. Equation (163) thus becomes

$$[\,[K^o] + \lambda [K_2^o]\,]\{\delta U^o\} = \{\delta S^o\} \qquad (165)$$

If the element stiffness matrices are referred to the following displacement vector

$$\{u\} = \{u_1, v_1, \theta_{z1}, u_2, v_2, \theta_{z2}, u_3, v_3, \theta_{z3},$$

$$w_1, \theta_{x1}, \theta_{y1}, w_2, \theta_{x2}, \theta_{y2}, w_3, \theta_{x3}, \theta_{y3}\} \qquad (166)$$

then they take the form

$$[k] = \begin{bmatrix} k_p & 0 \\ 0 & k_b \end{bmatrix} \qquad [k_1] = \begin{bmatrix} k_{1p} & 0 \\ 0 & k_{1b} \end{bmatrix} \qquad (167)$$

where p denotes in-plane effects and b bending effects. Before buckling no lateral deflections occur, and so the rotation from local to global axes is simply a rotation about the vertical axis O^oZ^o. Thus the stiffness matrices referred to global axes take on a similar form. That is

$$[k^o] = \begin{bmatrix} k^o_p & 0 \\ 0 & k^o_b \end{bmatrix} \qquad [k^o_1] = \begin{bmatrix} k^o_{1p} & 0 \\ 0 & k^o_{1b} \end{bmatrix} \qquad (168)$$

Equation (165) may now be written

$$\left[\begin{bmatrix} K^o_p & 0 \\ 0 & K^o_b \end{bmatrix} + \lambda \begin{bmatrix} K^o_{2p} & 0 \\ 0 & K^o_{2b} \end{bmatrix}\right] \begin{bmatrix} \delta U^o_p \\ \delta U^o_b \end{bmatrix} = \begin{bmatrix} \delta S^o_p \\ \delta S^o_b \end{bmatrix} \qquad (169)$$

This separates into two equations

$$[\,[K^o_p] + \lambda[K^o_{2p}]\,]\{\delta U^o_p\} = \{\delta S^o_p\} \qquad (170)$$

$$[\,[K^o_b] + \lambda[K^o_{2b}]\,]\{\delta U^o_b\} = \{\delta S^o_b\} \qquad (171)$$

The matrix $[K^o_{2p}]$ represents the change in the in-plane nodal forces dueto the rotation of the structural elements in the displacement $\{\delta U^o_p\}$. This effect is negligible below the buckling load, and so the in-plane displacements

may be calculated from the equation

$$[K_p^o]\{\delta U_p^o\}=\{\delta S_p^o\} \qquad (172)$$

These displacements may then be used in conjunction with the element stiffness matrices to calculate the nodal forces $S^{\bar{x}2}$, $S^{\bar{x}3}$ and $S^{\bar{y}3}$ for each element.

At buckling arbitrary displacements $\{\delta U_b^o\}$ may be sustained without any external loads $\{\delta S_b^o\}$. Thus the equation

$$\left[[K_b^o] + \lambda[K_{2b}^o] \right]\{\delta U_b^o\} = 0 \qquad (173)$$

has a non-trivial solution. The solution to this equation gives the critical load intensity factor λ and the buckling mode $\{\delta U_b^o\}$.

To illustrate the application of this type of analysis, the buckling load of a simply-supported rectangular plate of dimensions 13·5 x 20·0 ins., subject to a uniform compressive load over the longer sides, has been determined. Four different idealisations were considered as illustrated in figure 29.

The exact solution to this problem for the buckling stress σ_b is

$$\sigma_b = \frac{\pi^2 D}{b^2 t}\left(\frac{b}{a} + \frac{a}{b}\right)^2 \qquad (174)$$

whenever $a/b < \sqrt{2}$, where a and b are the plate dimensions, t the plate thickness and D flexural rigidity. The comparison between the finite element solutions and this exact solution is shown in figure 41. The buckling stress is underestimated for all the four idealisations considered. As the mesh is made successively finer, the finite element solution converges towards the true solution. Both these factors emerged when considering the frequencies of vibration of this plate in chapter 4. The curve for the buckling stress given in figure 41 may be compared with the curve for the fundamental mode of vibration in figure 30. The convergence characteristics of the two are very similar, but the error for the buckling stress is about 4% greater than the error for the fundamental frequency. The reason for this is that in

calculating the geometrical stiffness matrix it was assumed that the curvature of the individual elements was negligible. This is equivalent to assuming a lumped mass representation for the inertia forces in the vibration problem. Zienkiewicz has shown [31] that by taking a lumped mass representation, the errors in frequency are greater than those obtained by taking a consistent mass matrix as given in chapter 3.

6.7 Vibration of a Plate Subject to Static Loads along the Boundary

Consider a plate which is subjected to static loads along its boundary. The characteristics of small amplitude vibrations of the plate in this configuration may be evaluated in the following manner. First, apply the static load to the plate by means of the step-by-step procedure to determine the deflected shape and the element nodal forces. Next, calculate the matrix $[K_c^o]$ which is the stiffness matrix for small displacements at the given loading. Finally, the inertia matrix $[M_s^o]$ may be determined by the procedure described for shells in chapter 5. The frequencies and modes of vibration may then be calculated from the equation

$$[K_c^o]\{U^o\} - \Omega^2[M_s^o]\{U^o\} = 0 \qquad (175)$$

As in the case of stability analysis, we may assume that the distribution of in-plane forces is fixed below the buckling load of the plate. In this case the flexural vibrations of the plate may be determined from the reduced equation

$$\left[[K_b^o] + \lambda[K_{2b}^o] \right]\{U_b^o\} - \Omega^2[M_b^o]\{U^o\} = 0 \qquad (176)$$

The problem is thus reduced to calculating the in-plane stress distribution, from which may be calculated $[K_{2b}^o]$, and then solving equation (176) for a given value of λ. This procedure eliminates the necessity of carrying out the step-by-step analysis.

In order to determine the accuracy to which the frequency of vibration may be determined for any given loading below the buckling load, a simply supported plate 13·5 x 20·0 ins. subject to a uniform compressive load was considered. The first two doubly symmetric modes of vibration were calculated

for a mesh size of 5 and a range of applied loads. The exact solution to this problem [32] gives the following frequency expression

$$f = f_o \left[1 - \frac{(m-1)^2}{\left[(m-1)^2 \frac{b}{a} + (n-1)^2 \frac{a}{b}\right]^2} \left(\frac{b^2 t}{\pi^2 D}\right) \sigma_b \mu \right]^{\frac{1}{2}} \qquad (177)$$

where f_o is the frequency of the plate under zero load, m and n denote the number of nodal lines in the direction of a and b respectively, and μ is the ratio of applied stress to buckling stress. Other quantities are as previously defined.

The finite element solutions are compared with these solutions in figure 42. It may be seen that the fundamental mode has been predicted to within 4 c.p.s. when the applied stress is less than 80% of the true buckling stress. The increase in error above this stress is due to the error in predicting the buckling stress. The second doubly symmetric mode has been predicted to within 9 c.p.s. for all stresses up to the buckling stress.

7. THEORETICAL ANALYSIS OF CRACKED PLATES IN TENSION

7.1 Introduction

In this chapter finite element displacement theory, as developed in chapters 3 to 6, is used to determine the vibration characteristics of rectangular plates which contain a central crack and are subject to tensile loads in a direction perpendicular to the crack. Where possible, the results obtained are compared with experimental measurements obtained from either reference [2] or chapter 2.

The dynamic characteristics are effected by the distribution of static stresses within the plate. The initial investigation is therefore confined to determining the accuracy of the calculated distributions. The major effect on the frequency of vibration is caused by compressive stresses in the direction parallel to the free edge of the crack. As the applied load is increased the magnitude of the compressive stresses increase. Eventually the free edge of the crack becomes unstable and buckles permanently. At this point the frequency of vibration is a minimum. The second stage in the investigation is therefore to consider the accuracy of the buckling stresses calculated from small displacement theory. The effect of variations in plate width is also determined, and the phenomena observed in chapter 2 is discussed. Finally the variation of the frequency and shape of the fundamental mode of vibration of the plate with increasing applied load is considered. For applied loads greater than the critical buckling load, the analysis involves determining the deflected shape of the buckled plate by the step-by-step procedure which is given in chapter 6.

For a majority of the investigations a plate 13·5 in. long, 10 in. wide and 0·064 in. thick is considered. The effect of variations in plate width is determined by successively increasing this dimension to 20 in. and 40 in. Crack lengths of 3·5 in. and 5·0 in. have been considered.

7.2 Static Stress Distribution

The static stress distributions of a plate 13·5 in. long and 10 in. wide, containing a central crack 3·5 in. long in the direction of the short dimension, have been calculated. The idealisation into an assemblage of triangular elements is shown in figure 43. Only one quarter of the plate is shown as it is symmetrical with respect to both horizontal and vertical centre lines. The construction of the idealisation consisted of first dividing the plate up by elliptical arcs having the centre line through the crack as major axis. The area between two consecutive arcs was then divided up into triangles which were as near to being equilateral as possible. This technique was successfully used by Clough [15] when analysing the stresses in a plate containing an elliptical hole. In the present investigation the crack was represented by a slot 1/20 in. wide and having circular holes of diameter 3/32 in. at each end. The calculated stresses are thus directly comparable with the measured ones presented in reference [2]. The complete idealisation consists of 114 elements interconnected at 73 nodal points. The factor restricting the number of nodal points is the computer storage requirements for analysing the vibration characteristics of the plate when in a buckled state, which is to be considered in section 7.6

The initial step in the analysis is to calculate the stiffness matrix $[k^o]$, referred to global coordinates, of each element as given in chapter 5. The stiffness matrix $[K_p^o]$ for the complete plate is obtained from the relation

$$[K_p^o] = \sum_g [a_g]^T [k_g^o] [a_g] \qquad (178)$$

The equilibrium equation

$$\{S^o\} = [K_p^o]\{U^o\} \qquad (179)$$

is now solved for the displacements $\{U^o\}$ corresponding to a given set of applied loads $\{S^o\}$. This matrix represents a set of concentrated loads applied at the nodes. These discrete loads are such that in any virtual displacement the work done by them is equal to the work done by the actual

distributed loading. In the present application the distributed loading was taken to be a uniform distribution over the edges parallel to the crack. In this particular case the nodal forces may be calculated by a simpler, but equivalent process. The total distributed load on the side of an element is assigned as two equal concentrated loads at the nodes. When solving equation (179) it is assumed that, due to symmetry, the vertical displacements over AB and the horizontal displacements over DE are zero. In addition the horizontal displacements over CD are also assumed zero since this edge was clamped when the experimental stresses were determined. Once the nodal displacements $\{U^o\}$ have been determined the stresses within an element are calculated from equation (26), namely

$$\{\sigma\} = [D][B][C^{-1}]\{u_i\} \qquad (180)$$

the matrices being interpreted as in chapter 5.

It may be noted that, because the displacements have been assumed to vary linearly, the stresses are constant within any one element. Hence the computed stress distributions will be discontinuous. It is thus necessary to employ a smoothing process. Clough [33] used a graphical process, whilst Turner [29] assumes the stress at a nodal point to be equal to the average value of the stresses within the elements surrounding it. In the present investigation it was found necessary only to employ a smoothing technique to elements within two adjacent elliptic arcs. The distributions in directions normal to the arcs were found to be relatively smooth. The method adopted was to assign the average stresses within two adjacent elements to the midpoint of the common side.

The distribution of the horizontal stress component σ_x along the plate centre line normal to the crack is shown in figure 44. The finite element solution has been compared with the experimental results presented in reference [2] and also the analytical solution for an infinite plate due to Inglis [34]. It may be seen that there is excellent agreement between all three, particularly in regions of high stress. The

major feature of this distribution is that the stress is compressive, and equal to the applied stress, at the free edte of the crack, reducing to zero at a distance approximately equal to half the length of the crack.

The distribution of the vertical stress component σ_y along the plate centreline in the direction of the crack is given in figure 45. A comparison with experimental and theoretical distributions again shows very close agreement. Experimentally determined stresses, for an applied stress of 22, 255 lb./in.^{2}, when the free edge of the crack is permanently buckled, is also shown. The infinite plate theory predicts an infinite stress at the tip of the crack. In practice this does not arise since plastic deformations occur which reduce the stress concentration. This plastic yielding effect has not been taken into account in the finite element solution, which is a purely elastic analysis. In spite of this, finite stresses occur at the crack tip. This is due to the averaging effect of the constant stress assumed within each element.

Contours of constant stress over one quarter of the plate for the direct stresses σ_x and σ_y, and also the shear stress τ_{xy} are given in figures 46 to 48. A comparison is made with the corresponding contours for an infinite plate. The two solutions again show remarkable agreement. As may be expected, the accuracy is not quite so good in areas where the triangular elements used are too large to predict the large stress gradients which exist.

7.3 Buckling Analysis

The stability analysis, presented in chapter 6, may be used to determine the applied stress at which the free edge of the crack buckles permanently. The first case which was considered was the configuration shown in figure 43. This analysis gave a buckling stress of $21{\cdot}09 \times 10^3$ lb./in.^{2} compared with an experimental value of $17{\cdot}2 \times 10^3$ lb./in.^{2} The deflected shape of the free edge of the crack at buckling is compared with the experimentally measured shape in figure 49.

In an attempt to resolve the variation in the buckling stress-crack

length curves, as determined experimentally in chapter 2, three plates of width 10 in., 20 in. and 40 in. were considered. Each of these plates were assumed to have a 5 in. crack. The idealisation process followed a similar pattern to the one described in section 7.2. In addition, it was arranged that the common areas of the three plates should have identical idealisations. In all 150, 183 and 230 elements were used involving 93, 112 and 140 nodal points respectively. The computed buckling stresses are compared with the experimental ones in table 7 showing reasonable agreement. The deflected shapes at buckling along and normal to the crack are shown in figures 50 and 51. Along the line of the crack, the effect of increasing the width of the plate is to decrease the amplitude in the area away from the crack, and hence increasing the curvature of the platein the region of the crack tip. In the direction normal to the crack, the effect of increasing the plate width is to reduce the area of buckling. These effects may be explained by examining the various stress distributions given in figures 52 , 53 and 54.

Figure 52 shows the variation of the longitudinal direct stress σ_y along the plate centreline normal to the crack. It is zero at the free edge of the crack and increases to the applied stress at the boundary. Very little variation in the distribution occurs when the width of the plate is increased. The distribution of the horizontal component of direct stress σ_x in the direction normal to the crack is shown in figure 53. Increasing the plate width has reduced the compressive stress along the free edge of the crack to about 80% of the applied stress. For the narrower plates the compressive stresses occur over a distance equal to half the crack length, but for the wider plate this distance is only one quarter of the crack length. Both these effects will increase the value of the applied stress at which buckling occurs. This explains why the buckling stresses for the 40 in. plates were found to be greater (by a factor of 3) than the buckling stresses for the 10 in. and 20 in. plates. It does not, however, explain the departure from a linear relationship between the buckling stress σ_b and the inverse square of half the crack length $1/\ell^2$. This occurs for crack lengths less than 6·26 in.

Photoelastic coating measurements on a 20 in. wide plate with a 5 in. crack have shown that the stress concentration factor K_1 at the tip of the crack is 3·13. We may calculate the corresponding stress concentration factor K_2 for a 40 in. plate containing a 6·26 in. crack using Dixon's work [**35**] . This gives

$$\frac{K_2}{K_1} = \left[\frac{1 - (\ell_1/a_1)^2}{1 - (\ell_2/a_2)^2} \right]^{\frac{1}{2}} \qquad (181)$$

where 2a denotes plate width. This gives a value of 3·07 for K_2. The buckling stress for a 6·26 in. crack in a 40 in. plate was found to be 16×10^3 lb./in.^{2}, and so the tensile stress at the tip of the crack at buckling is $3{\cdot}07 \times 16 \times 10^3 = 49 \times 10^3$ lb./in.^{2}. Now the 0·1% yield stress for the material is 47×10^3 lb./in.^{2}, and so for crack lengths less than 6·26 in., plastic flow occurs at the tip of the crack before buckling, thereby reducing the buckling stress to a value below that given by an elastic analysis.

The variation of the longitudinal direct stress σ_y along the line of the crack is shown in figure 54. The stresses in the region of the crack tip are relatively insensitive to variations in plate width. Away from the crack, the stresses reduce fairly rapidly for the narrower plates, but remain almost constant, and approximately equal to the applied stress, for the widest plate. This, together with the increased value of the buckling stress, produces the reduced amplitudes away from the crack in the 40 in. plate.

7.4 Vibration Analysis before Buckling

For applied loads which are less than the critical buckling load of the plate, the natural frequencies and modes of vibration may be determined by the simplified analysis given in section 6.7. This has been done for a 10 in. wide plate containing a 3·5 in. crack, the idealisation being identical to the one shown in figure 43.

The variation of the frequency of the fundamental mode of vibration with applied load as calculated, is compared with the measured values in figure 55. At low applied stresses the agreement is very close. There is, however, an overestimate of 30% in the maximum frequency, and of 23% in the buckling stress where the minimum frequency occurs. Both these errors may be reduced by increasing the fineness of the network in the idealisation.

The variation in the shape of the fundamental mode of vibration with the ratio μ of applied stress to the calculated buckling stress, is shown in figure 56. At zero stress the plate vibrates similarly to a plate without a crack. As μ is increased the amplitude of the edge of the plate is gradually reduced until the predominant vibrations are finally confined to an area around the crack. The calculated mode shape for an applied stress of 13,300 lb./in.^{2} is compared with the measured one in figure 57, the two showing very close agreement.

7.5 Post-buckling Behaviour

The deflected shape of a cracked plate, for applied loads greater than the buckling load, may be calculated using the step-by-step procedure presented in chapter 6. In the analysis, coupling terms between the in-plane and bending effects, only appear when lateral deflections of the plate are present. In practice, lateral deflections occur at the buckling load because of the presence of initial imperfections in the geometry of the system. Thus, in order to initiate lateral displacements at buckling in the mathematical solution, an artificial initial imperfection is introduced. It is convenient to take as this initial imperfection, the buckling mode calculated from small displacement theory, with an amplitude factor which may be arbitrarily chosen.

This technique has been used to determine the post-buckling behaviour of a plate 13·5 in. long, 10·0 in. wide and 0·064 in. thick containing a 3·5 in. crack. The small displacement buckling mode, which was used, is given in figure 49. The deflection of the centre of the crack

for various applied loads, when the amplitude factor is taken to be 0·005 in., is shown in figure 58. In the step-by-step analysis, the initial load was taken to be $0{\cdot}8\sigma_b$ and subsequent incremental loads were $0{\cdot}05\ \sigma_b$, where σ_b is the buckling stress. The deflected shape of the plate did not change appreciably from the assumed shape of the initial imperfection.

The deflections of the mid point of the crack, for applied loads less than the buckling load, may be used in a Southwell plot [36] to determine the buckling load. This has been done in figure 59. This technique estimates a buckling stress of $23{\cdot}6 \times 10^3$ lb./in.^{2} compared with the small displacement solution of $21{\cdot}1 \times 10^3$ lb./in.^{2}. This suggests that in the step-by-step procedure, smaller incremental loads should have been used.

7.6 Vibration Analysis after Buckling

The method of determining the frequencies and modes of vibration, for applied loads greater than the buckling load, has been given in section 6.7. This involves calculating the small displacement stiffness matrix, at the given loading, by the step-by-step procedure. The inertia matrix is then calculated, for the plate in the deflected state, by the procedure described for shells in chapter 5.

This method of analysis has been applied to the plate which is 13·5 in. long, 10·0 in. wide and 0·064 in. thick and contains a 3·5 in. crack. The frequencies obtained are shown in figure 55. The general trend, in this region, of increasing frequency with increase of applied load, as shown by the experimental observations, has been obtained. The actual values of the frequencies are grossly underestimated by the finite element solution. This is due to the coarseness of both the idealisation and the step size in the step-by-step procedure, and also the inability of the assumed displacement functions to maintain continuity of displacement between adjacent elements, as shown in chapter 5. The shape of the mode of vibration when $\mu = 1{\cdot}15$ is shown in figure 56. It may be seen that the process of reducing the amplitude at the edge of the plate, and also reducing the area of predominant vibrations, continues when μ is greater than one.

8. GENERAL DISCUSSION AND CONCLUSIONS

The finite element displacement method of analysis has been applied to a number of static and dynamic problems, and the results obtained have been compared with either analytical solutions or experimental data. The particular problem of a rectangular plate containing a central crack and subject to tensile loads has also been studied and comparisons made with experiment.

In this work the triangular element only has been considered. The lateral displacements within an element have been represented by a simple polynomial function equation (37) which does not give continuity of normal slope between adjacent elements. It also varies with the choice of local axes. In spite of these drawbacks, it has been found that good accuracy may be obtained provided a sufficient number of elements are used, and that the elements are almost equilateral. The general variation in the calculated frequency has been to, first of all, overestimate the true value when only a few elements have been used, and then to rapidly underestimate it as the number of elements are increased. Further increases in the number of elements then show a convergence towards the true solution.

Increasing the number of elements, and hence the number of nodal points, to obtain the required accuracy, leads to a considerable increase in computer storage requirements for the stiffness and inertia matrices. Figure 60 shows the storage requirements for the various problems considered when

$$\underset{I}{\text{Maximum}} \quad \{NPC(I)\} = n = NPR \tag{182}$$

the notation being defined as in chapter 4. Inevitably, this will lead to a vast increase in the computing time required to solve the eigenvalue

problem. One must therefore seek a more accurate representation of the element displacement function, which produces the required accuracy for a reduced total number of degrees of freedom.

A displacement function for a triangular element in bending, which ensures continuity of normal slope between adjacent elements, has been proposed in reference [19]. This function has been expressed in terms of the area coordinates of the triangle instead of the more usual cartesian system. However, the one example quoted - a cantilever plate using four elements - shows frequency errors, greater than the ones obtained using a similar displacement function which did not give continuity of normal slope. It would be instructive to compare the solutions for both this and other applications, using an increased number of elements.

An alternative method would be to make use of higher order approximations for the element displacement function. That is, higher order derivatives of the lateral displacement w are treated as unknowns at the nodal points. For the triangular element, the lateral deflection may be expressed as a fifth order polynomial, namely

$$\begin{aligned} w = {} & A_1 + A_2x + A_3y + A_4x^2 + A_5xy + A_6y^2 \\ & + A_7x^3 + A_8x^2y + A_9xy^2 + A_{10}y^3 \\ & + A_{11}x^4 + A_{12}x^3y + A_{13}x^2y^2 + A_{14}xy^3 + A_{15}y^4 \\ & + A_{16}x^5 + A_{17}x^4y + A_{18}x^3y^2 + A_{19}x^2y^3 + A_{20}xy^4 + A_{21}y^5 \end{aligned} \tag{183}$$

The constants $A_1, A_2, \ldots, A_{21}$ in this expression may be expressed in terms of the values of w, $\partial w/\partial x$, $\partial w/\partial y$, $\partial^2 w/\partial x^2$, $\partial^2 w/\partial x \partial y$, $\partial^2 w/\partial y^2$ at the nodal points, and the normal slope $\partial w/\partial n$ at the mid points of the sides. This gives complete continuity of displacement and slope between elements. On the other hand, for a given number of nodal points in a structure, there will be an increase in the total number of degrees of freedom. Hence, the use of this function is justifiable, only if it is possible to reduce the number of nodal points to such an extent, that the total number of degrees of freedom are reduced.

As shown in chapter 5, a more sophisticated set of in-plane displacement functions are required to increase the accuracy of the solution of shell problems. The prime necessity is for a set of functions which are compatible with the bending displacements to ensure continuity of displacement between elements. If higher order approximations are used, then the strains and rotations should also be treated as nodal degrees of freedom.

The work described, has shown that the dynamic characteristics of cracked plates in tension may be analysed successfully by the finite element displacement method. The modes of vibration, presented in chapter 7 for varying static loads, may be used to calculate the distribution of dynamic stresses within the plate, relative to the stress at a reference point. Since the particular quantities of interest are the stresses at the tip of the crack, then the effect of plastic yielding there should be included in the analysis. The response of the plate to representative boundary layer pressure fluctuations may then be obtained and the actual dynamic stresses calculated. In order that the analysis may be applied to more representative structures the effect of the fuselage longitudinal stress, the presence of frames and stringers, and the curvature of the skin should be considered.

REFERENCES

1. Zienkiewicz, O.C. and Holister, G.S. (Editors), "Stress Analysis", J. Wiley Press, 1965.

2. Clarkson, B. L., "The Propagation of Fatigue Cracks in a Tensioned Plate Subject to Acoustic Loads", in Acoustical Fatigue in Aerospace Structures, edited by W. J. Trapp and D. M. Forney, Jr. (Syracuse University Press, Syracuse, N. Y., 1965), Chapter 18 pp. 361-388.

3. Buckingham, E., "On Physically Similar Systems; Illustrations of the Use of Dimensional Equations", Physics Review, Vol. 4, No. 4, (1914).

4. Van Driest, E. R., "On Dimensional Analysis and the Presentation of Data in Fluid Flow Problems", J. App. Mech., Vol. 13 (1946).

5. Mansfield, E. H., "On Theoretical Plasticity and Crack Propagation", A.R.C.C.P. No. 688, Aeronautical Research Council, Great Britain (1963).

6. Ramberg, W. and Osgood, W. R., "Description of Stress-Strain Curves by Three Parameters", NACA TN 902 (1943).

7. Argyris, J. H., Energy Theorems and Structural Analysis (Butterworths Press, London, 1960).

8. Argyris, J. H., Recent Advances in Matrix Methods of Structural Analysis, (Pergamon Press, New York, 1964).

9. Taig, I. C. and Kerr, R. I., "Some Problems in the Discrete Element Representation of Aircraft Structures", in Matrix Methods of Structural Analysis, edited by B. Fraijs de Veubeke (Pergamon Press, New York, 1964), pp. 267-315.

10. Hessel, A., "Analysis of Plates and Shells by Matrix Methods", SAAB TN 48.

11. Denke, P. H., "Digital Analysis of Non-Linear Structures by the Force Method", in Matrix Methods of Structural Analysis, edited by B. Fraijs de Veubeke (Pergamon Press, New York, 1964) pp. 317-342.

12. Clough, R. W., "The Finite Element Method in Plane Stress Analysis", Proc. Second Int. Conf. on Electronic Computati Am. Soc. Civil Engineering (1960).

13. Clough, R. W. and Tocher, J. L., "Analysis of Thin Arch Dams by the Finite Element Method", Proc. of the Int. Symp. on the Theory of Arch Dams, Southampton University, England, (1964), pp. 107-121.

14. Zienkiewicz, O. C. and Cheung, Y. K., "Finite Element Method of Analysis for Arch Dam Shells and Comparison with Finite Difference Procedures", Proceedings of The International Symposium on the Theory of Arch Dams, Southampton University, England, pp.123-140 (1964).

15. Clough, R. W., "The Finite Element Method in Structural Mechanics", Stress Analysis, Editors, Zienkiewicz, O.C. and Holister, G. S. (J. Wiley, 1965), Chapter 7.

16. Melosh, R. J., "Basis for Derivation of Matrices for the Direct Stiffness Method", AIAA Journal, Vol. 1, PP. 1631-1637 (1963).

17. Pian, T. H. H., "Derivation of Element Stiffness Matrices by Assumed Stress Distribution", AIAA Journal, Vol. 2, pp. 1333 - 1336 (1964).

18. Fraeijs de Veubeke, J., "Displacement and Equilibrium Models in the Finite Element Method", Stress Analysis, Editors, Zienkiewicz, O. C. and Holister, G. S. (J. Wiley, 1965), Chapter 9.

19. Irons, B., Proc. Instn. of Civil Engrs., Vol. 33, pp. 322 - 335 (1966) [Discussion of "The Finite Element Method for Analysis of Elastic Isotropic and Orthotropic Slabs" by Zienkiewicz, O. C. and Cheung, Y. K., Proc. Instn. of Civil Engrs., Vol. 28, pp. 471-488 (1964)].

20. Fox, L., An Introduction to Numerical Linear Algebra, (Clarendon Press, Oxford,England, 1964).

21. Wilkinson, J. H., "Householders Method for the Solution of the Algebraic Eigen Problem", Computer Journal, Vol. 3, No. 1, pp. 23-27 (1960).

22. Booth, A. D., Numerical Methods (Butterworths Scientific Publications, 1955).

23. Timoshenko, S., **Vibration Problems in Engineering**, (D. Van Nostrand Co.)

24. Silberstein, J.P.O., "Static Loading and Free Vibrations of Plates", Report No. ARL/SM 290 (1962).

25. Gustafson, P. N., Stokey, W. F. and Zorowski, C. F., "An Experimental Study of Natural Vibrations of Cantilevered Triangular Plates", J. Aero. Sci., Vol. 20, pp. 331 - 337 (1953).

26. Zienkiewicz, O. C., "Finite Element Procedures in the Solution of Plate and Shell Problems", Stress Analysis, Editors, Zienkiewicz, O. C. and Holister, G. S., (J. Wiley, 1965), Chapter 8.

27. Arnold, R. N. and Warburton, G. B., "Flexural Vibrations of the Walls of Thin Cylindrical Shells having Freely Supported Ends", Proc. Roy. Soc., A, Vol. 197, pp. 238-257 (1949).

28. Novozhilov, V. V., "Foundations of the Non-Linear Theory of Elasticity" (Graylock Press, Rochester, N. Y., 1953).

29. Turner, M. J., Martin, H. C. and Weikel, R. C., "Further Development and Applications of the Stiffness Method", Matrix Methods of Structural Analysis, editor Fraeijs de Veubeke, B. (Pergamon Press, 1964), pp. 203-266.

30. Clough, R. W., Wilson, E. L. and King, I. P., "Large Capacity Multistory Frame Analysis Programs", Proc. Am. Soc. Civil Engrs. (Structural Div.), pp. 179 - 204 (1963).

31. Zienkiewicz, O. C., Irons, B. and Nath, B., "Natural Frequencies of Complex, Free or Submerged,Structures by the Finite Element Method", Proc. of the Symposium on Vibrations in Civil Engineering, London, pp. 83 - 90 (1965).

32. Harris, C. M. and Crede, C. E., (eds.) Shock and Vibration Handbook, Vol. 1 (McGraw-Hill Publishing Co., 1961).

33. Clough, R. W. and Wilson, E. L., "Stress Analysis of a Gravity Dam by the Finite Element Method", RILEM Bull., No. 19, pp. 45 - 54 (1963).

34. Inglis, C. E., "Stresses in a Plate Due to the Presence of Cracks and Sharp Corners", Trans. Inst. Naval Architects (London), Vol. 55, pp. 219 - 230 (1913).

35. Dixon, J. R., "Stress Distribution Around a Central Crack in a Plate Loaded in Tension: Effect of Finite Width of Plate", J. Roy. Aero. Soc., Vol. 64, pp. 141 - 145

36. Southwell, R. V., "On the Analysis of Experimental Observations in Problems of Elastic Stability", Proc. Roy. Soc. of London, A, Vol.135, pp. 601 - 616 (1932).

APPENDIX

Evaluation of the integral $\int_{\Delta} x^m y^n dxdy$

(i) $\underline{x_3 \neq 0,\ x_3 \neq x_2}$

In figure 22 the equations of lines 13 and 23 respectively are

$$y = \frac{y_3}{x_3} x \tag{A .1}$$

$$y = \frac{-y_3(x - x_2)}{\delta x} \tag{A .2}$$

where $$\delta x = (x_2 - x_3) \tag{A .3}$$

The integral $\int_{\Delta} x^m y^n dxdy$ is evaluated, first by perfoming the integration with respect to x, and then the integration with respect to y. That is

$$\int_{\Delta} x^m y^n dxdy = \int_0^{y_3} y^n \left[\int_{\frac{x_3}{y_3} y}^{(x_2 - \frac{\delta x}{y_3} y)} x^m dx \right] dy \tag{A .4}$$

Now $$\int_{\frac{x_3}{y_3} y}^{(x_2 - \frac{\delta x}{y_3} y)} x^m dx = \frac{1}{m+1} \left[\left[x_2 - \frac{\delta x}{y_3} y \right]^{m+1} - \left[\frac{x_3}{y_3} y \right]^{m+1} \right]$$

$$= \frac{1}{m+1} \left[\sum_{r=0}^{m+1} \frac{(m+1)!}{(m+1-r)!r!} (-1)^r \left(\frac{\delta x}{y_3}\right)^r x_2^{m+1-r} y^r - \left(\frac{x_3}{y_3}\right)^{m+1} y^{m+1} \right] \tag{A .5}$$

25. Gustafson, P. N., Stokey, W. F. and Zorowski, C. F., "An Experimental Study of Natural Vibrations of Cantilevered Triangular Plates", J. Aero. Sci., Vol. 20, pp. 331 - 337 (1953).

26. Zienkiewicz, O. C., "Finite Element Procedures in the Solution of Plate and Shell Problems", Stress Analysis, Editors, Zienkiewicz, O. C. and Holister, G. S., (J. Wiley, 1965), Chapter 8.

27. Arnold, R. N. and Warburton, G. B., "Flexural Vibrations of the Walls of Thin Cylindrical Shells having Freely Supported Ends", Proc. Roy. Soc., A, Vol. 197, pp. 238-257 (1949).

28. Novozhilov, V. V., "Foundations of the Non-Linear Theory of Elasticity" (Graylock Press, Rochester, N. Y., 1953).

29. Turner, M. J., Martin, H. C. and Weikel, R. C., "Further Development and Applications of the Stiffness Method", Matrix Methods of Structural Analysis, editor Fraeijs de Veubeke, B. (Pergamon Press, 1964), pp. 203-266.

30. Clough, R. W., Wilson, E. L. and King, I. P., "Large Capacity Multistory Frame Analysis Programs", Proc. Am. Soc. Civil Engrs. (Structural Div.), pp. 179 - 204 (1963).

31. Zienkiewicz, O. C., Irons, B. and Nath, B., "Natural Frequencies of Complex, Free or Submerged,Structures by the Finite Element Method", Proc. of the Symposium on Vibrations in Civil Engineering, London, pp. 83 - 90 (1965).

32. Harris, C. M. and Crede, C. E., (eds.) Shock and Vibration Handbook, Vol. 1 (McGraw-Hill Publishing Co., 1961).

33. Clough, R. W. and Wilson, E. L., "Stress Analysis of a Gravity Dam by the Finite Element Method", RILEM Bull., No. 19, pp. 45 - 54 (1963).

34. Inglis, C. E., "Stresses in a Plate Due to the Presence of Cracks and Sharp Corners", Trans. Inst. Naval Architects (London), Vol. 55, pp. 219 - 230 (1913).

35. Dixon, J. R., "Stress Distribution Around a Central Crack in a Plate Loaded in Tension: Effect of Finite Width of Plate", J. Roy. Aero. Soc., Vol. 64, pp. 141 - 145

36. Southwell, R. V., "On the Analysis of Experimental Observations in Problems of Elastic Stability", Proc. Roy. Soc. of London, A, Vol.135, pp. 601 - 616 (1932).

APPENDIX

Evaluation of the integral $\int_{\Delta} x^m y^n dxdy$

(i) $x_3 \neq 0,\ x_3 \neq x_2$

In figure 22 the equations of lines 13 and 23 respectively are

$$y = \frac{y_3}{x_3} x \tag{A .1}$$

$$y = \frac{-y_3(x - x_2)}{\delta x} \tag{A .2}$$

where $$\delta x = (x_2 - x_3) \tag{A .3}$$

The integral $\int_{\Delta} x^m y^n dxdy$ is evaluated, first by performing the integration with respect to x, and then the integration with respect to y. That is

$$\int_{\Delta} x^m y^n dxdy = \int_0^{y_3} y^n \left[\int_{\frac{x_3}{y_3} y}^{(x_2 - \frac{\delta x}{y_3} y)} x^m dx \right] dy \tag{A .4}$$

Now $$\int_{\frac{x_3}{y_3} y}^{(x_2 - \frac{\delta x}{y_3} y)} x^m dx = \frac{1}{m+1} \left[\left[x_2 - \frac{\delta x}{y_3} y \right]^{m+1} - \left[\frac{x_3}{y_3} y \right]^{m+1} \right]$$

$$= \frac{1}{m+1} \left[\sum_{r=0}^{m+1} \frac{(m+1)!}{(m+1-r)!r!} (-1)^r \left(\frac{\delta x}{y_3}\right)^r x_2^{m+1-r} y^r - \left(\frac{x_3}{y_3}\right)^{m+1} y^{m+1} \right] \tag{A .5}$$

which is obtained by using the Binomial expansion of $\{x_2 - \frac{\delta x}{y_3} y\}^{m+1}$. Multiplying by y^n and integrating with respect to y gives

$$\int_\Delta x^m y^n dxdy = \frac{y_3^{n+1}}{m+1} \left[\sum_{r=0}^{m+1} \frac{(-1)^r (m+1)!}{(m+1-r)!r!(n+r+1)} (\delta x)^r x_2^{m+1-r} - \frac{x_3^{m+1}}{(m+n+2)} \right] \qquad (A .6)$$

Now the binomial expansion of $(\delta x)^r$ is

$$(\delta x)^r = (x_2 - x_3)^r = \sum_{s=0}^{r} \frac{(-1)^s r!}{(r-s)!s!} x_2^{r-s} x_3^s \qquad (A .7)$$

Substituting (A .7) into (A .6) gives the final result that

$$\int_\Delta x^m y^n dxdy = y_3^{n+1} \left[\sum_{r=0}^{m+1} \sum_{s=0}^{r} \frac{(-1)^{r+s} m!}{(m+1-r)!(r-s)!s!(n+r+1)} x_2^{m+1-s} x_3^s - \frac{x_3^{m+1}}{(m+1)(m+n+2)} \right] \qquad (A .8)$$

(ii) $x_3 = 0$

The value of the integral when $x_3 = 0$ may be obtained by putting $x_3 = 0$ in (A .6), in which case

$$\int_\Delta x^m y^n dxdy = y_3^{n+1} x_2^{m+1} \sum_{r=0}^{m+1} \frac{(-1)^r m!}{(m+1-r)!r!(n+r+1)} \qquad (A .9)$$

(iii) $x_3 = x_2$

When $x_3 = x_2$ the integration with respect to x reduces to

$$\int_{\frac{x_3}{y_3}y}^{x_2} x^m dx = \frac{1}{m+1}\left[x_2^{m+1} - \left(\frac{x_2}{y_3}\right)^{m+1} y^{m+1} \right] \qquad \text{(A .10)}$$

Multiplying by y^n and integrating with respect to y yields

$$\int_{\Delta} x^m y^n dxdy = \frac{y_3^{n+1} x_2^{m+1}}{(n+1)(m+n+2)} \qquad \text{(A .11)}$$

TABLE NO. 1

Percentage Error in Frequency

For a Simply Supported

Rectangular Plate

Configuration	Mode Number	% Error	m	n
27 (a)	1	-2•37	2	2
27 (b)	1	-2•02	2	2
	2	-4•31	2	3
	3	+7•37	3	2
	4	-5•20	2	4
27 (c)	1	-1•48	2	2
	2	-2•55	2	3
	3	-2•48	3	2
	4	-2•76	2	4
	5	-4•14	3	3
	6	-5•02	3	4

m = number of node lines including boundaries in the direction of the short sides.

n = number of node lines including boundaries in the direction of the long sides.

TABLE NO. 2

Number of nodal lines m and n in the directions of the short and long sides of a simply supported rectangular plate

Mode Number	m	n
1	2	2
2	2	3
3	3	2
4	2	4
5	3	3
6	3	4
7	2	5
8	4	2
9	4	3
10	3	5

TABLE No. 3

Comparison of calculated frequencies for different local axis systems of a simply supported rectangular plate

Mode Number	% Error in calculated frequency	
	28 (b)	28 (c)
1	-3·77	-15·22
2		
3	-3·31	-12·35
4	-4·42	-9·15
5	-1·74	+6·05
6	-5·05	+1·83
7	-2·11	-7·01
8	-2·97	-15·02
9	-1·36	+7·15
10	-3·98	+2·84

TABLE NO. 4

Comparison of calculated and experimental frequencies of a cantilevered triangular plate

Mode Number	Experimental Frequencies (ref. 29)	% Error in calculated frequency		
		ms = 5	ms = 5	ms = 10
		28 (a)	28 (b)	28 (b)
1	37·5	+2·40	-2·43	-2·88
2	161·0	+1·02	-0·82	-3·26
3	243·0	+0·49	+8·65	+0·75
4	392·0	+2·27	+9·43	-1·48
5	592·0	-1·84	+5·76	-0·76
6	744·0	+2·34	+18·98	+0·79

TABLE NO. 5

Comparison of finite element solution with a Rayleigh-Ritz solution of a clamped circular plate

Mode Number	n	s	% Error in frequency	
			m.s. = 5	m.s. = 8
1	0	0	-12·26	-5·65
2	1	0	-6·72	-3·01
3	2	0	-5·72	-1·89
4	0	1	-9·71	-5·51

n = number of nodal diameters. s = number of nodal circles.

TABLE No. 6

Natural frequencies of a cylindrical shell

Mode Number	m	n	Frequency Kc/s		% error
			Experimental	Finite Element	
1	1	2	2·06	2·25	+9·2
2	1	3	2·37	2·46	+3·8
3	2	3	4·05	2·96	-26·9
4	1	4	4·13	4·13	0·

m = number of axial half waves

n = number of circumferential waves

TABLE No. 7

Comparison of theoretical and experimental buckling stresses

Crack length ins.	Plate width ins.	Buckling stress lb./in.^{2}	
		Experimental	Theoretical
3·5	10·0	$17·2 \times 10^3$	$21·09 \times 10^3$
5·0	10·0	$7·6 \times 10^3$	$8·89 \times 10^3$
5·0	20·0	$7·6 \times 10^3$	$11·47 \times 10^3$
5·0	40·0	$21·6 \times 10^3$	$24·98 \times 10^3$

Fig.1. Variation in frequency of fundamental mode with applied tensile stress.

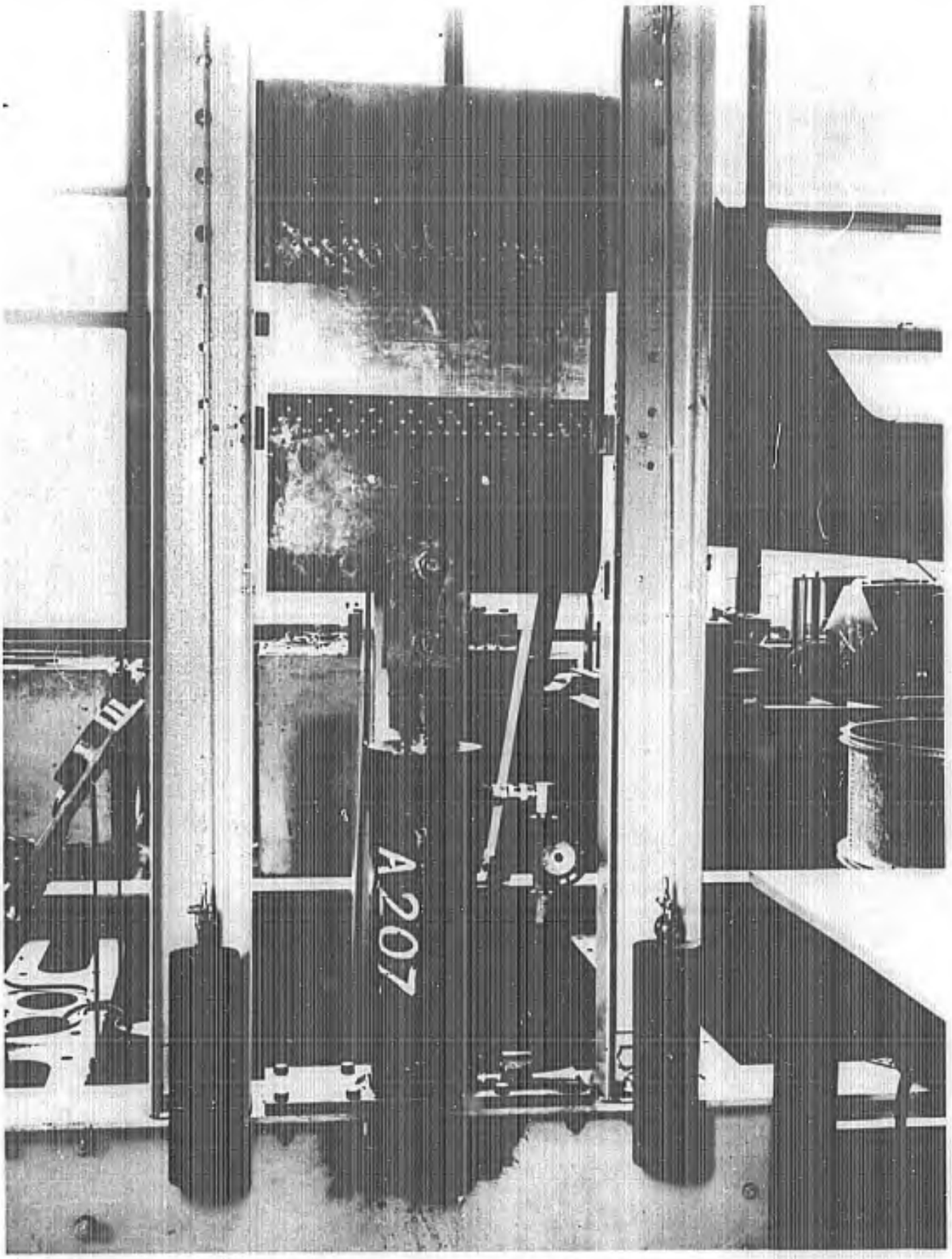

Fig. 2. View of test rig.

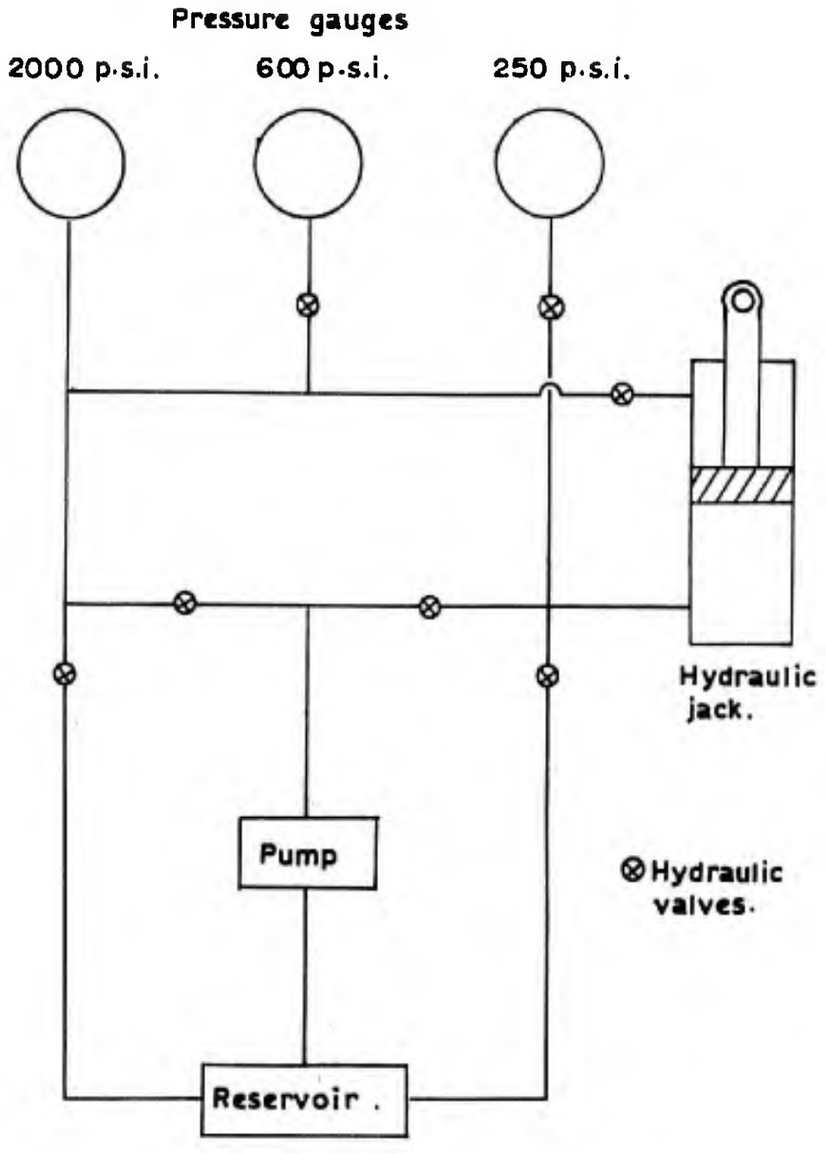

Fig. 3 Hydraulic system .

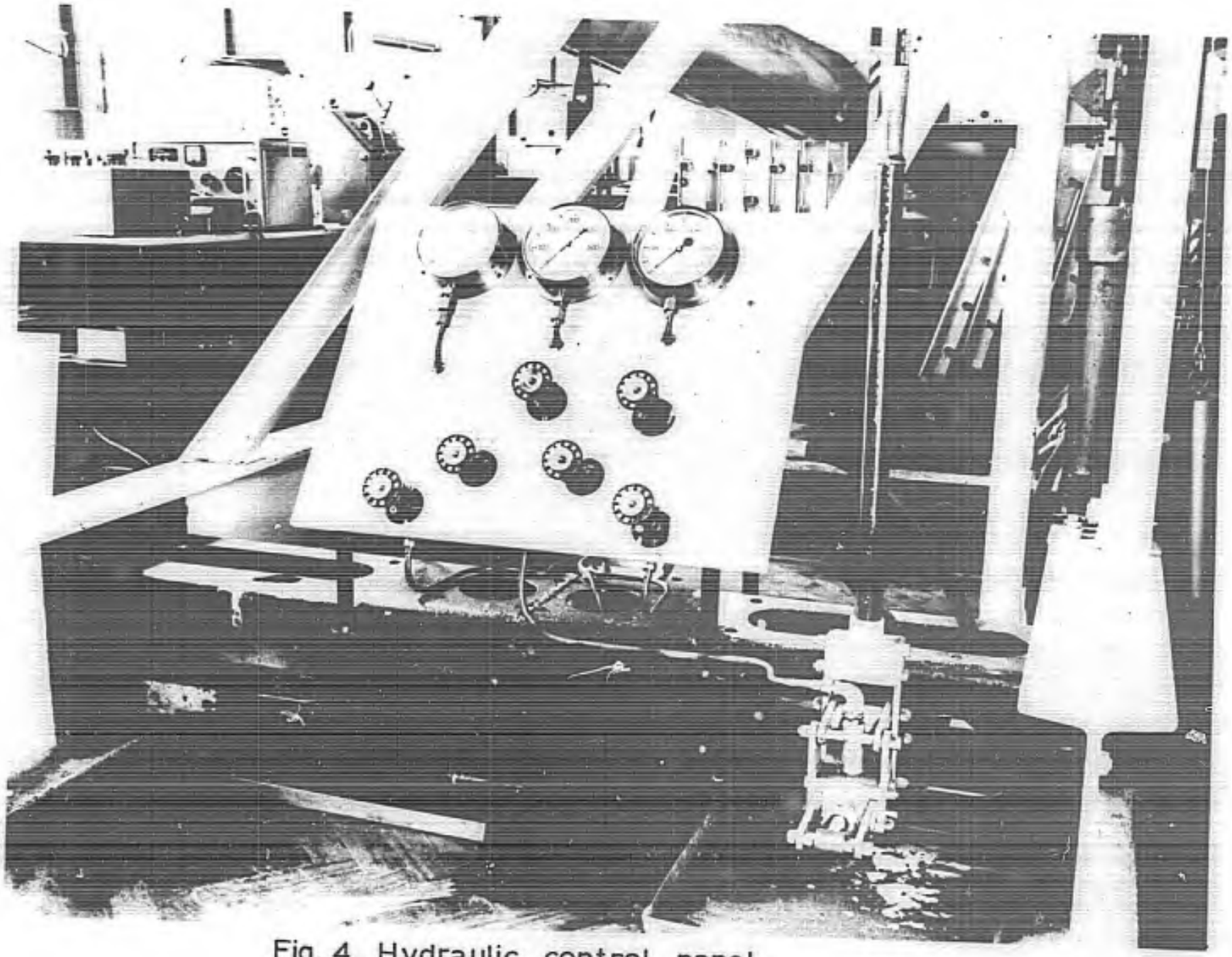

Fig. 4 Hydraulic control panel.

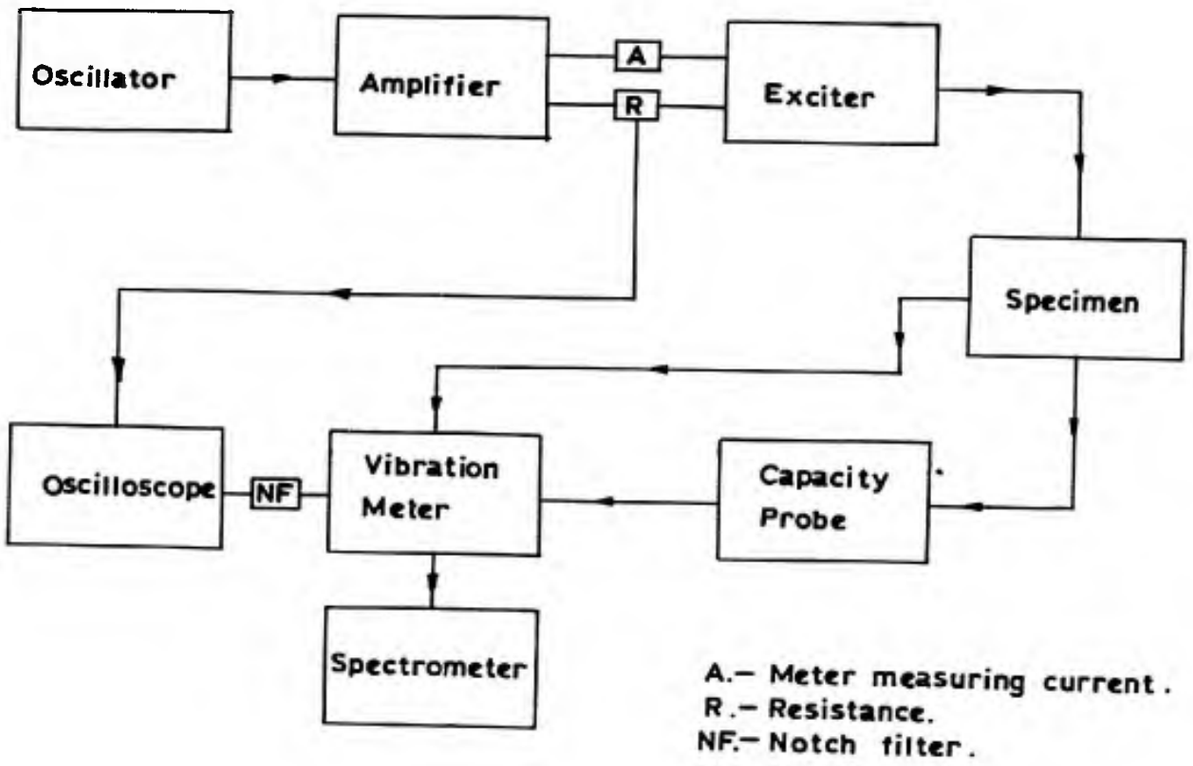

Fig. 5. Block diagram of instrumentation.

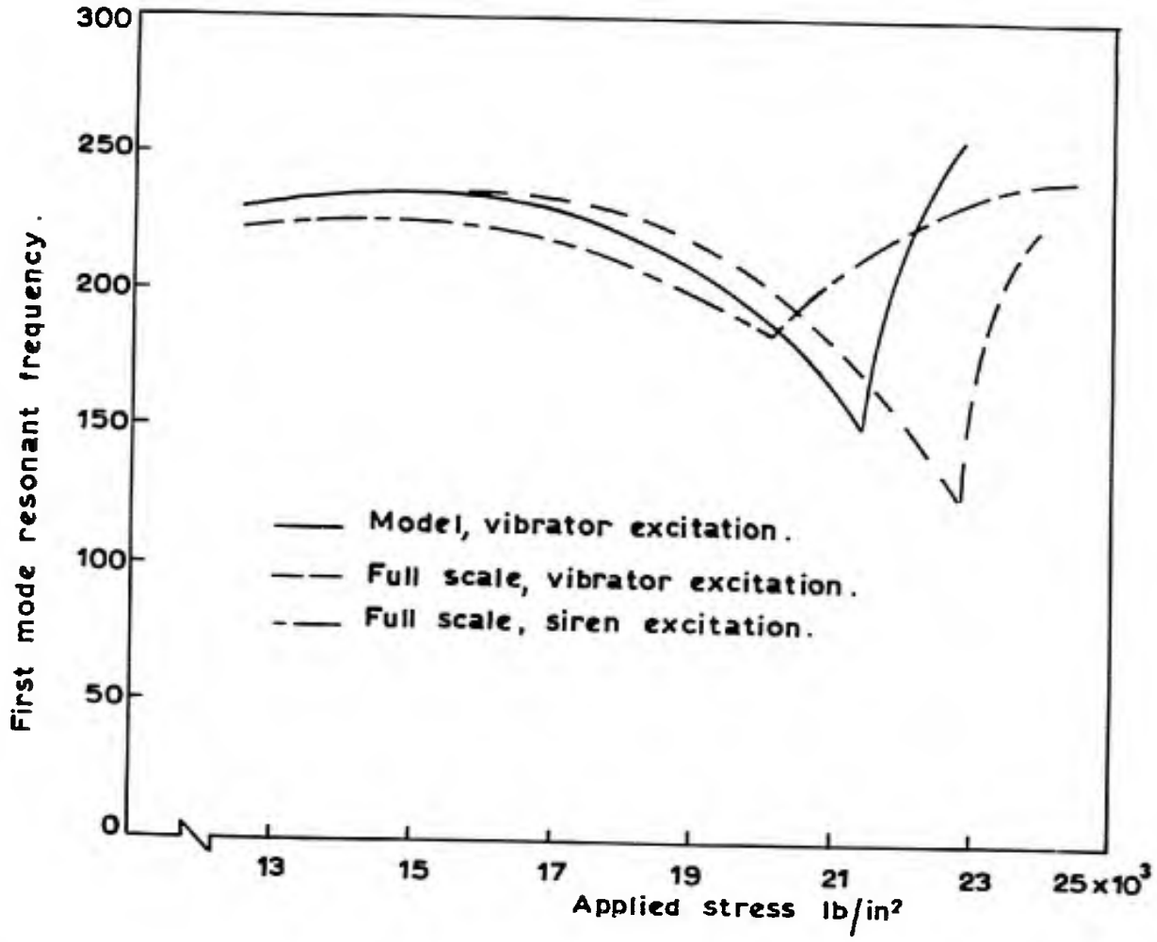

Fig. 6. Comparison of frequency-stress for model and full scale specimens.

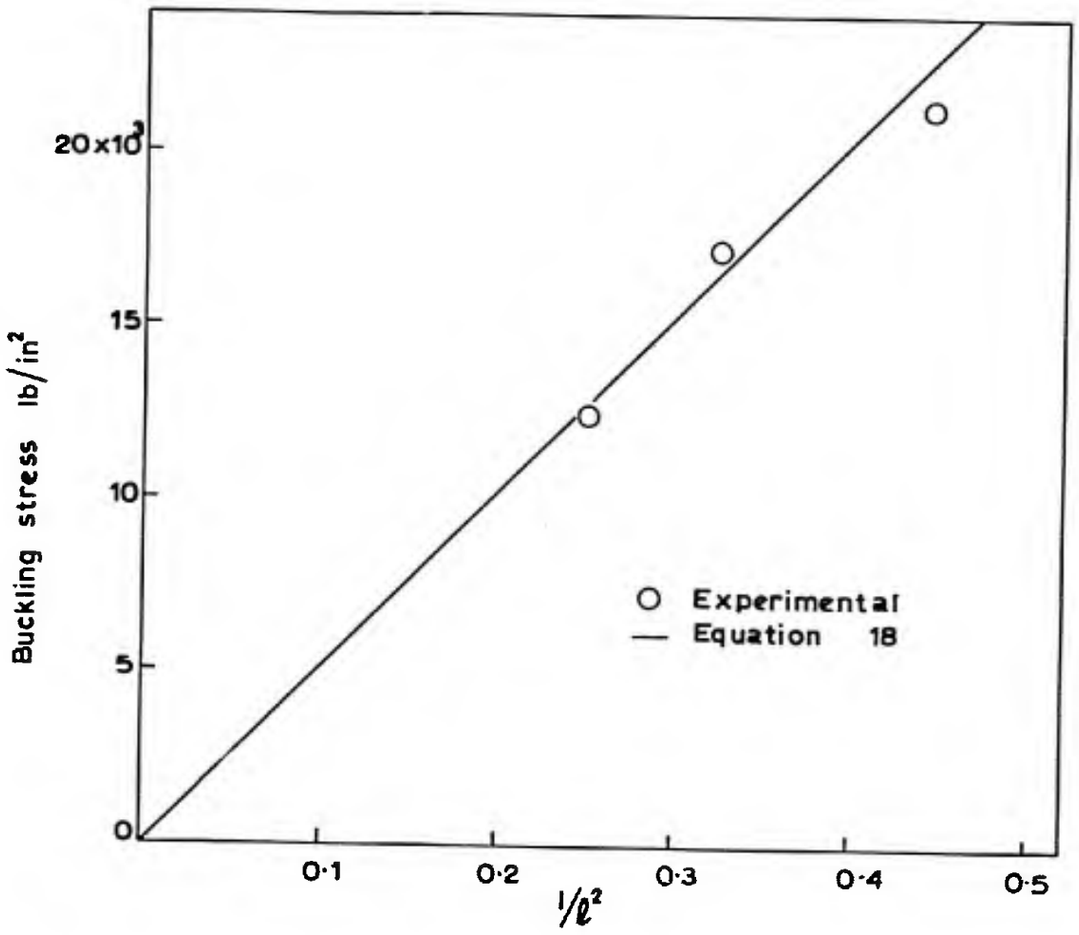

Fig. 7. Comparison of model and full scale buckling stresses.

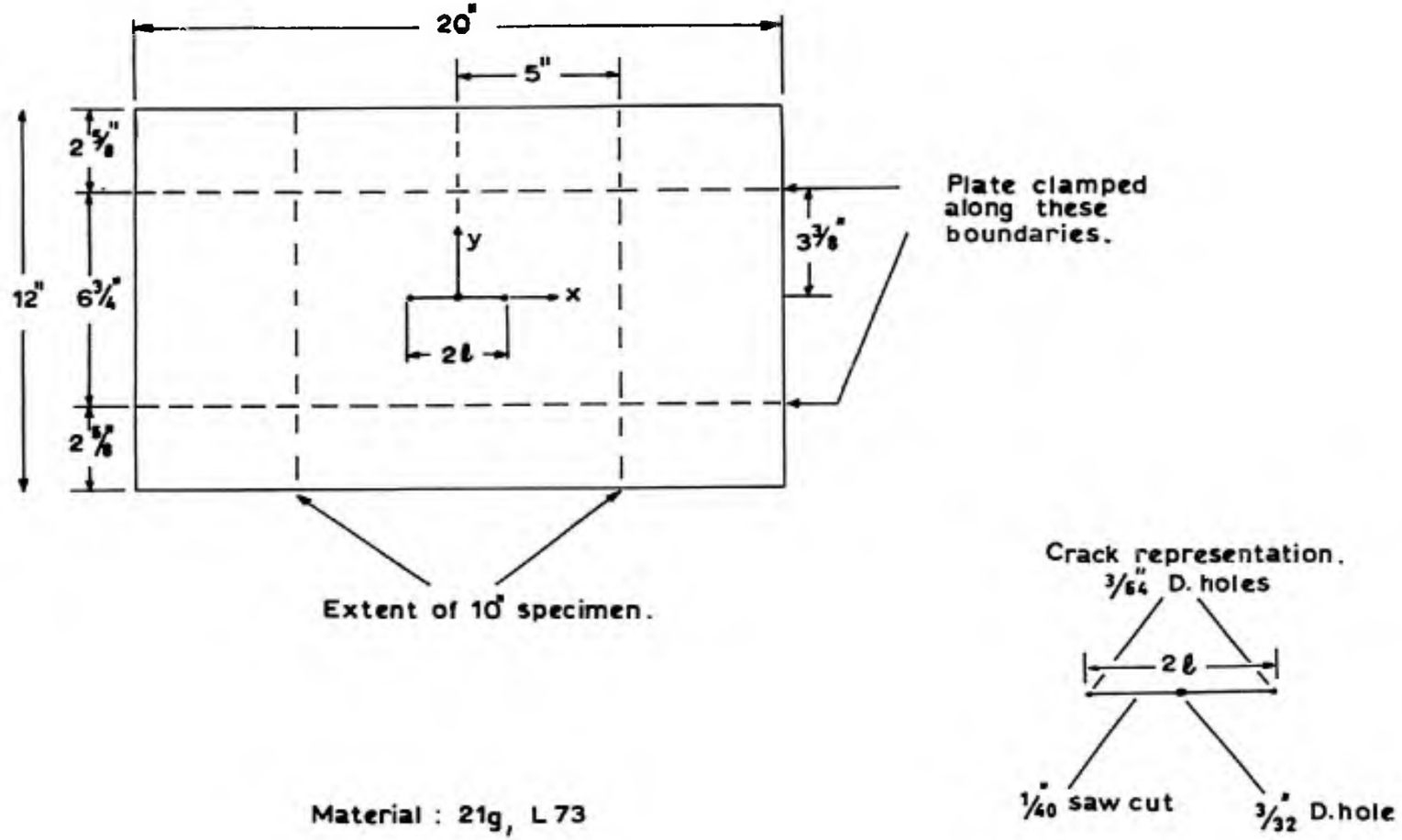

Fig. 8. Details of test specimens.

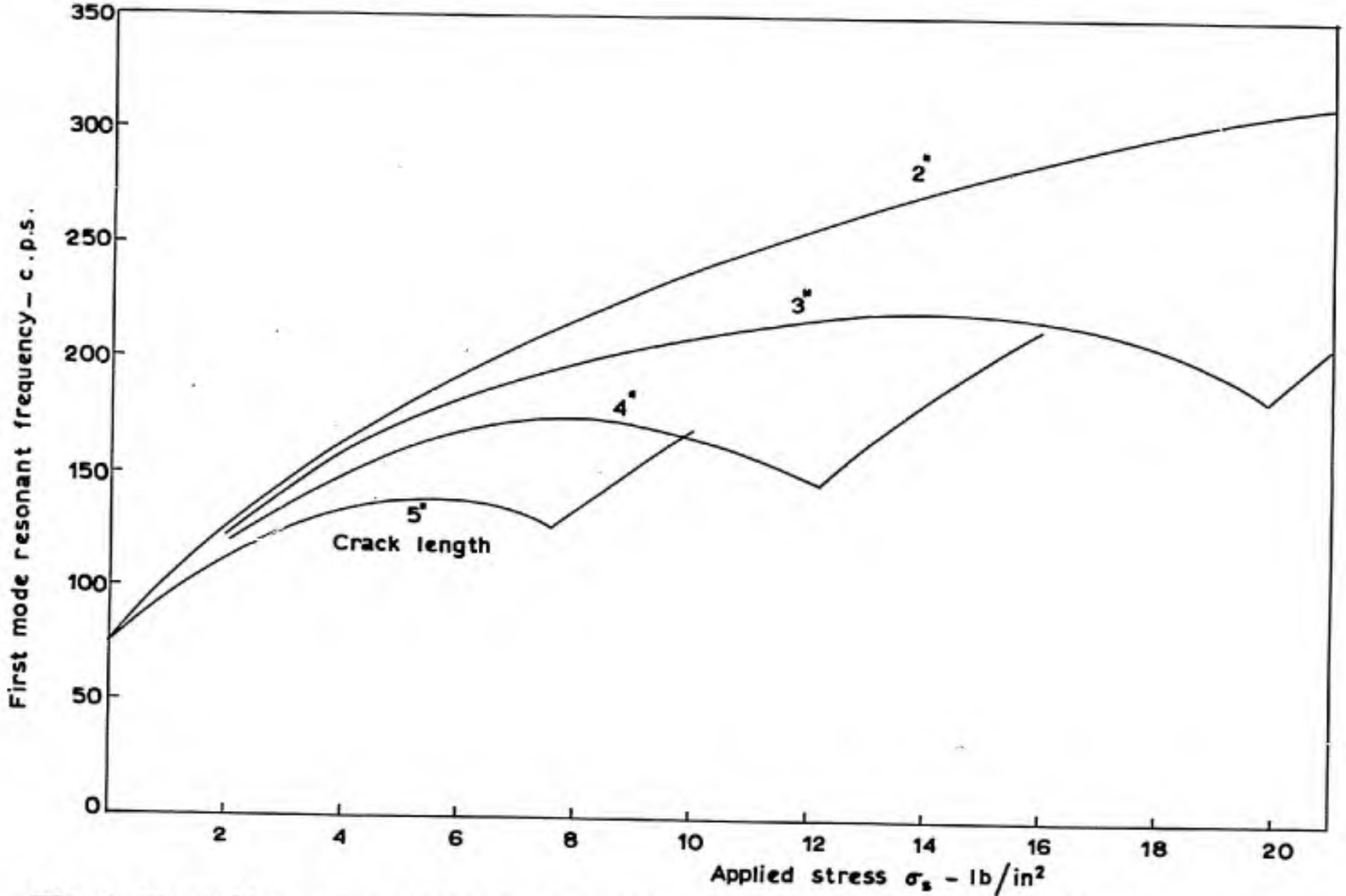

Fig. 9 . Variation of frequency with tensile stress and crack length for 10" wide plate.

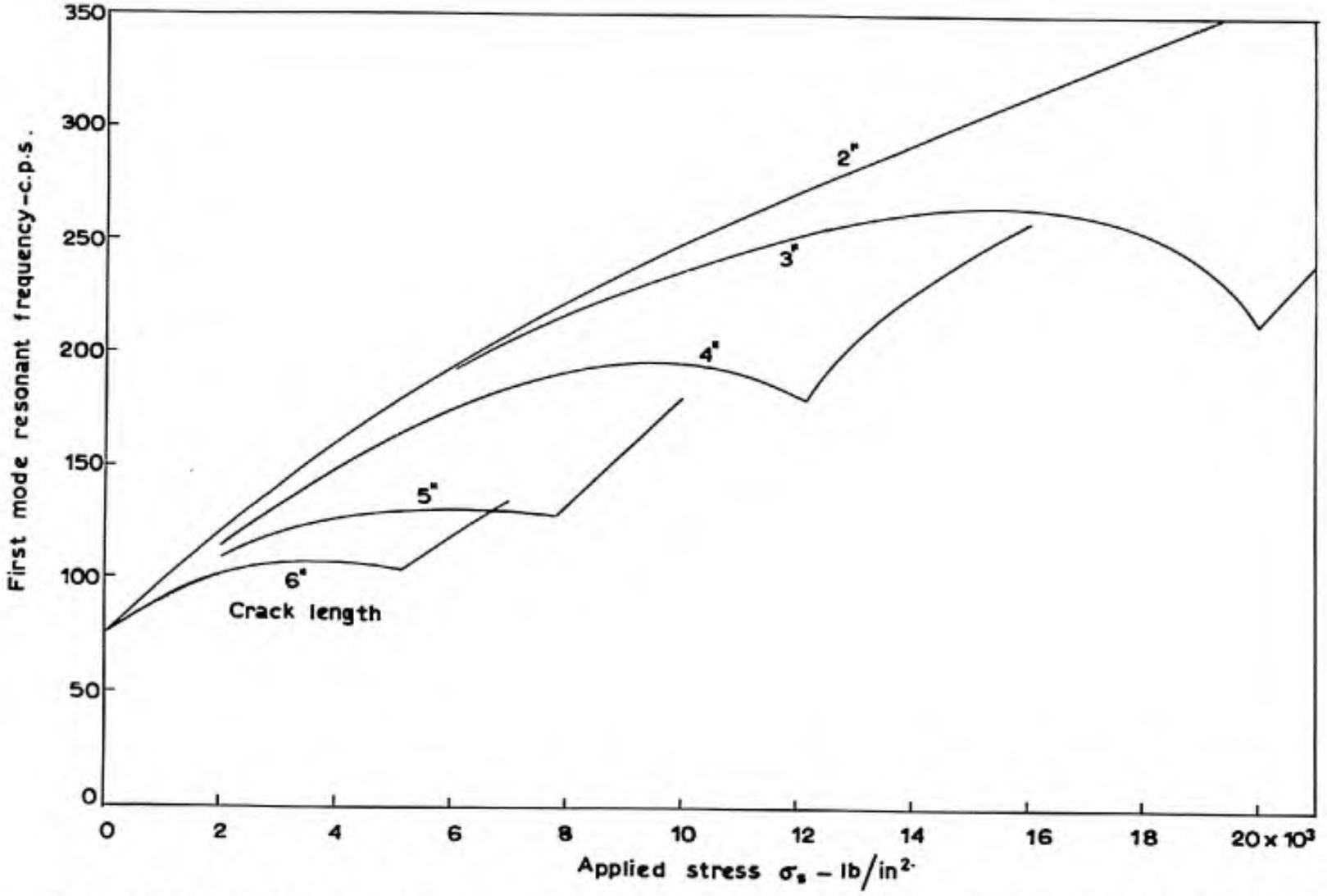

Fig. 10 Variation of frequency with tensile stress and crack length for 20" wide plate.

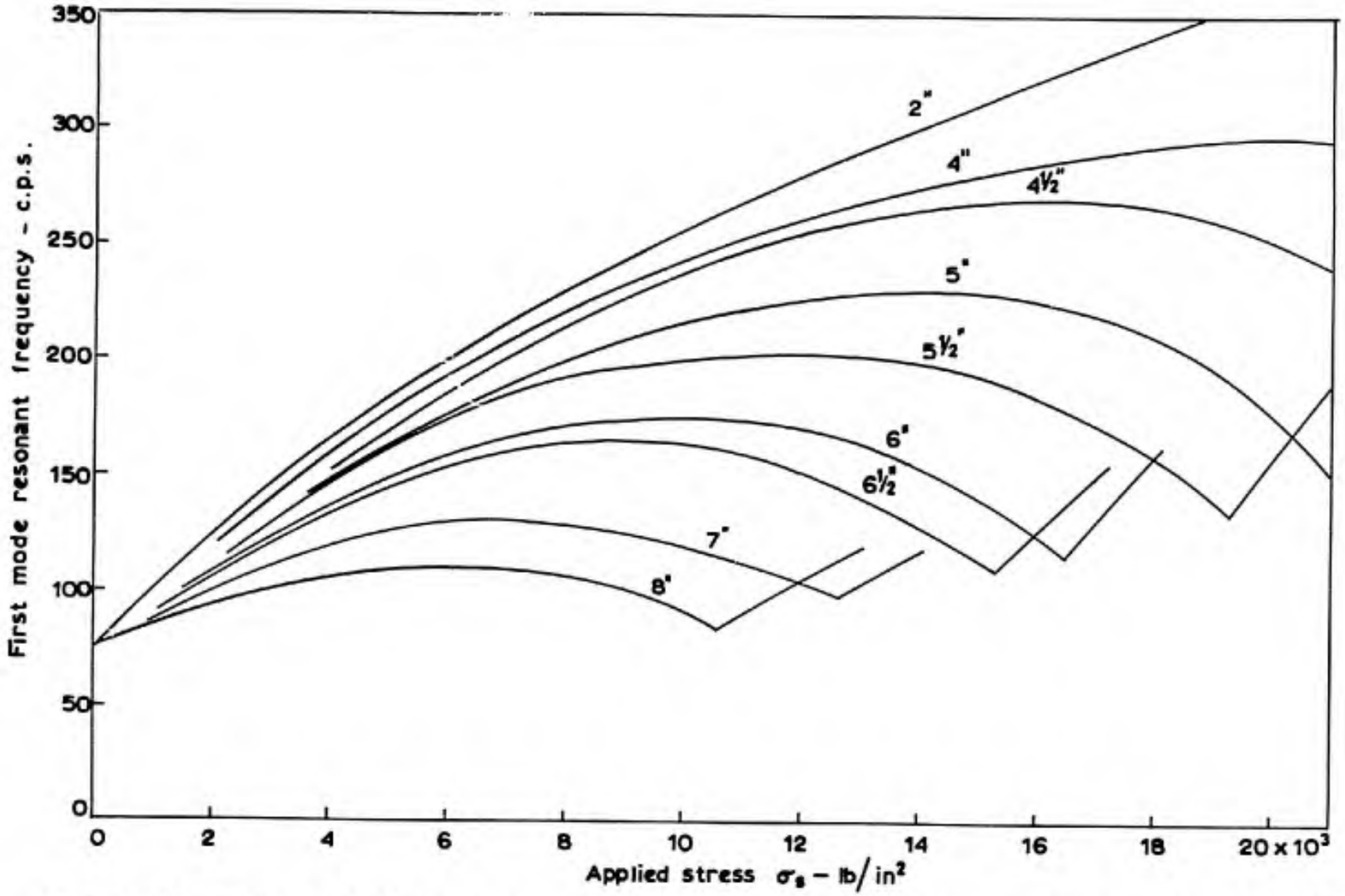

Fig. 11. Variation of frequency with tensile stress and crack length for 40" wide plate.

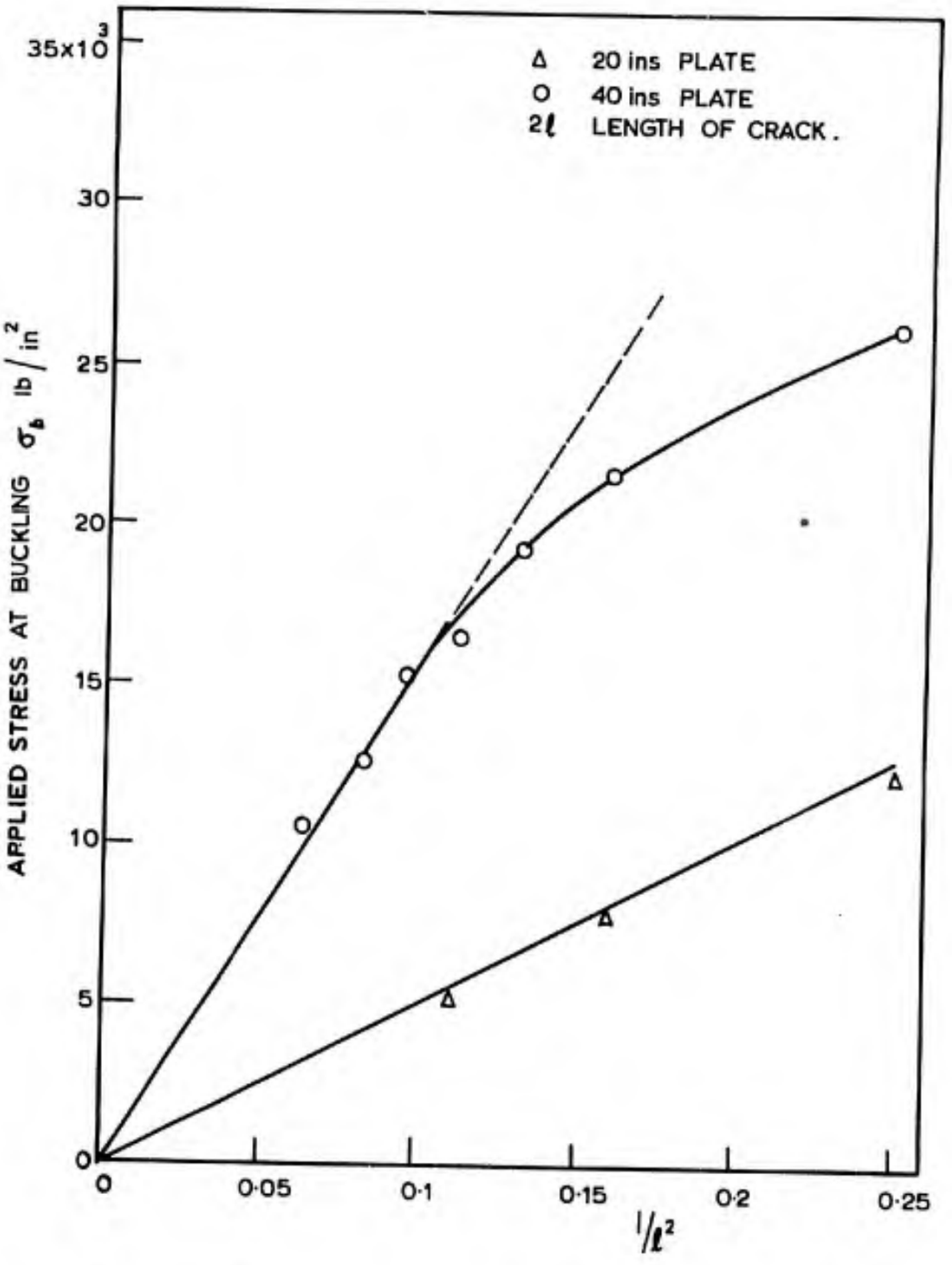

Figure 12 Variation of buckling stress with crack length and plate width.

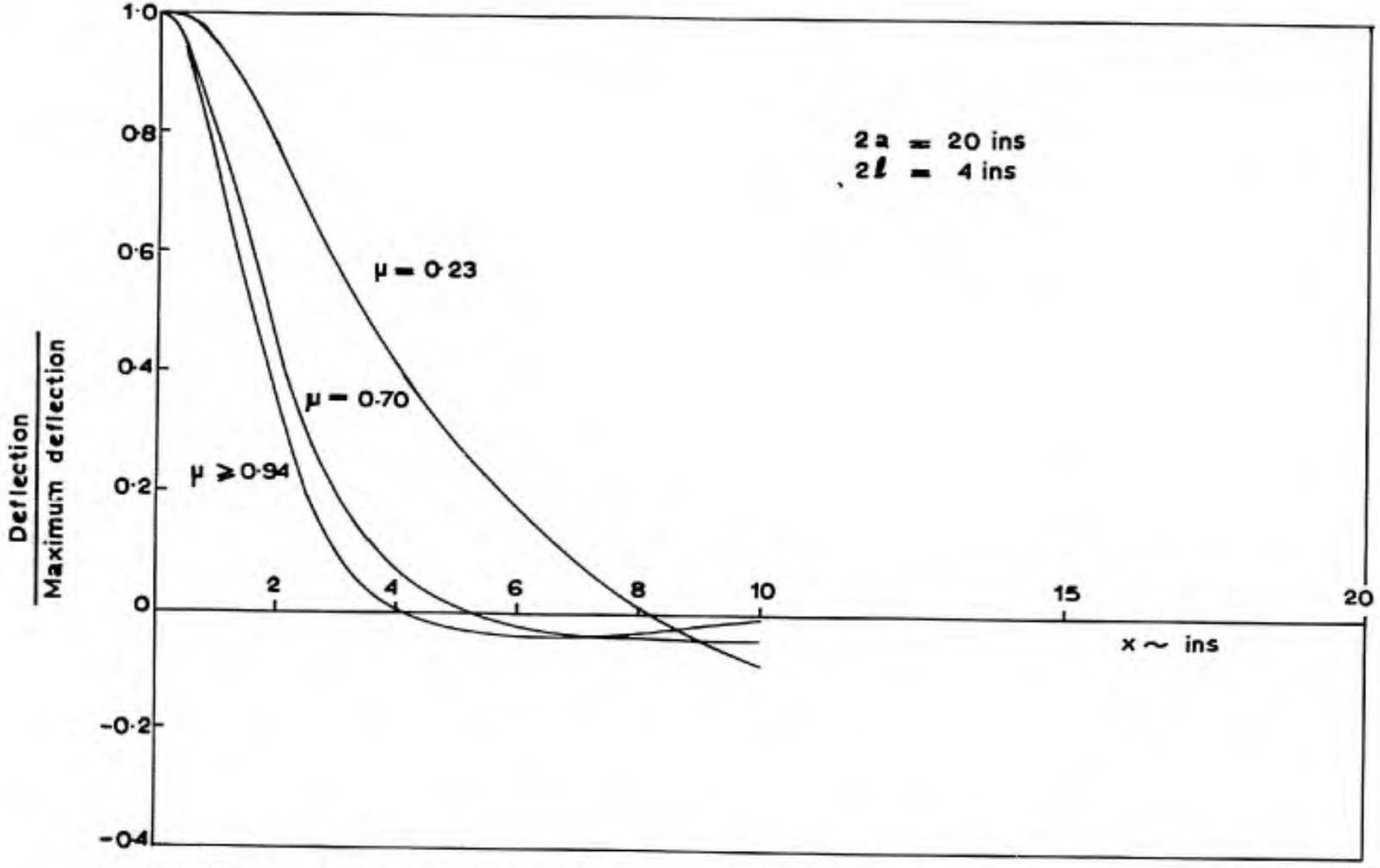

Fig.13. Dynamic deflection modes for varying stress.

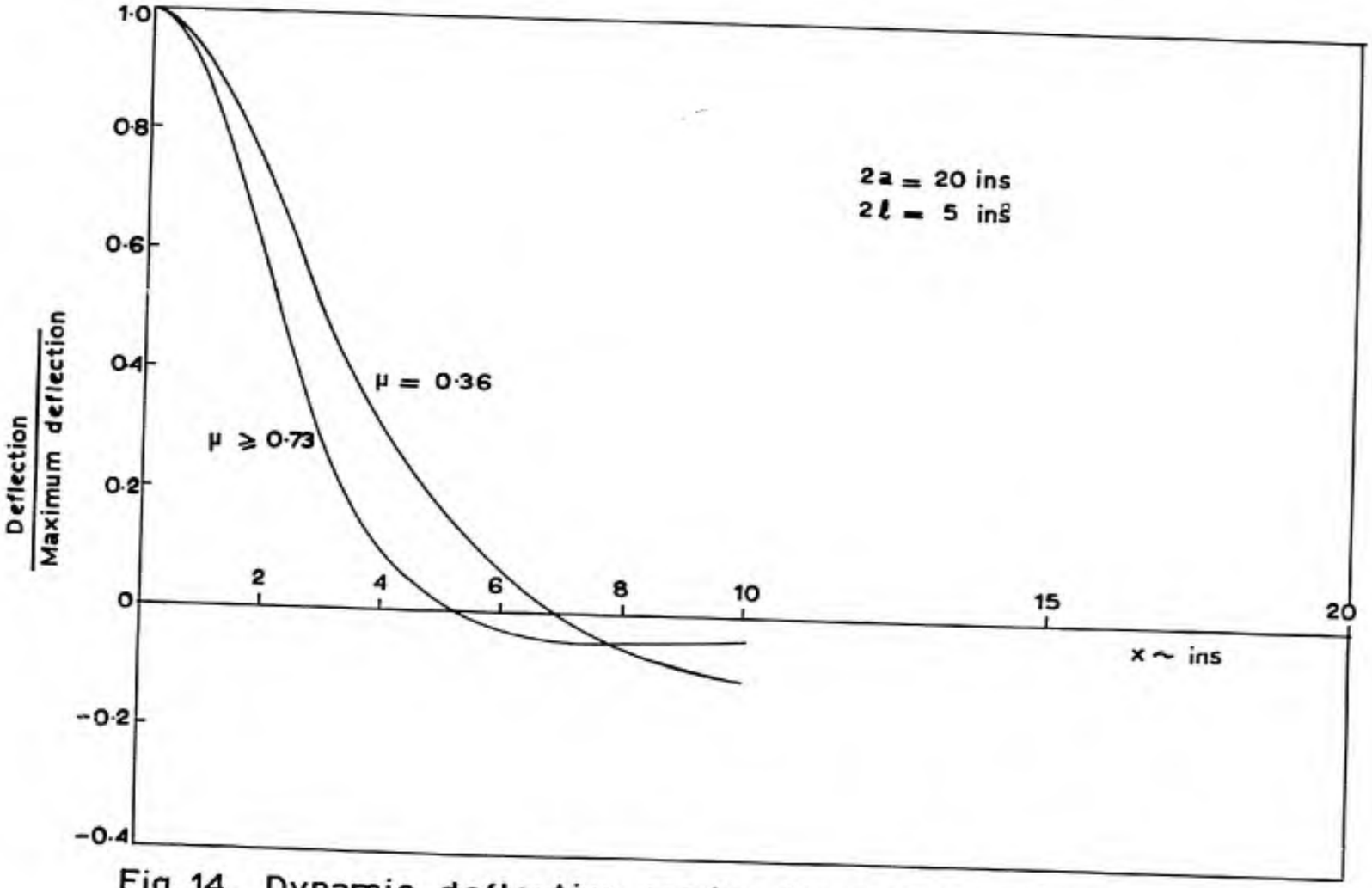

Fig. 14. Dynamic deflection modes for varying stress.

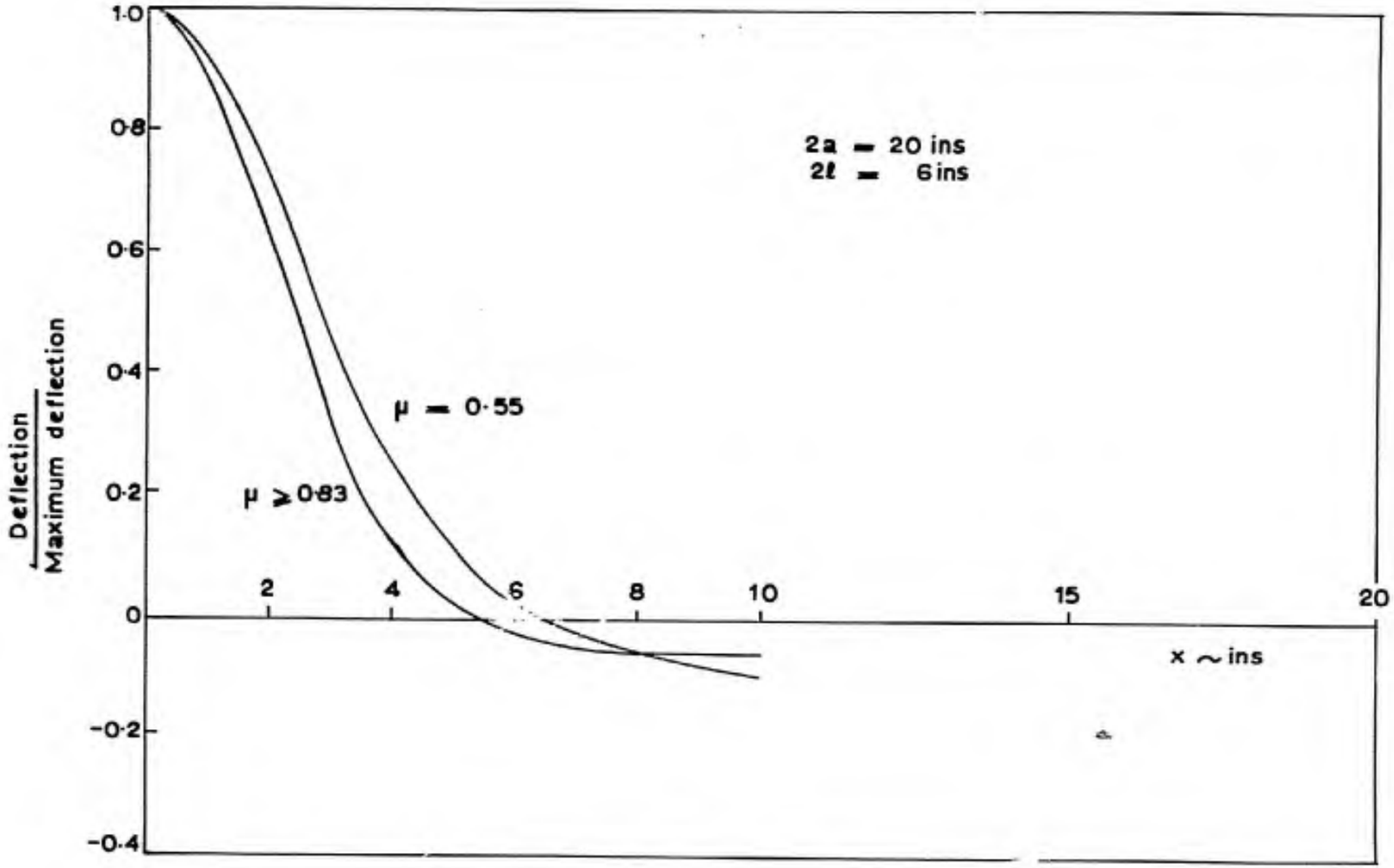

Fig. 15. Dynamic deflection modes for varying stress.

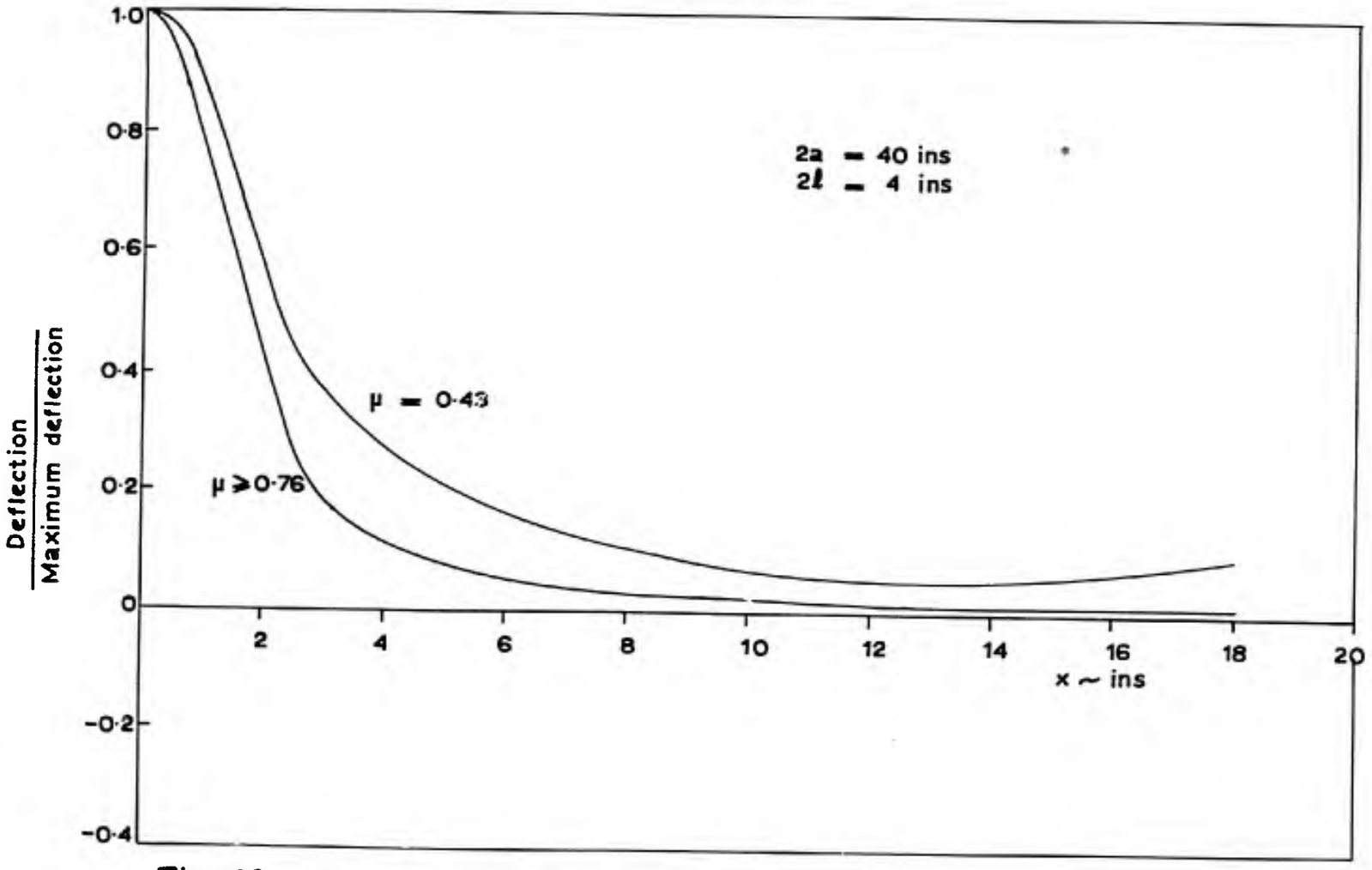

Fig. 16. Dynamic deflection modes for varying stress.

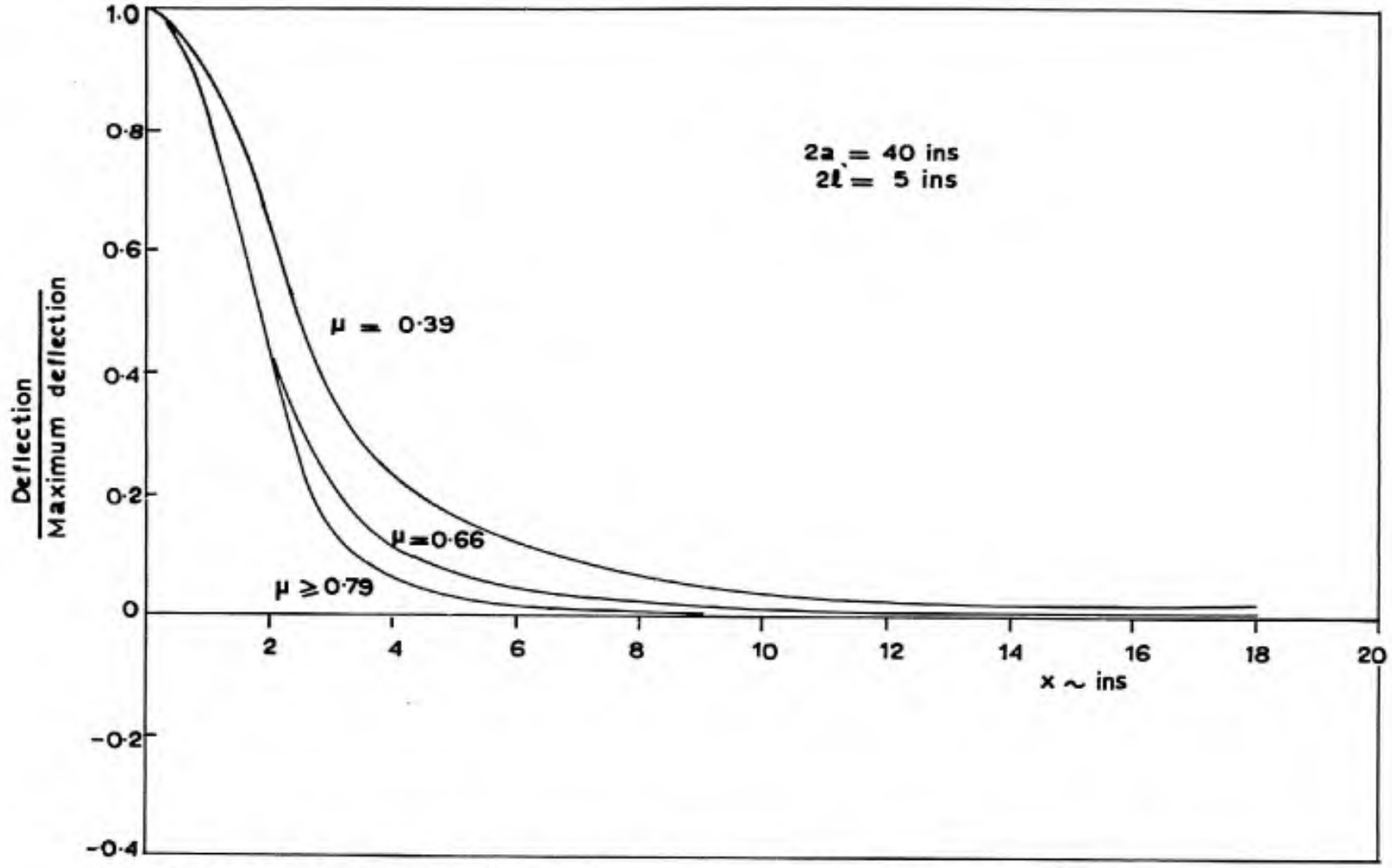

Fig. 17. Dynamic deflection modes for varying stress.

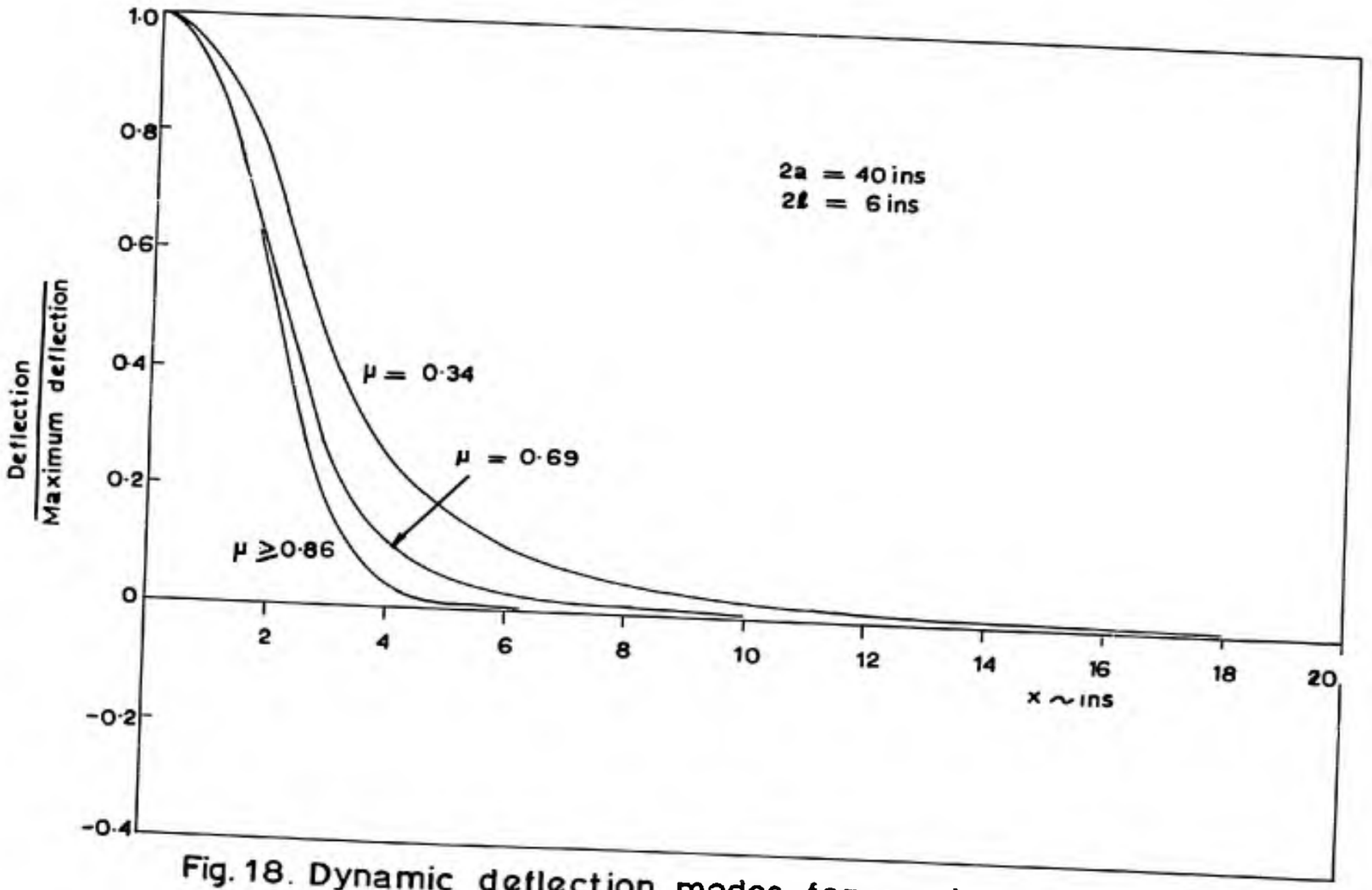

Fig. 18. Dynamic deflection modes for varying stress.

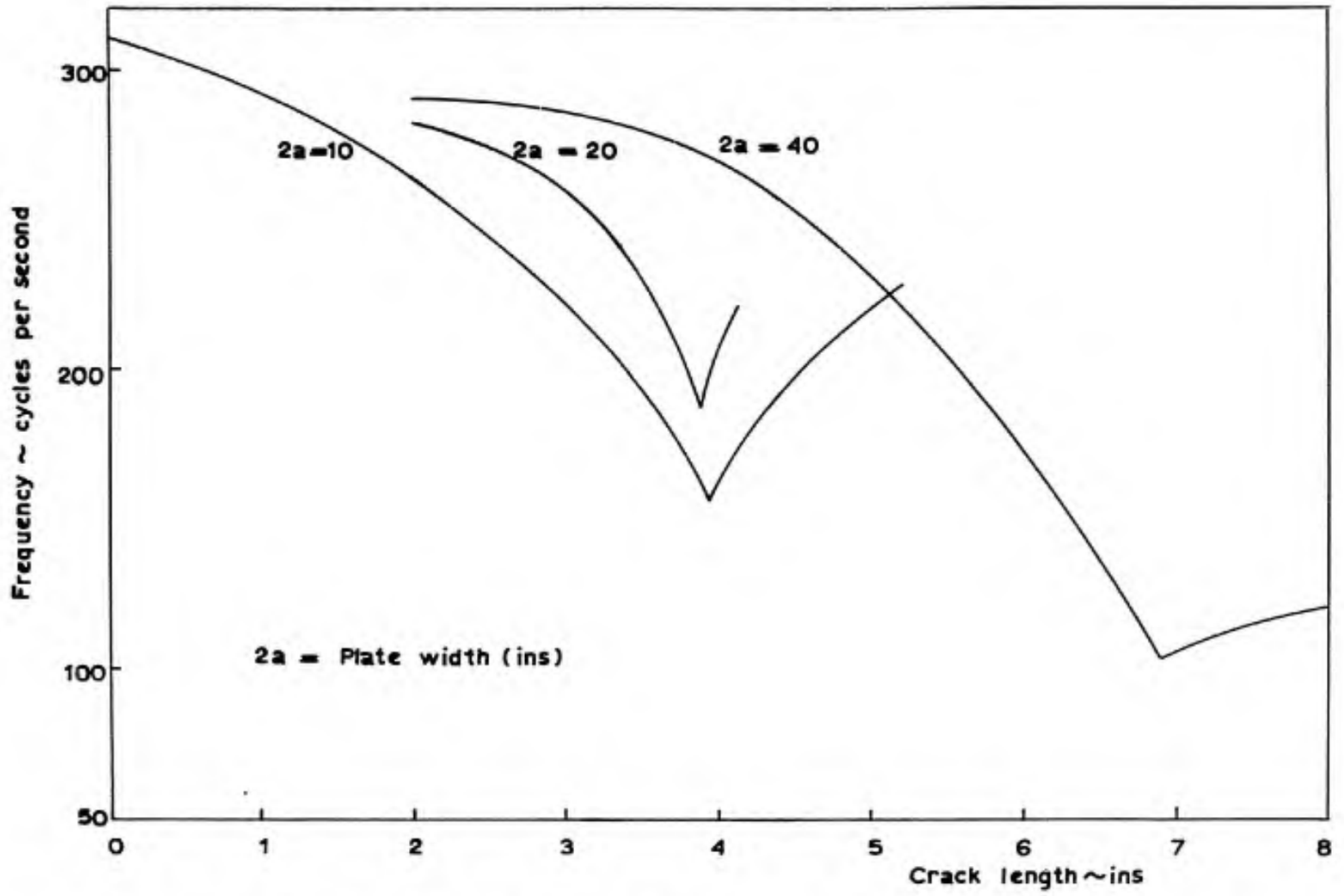

Fig. 19. Variation of frequency of fundamental mode with crack length σ_s = 13,000 lb/in^2

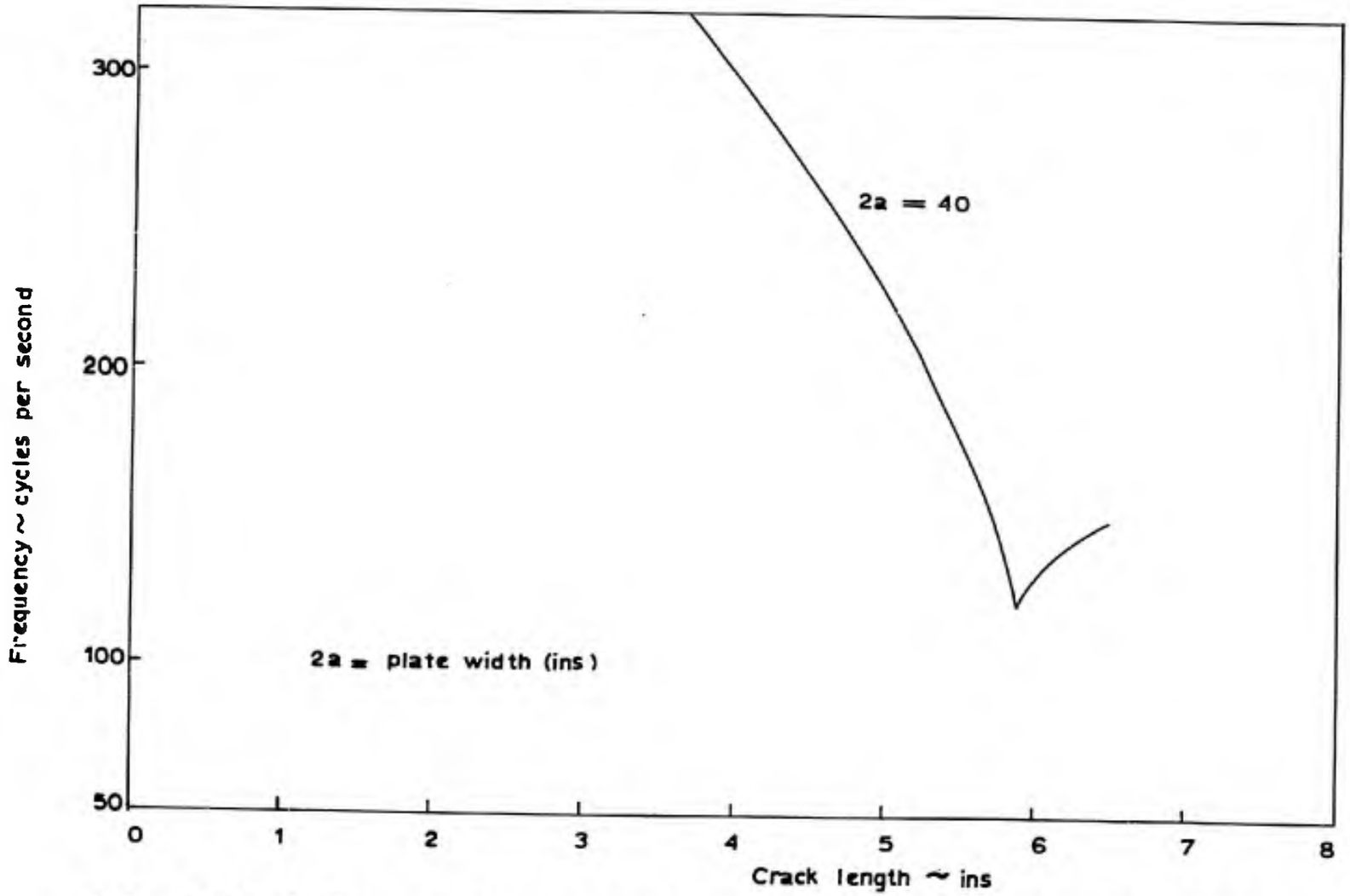

Fig. 20. Variation of frequency of fundamental mode with crack length σ_s = 17,000 lb/in^2

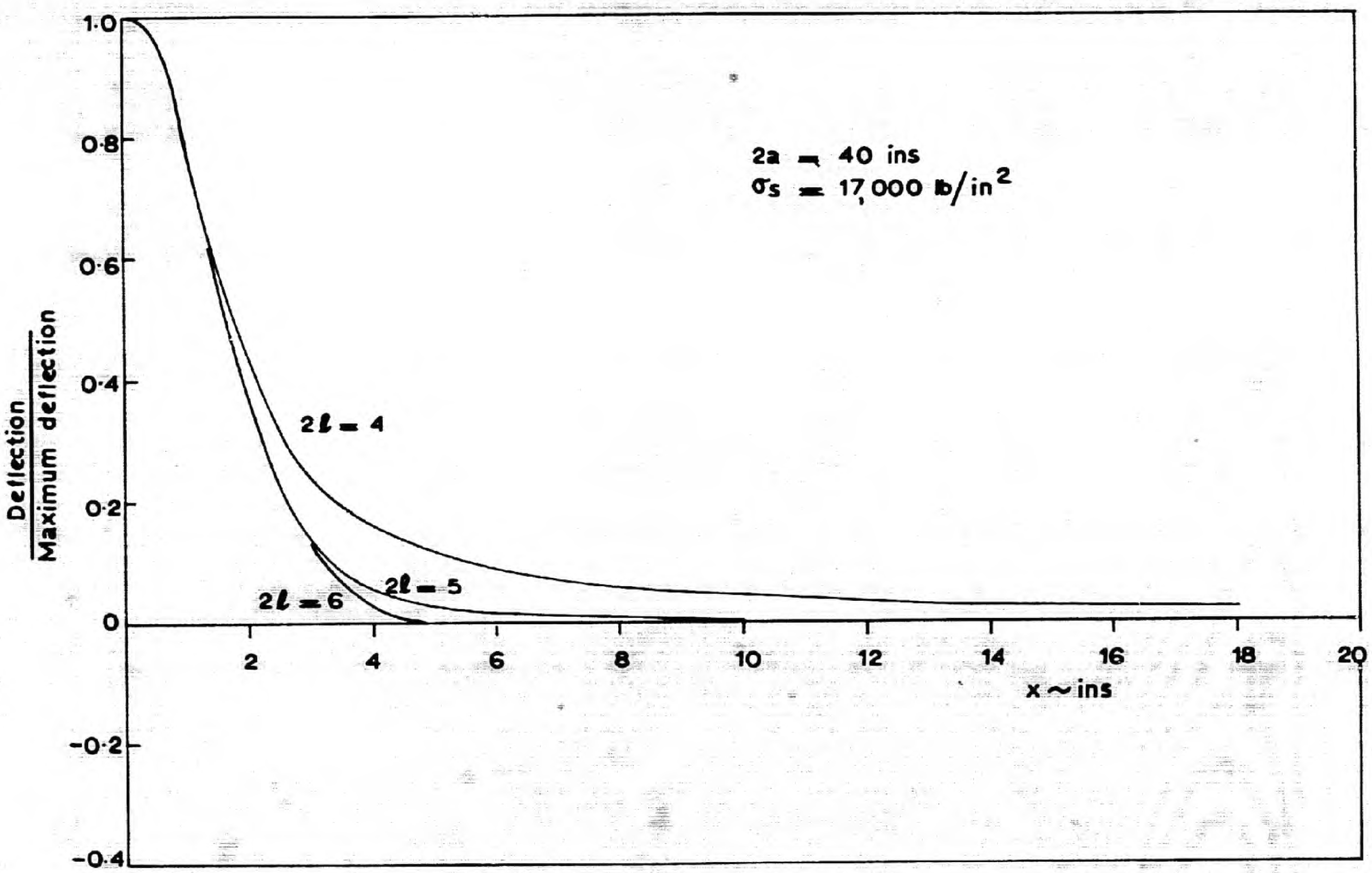

Fig. 21. Dynamic deflection modes for varying crack length.

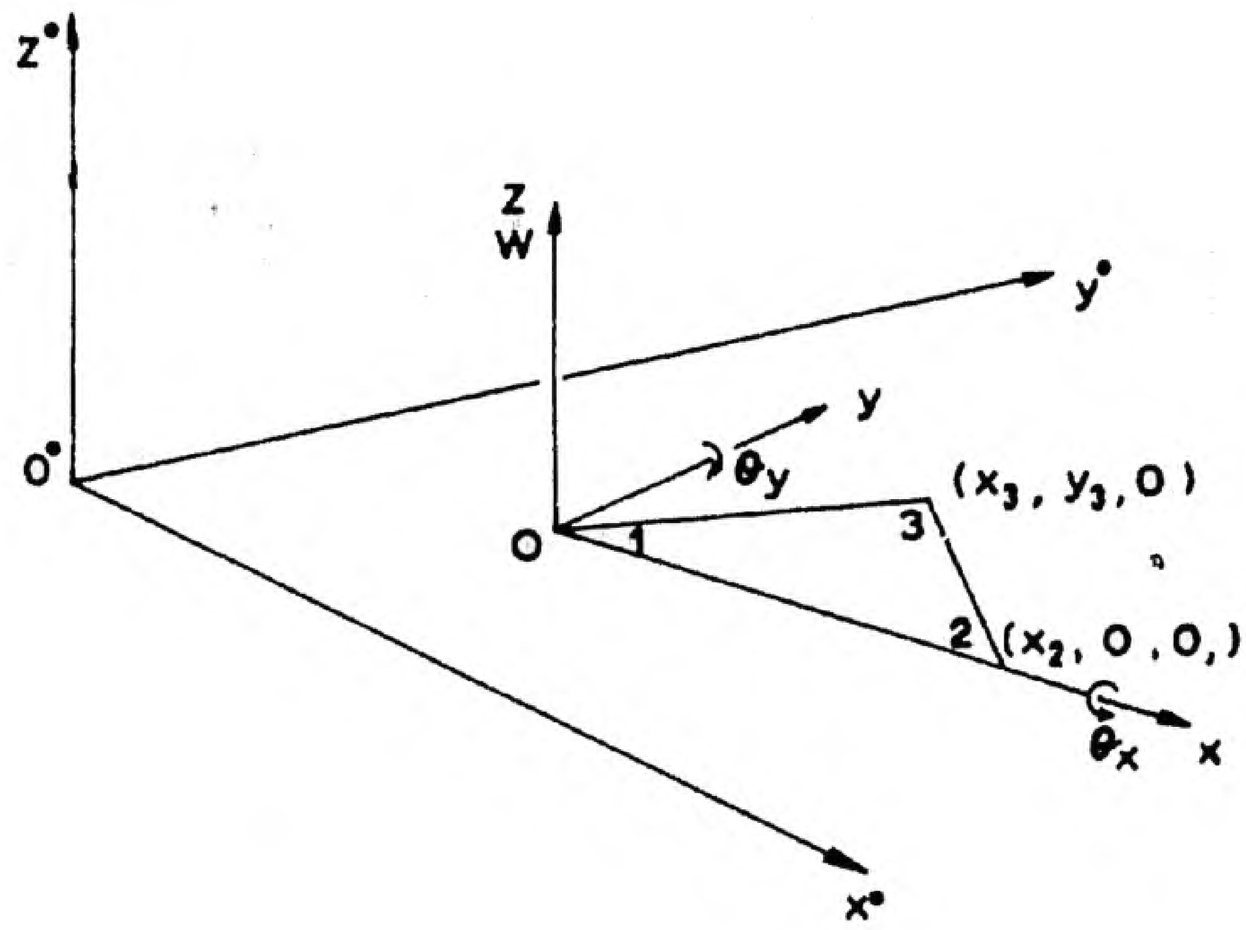

Fig. 22 Geometry of triangular element.

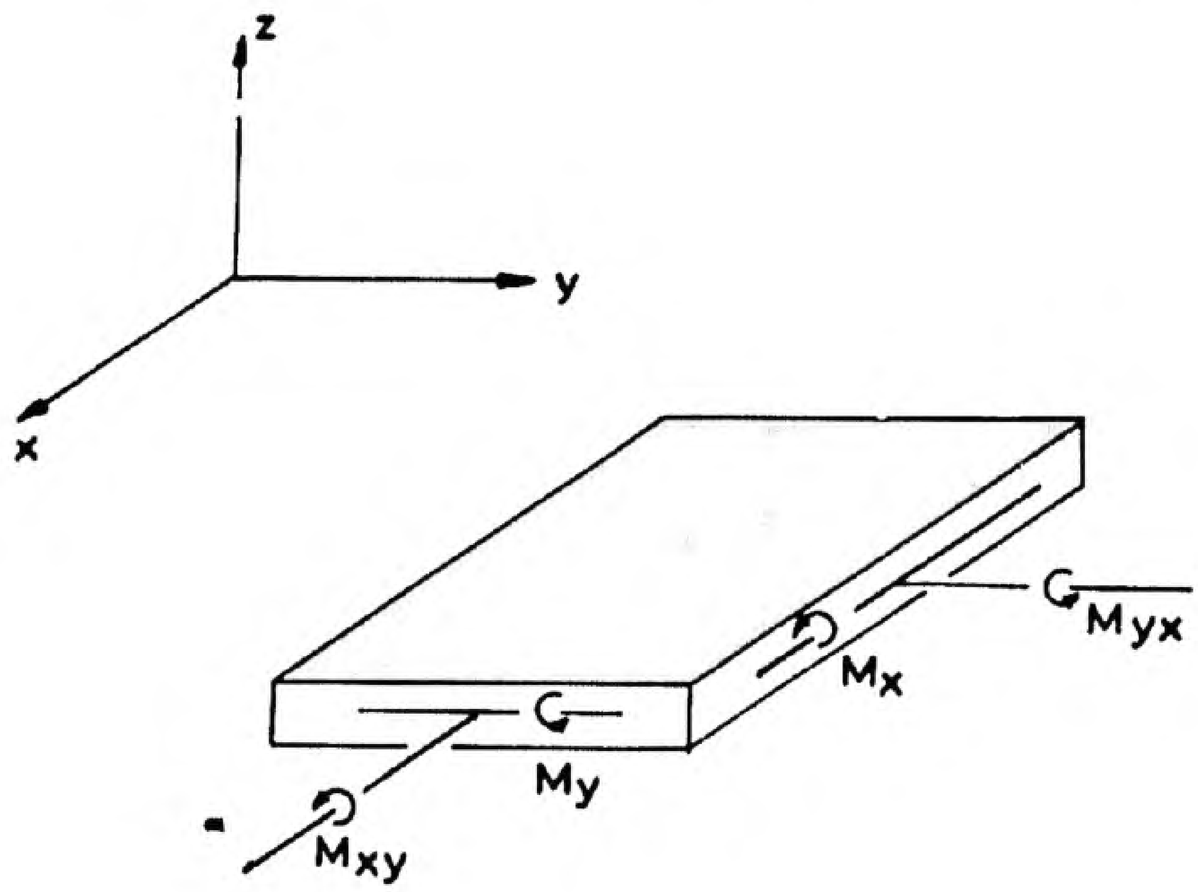

Fig. 23. Sign convention for stress resultants.
(Plate bending.)

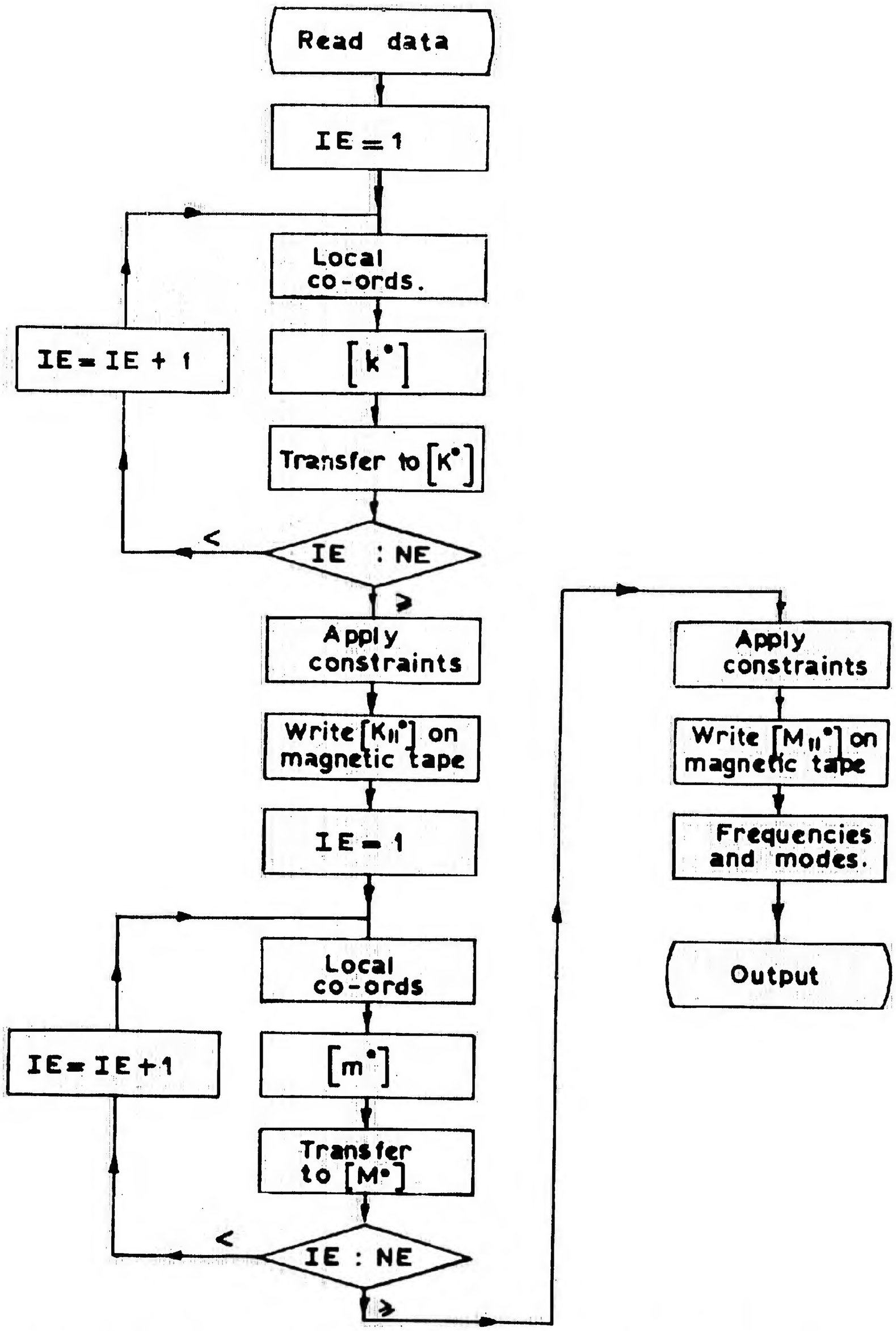

Fig. 24. Flow diagram for calculating flat plate vibrations.

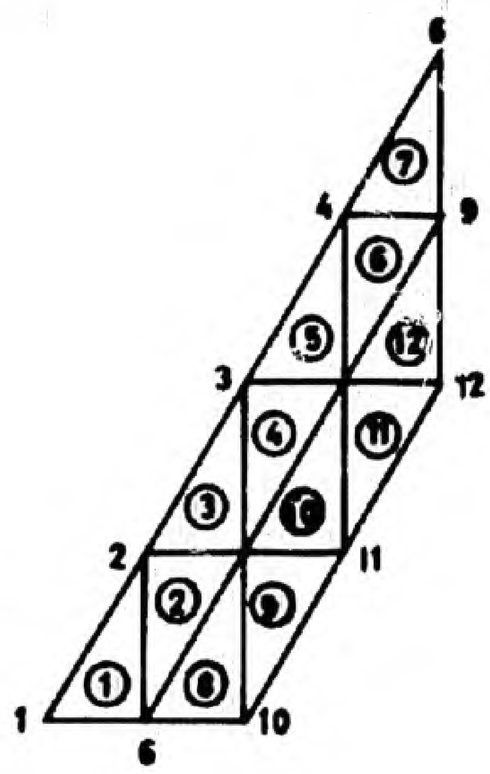

NE = 12 NP = 12 NPR = 3

$$\{NPC\} = \begin{bmatrix} 5 \\ 4 \\ 3 \end{bmatrix} \qquad [NGE] = \begin{bmatrix} 2 & 1 & 6 \\ 6 & 7 & 2 \\ \vdots & \vdots & \vdots \\ 9 & 8 & 12 \end{bmatrix}$$

Fig. 25. Idealisation and preparation of data for flat plates.

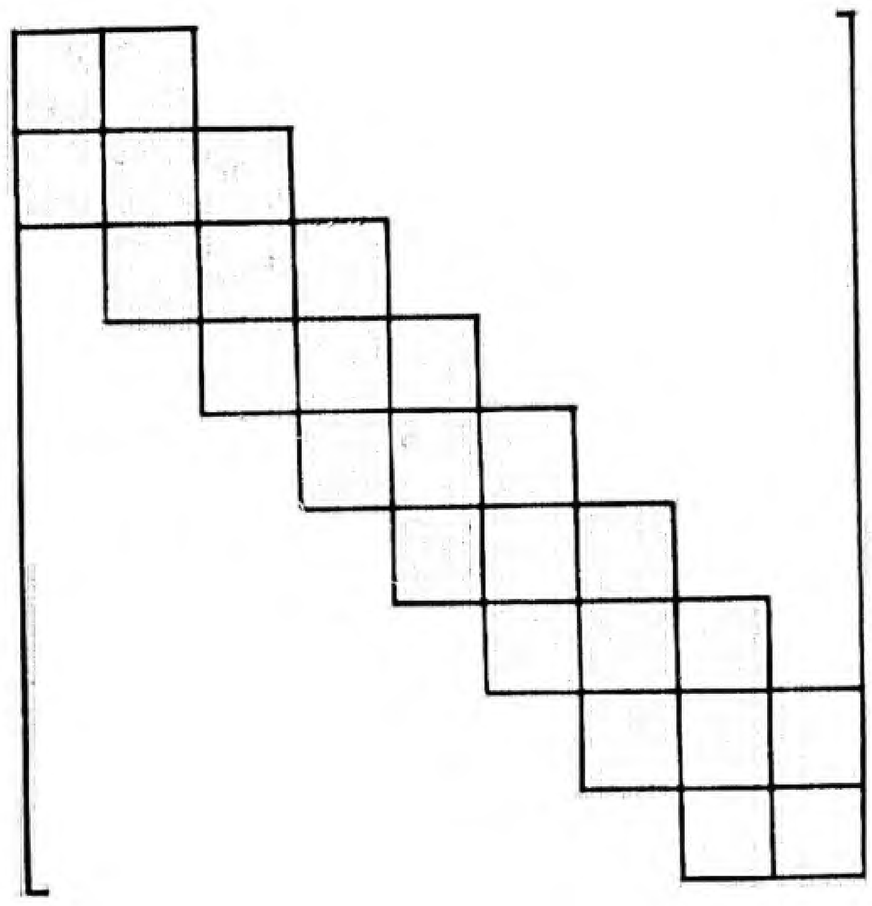

Fig. 26. Illustration of a triple band matrix.

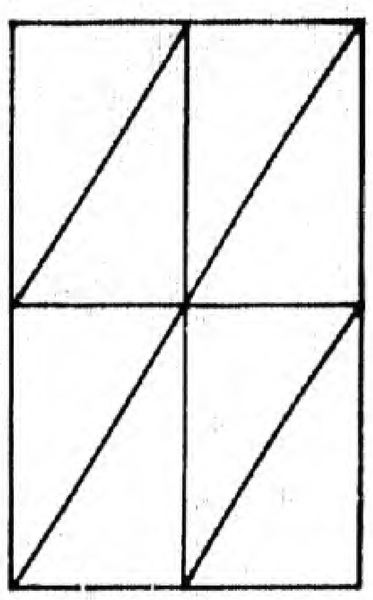

Fig 27 (a)

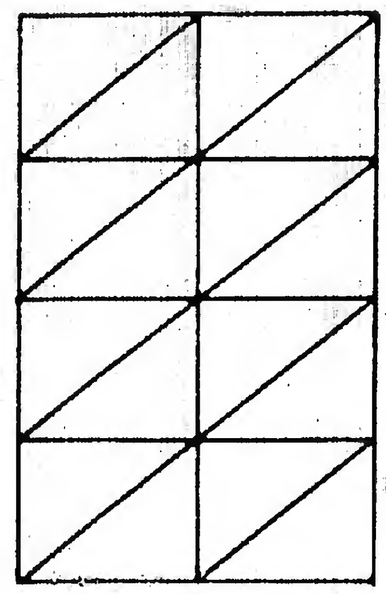

Fig. 27 (b)

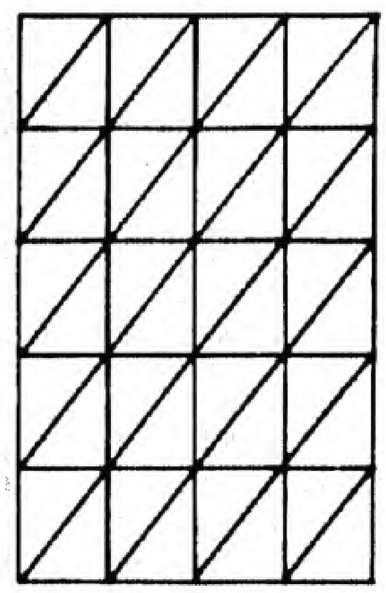

Fig. 27(c)

Fig. 27. Idealisation of a rectangular plate.

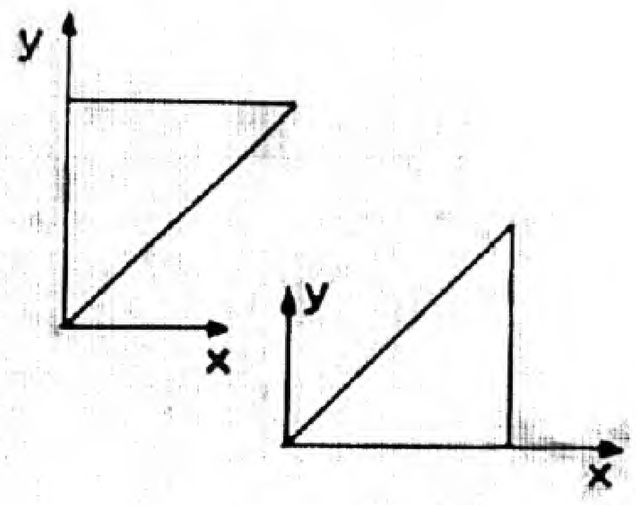

Fig. 28(a)

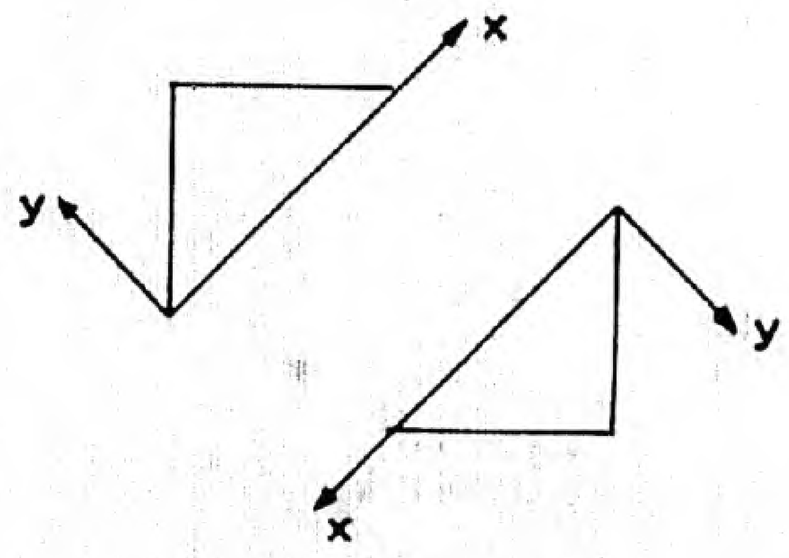

Fig. 28 (b)

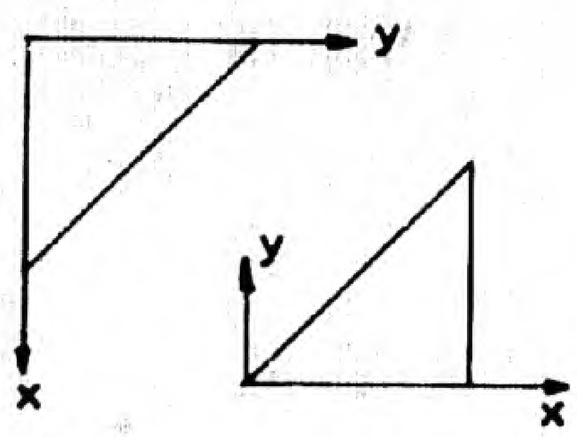

Fig. 28(c)

Fig. 28 Local axis systems.

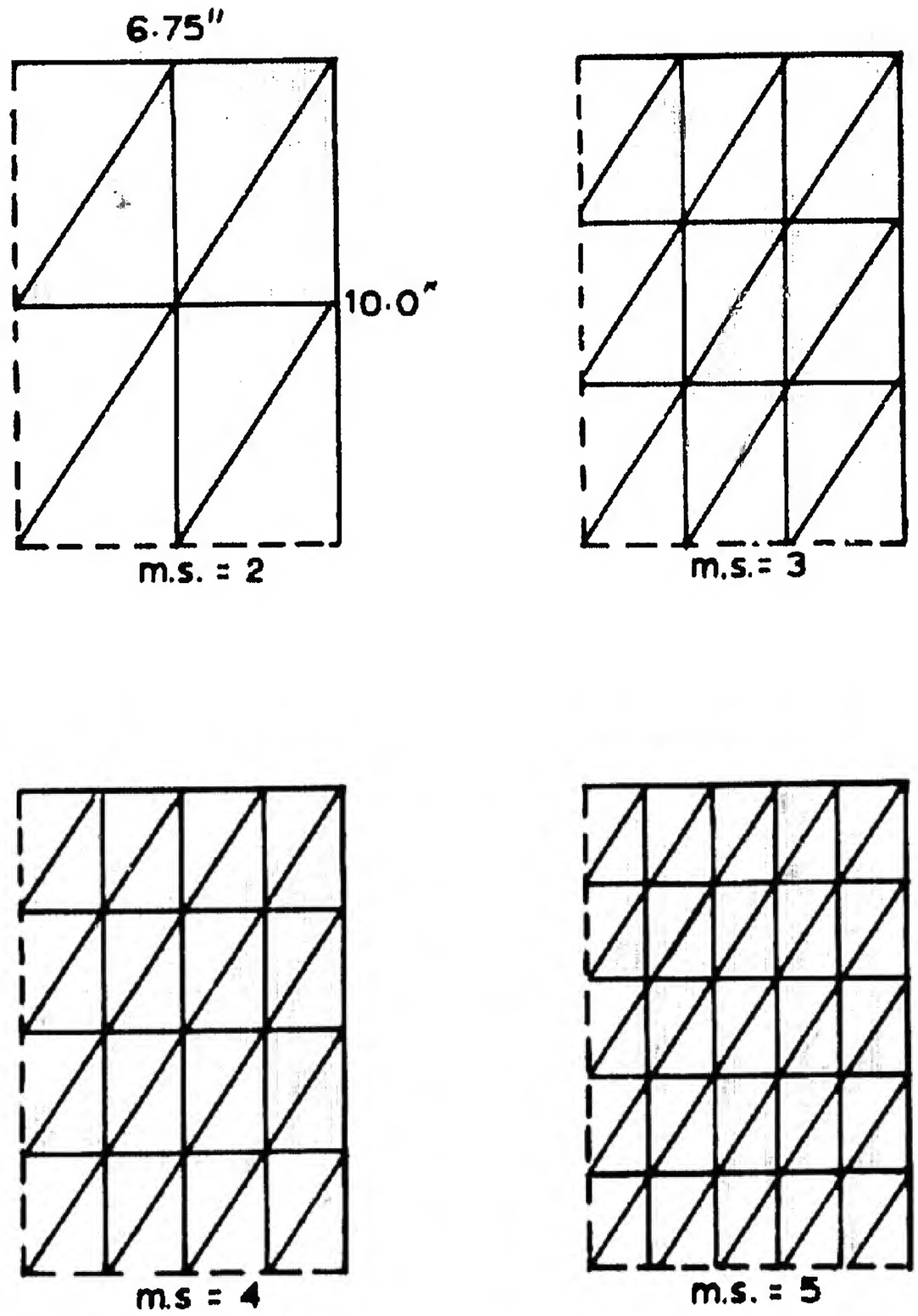

Figure 29. Idealisation of a rectangular plate using triangular elements.

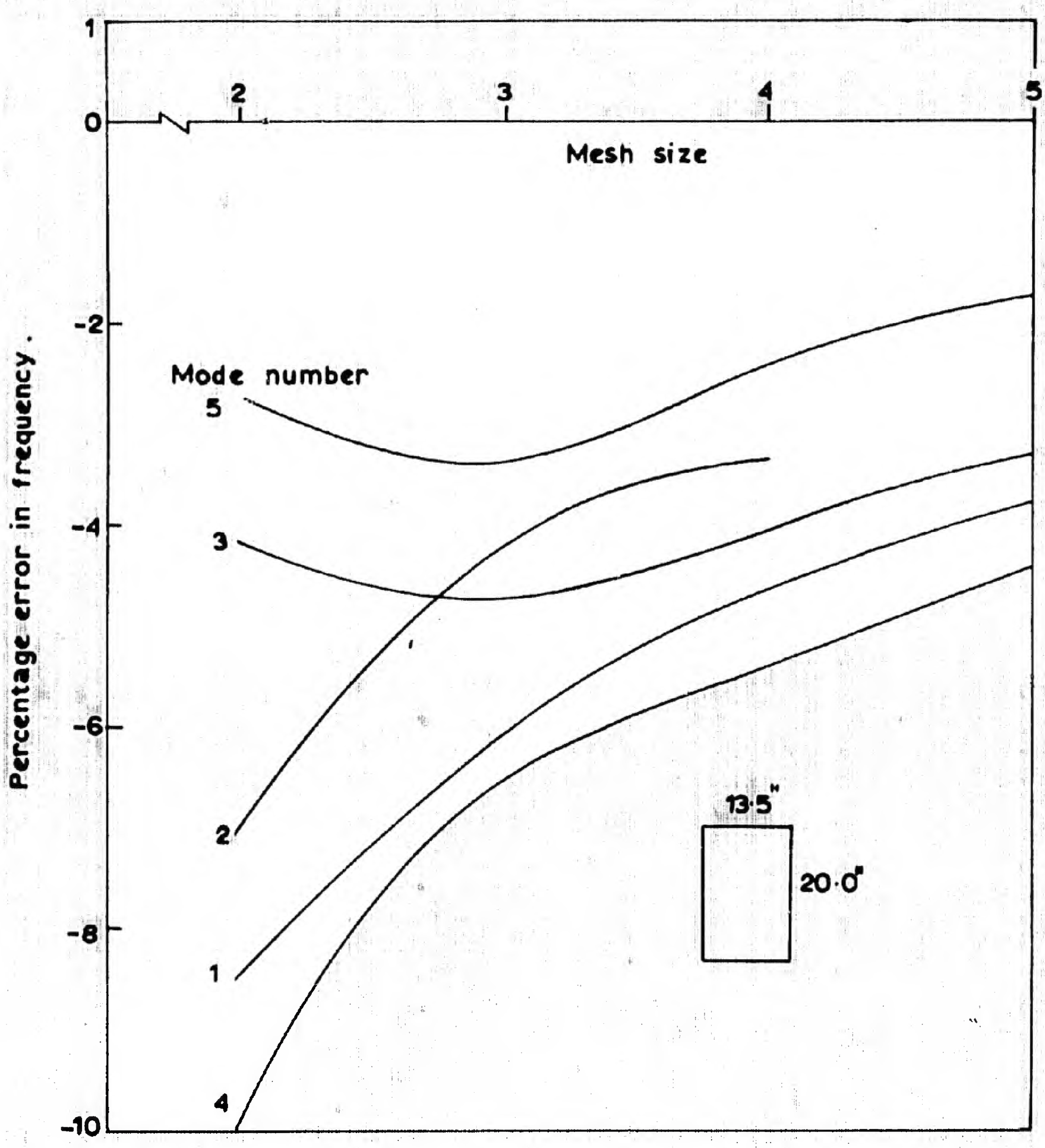

Fig. 30. Vibration of a simply supported rectangular plate.

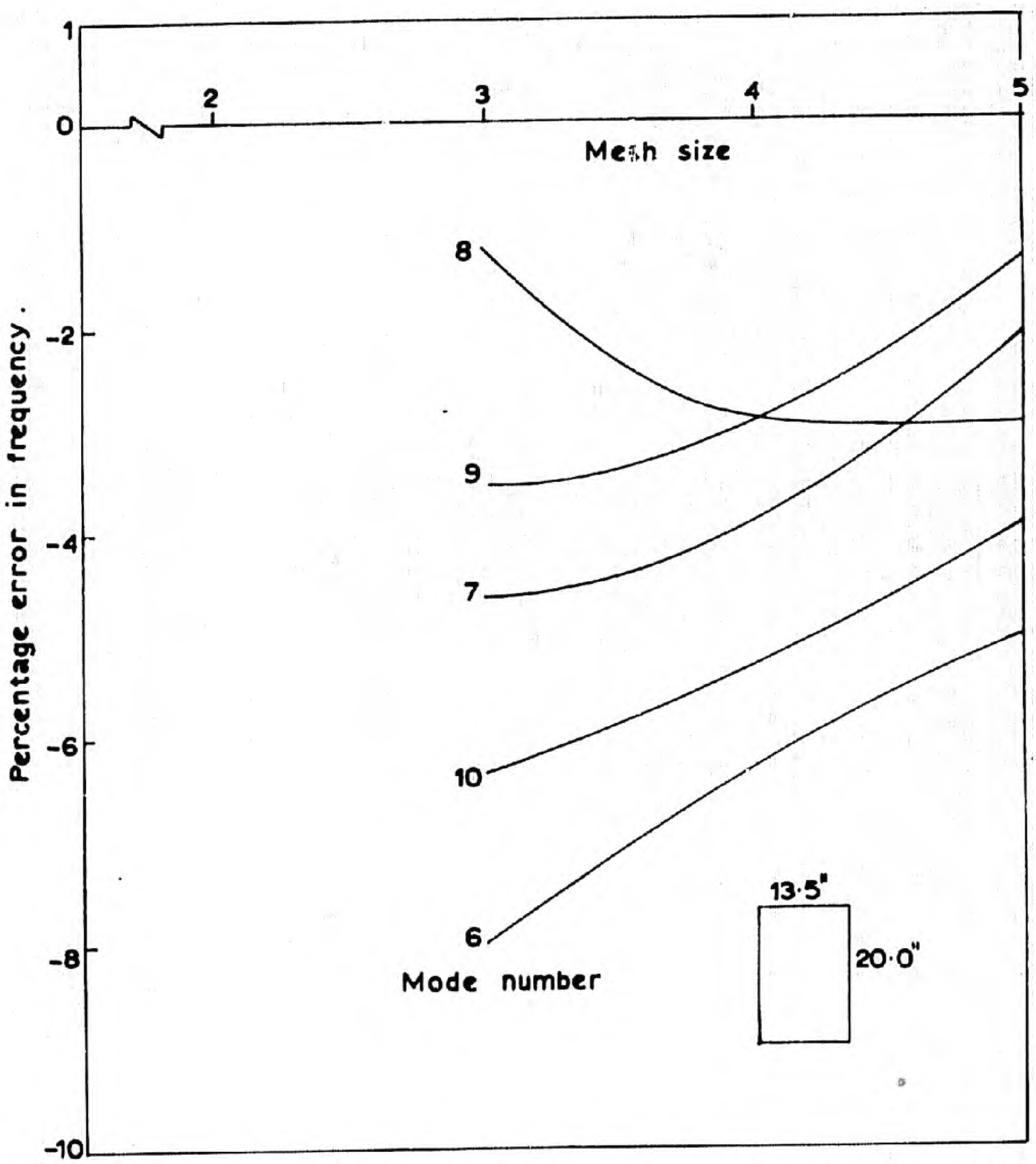

Fig. 31. Vibration of a simply supported rectangular plate.

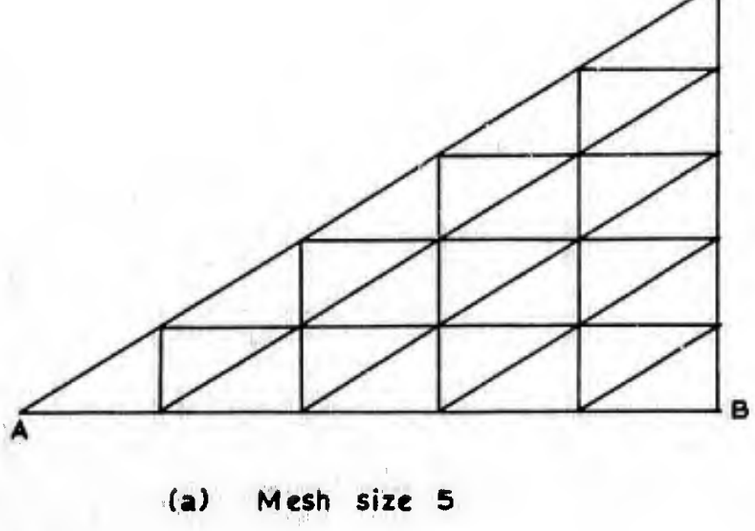

(a) Mesh size 5

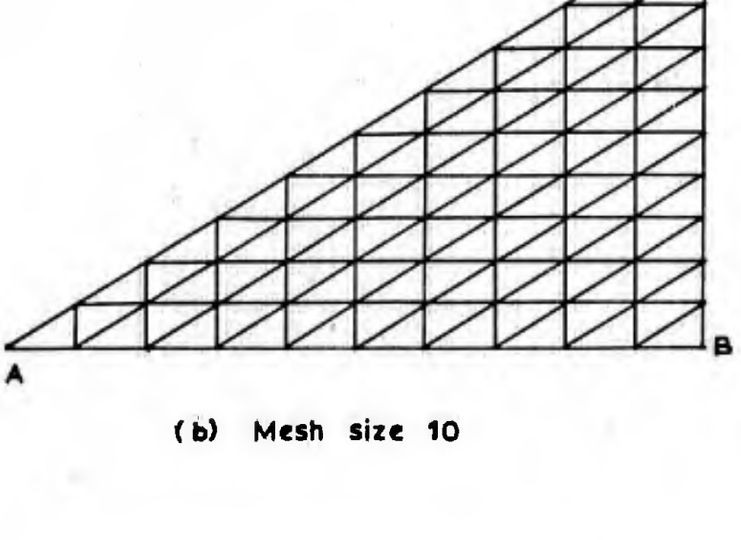

(b) Mesh size 10

Figure 32. Idealisation of a triangular plate using triangular elements.

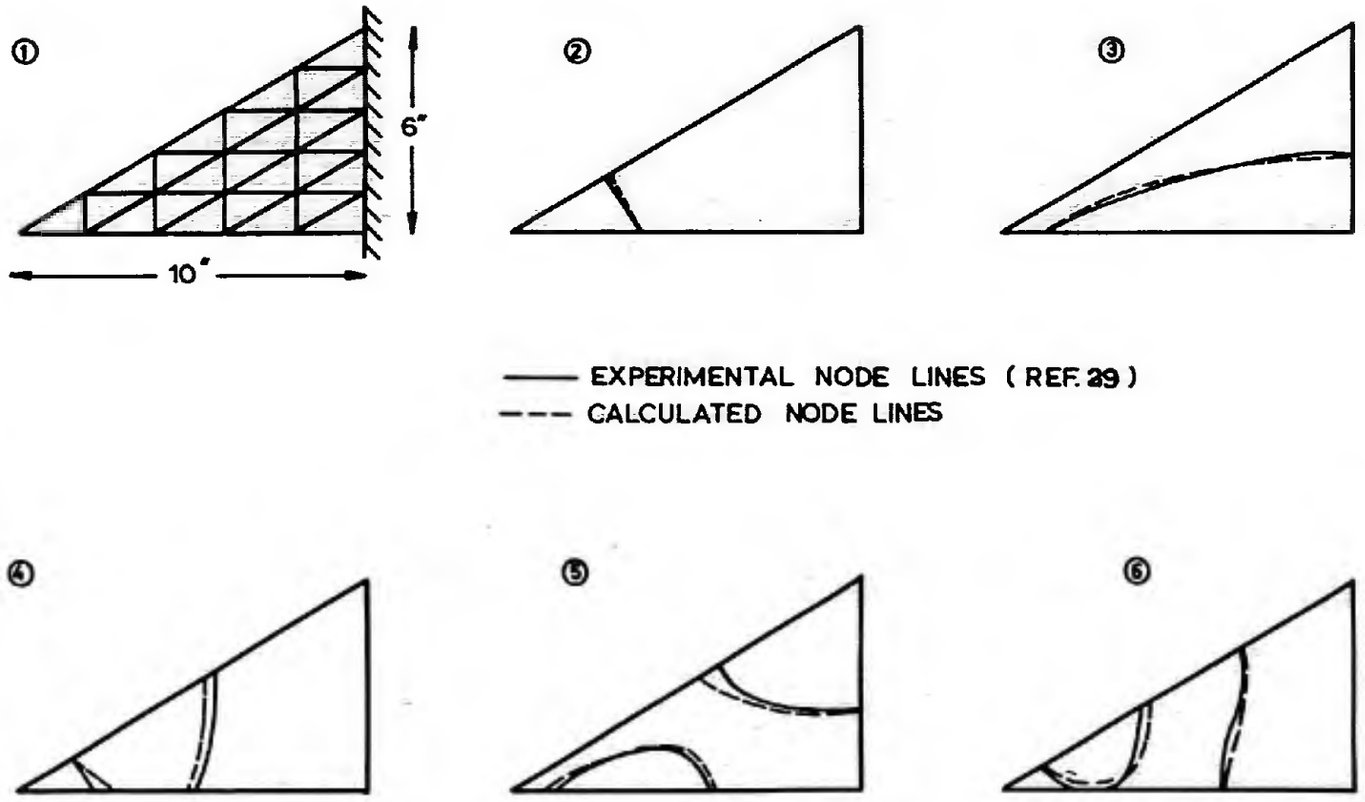

Figure 33. Comparison of calculated and measured nodal lines of a cantilevered triangular plate.

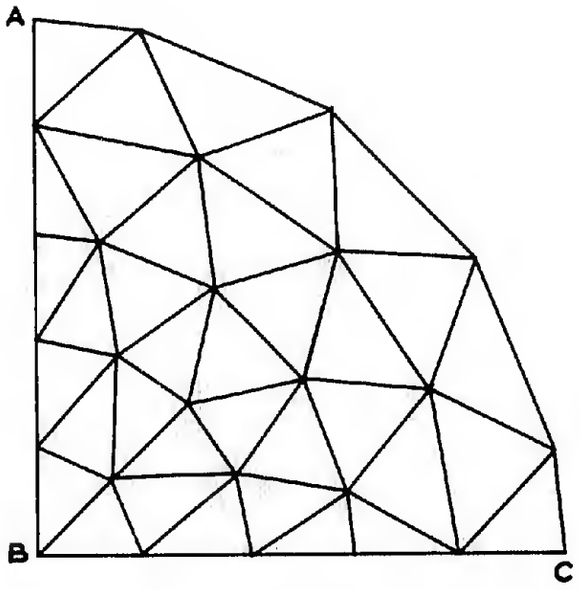

(a) Mesh size 5

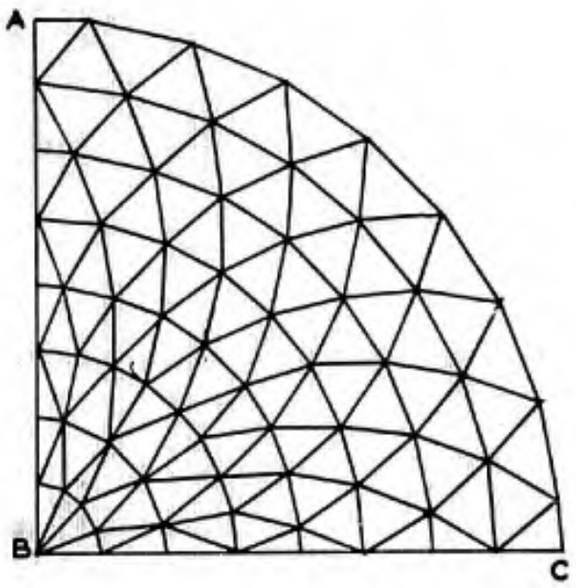

(b) Mesh size 8

Figure 34. Idealisation of a circular plate using triangular elements.

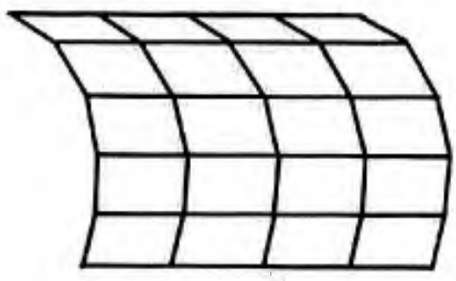

Figure 35a Cylindrical shell.

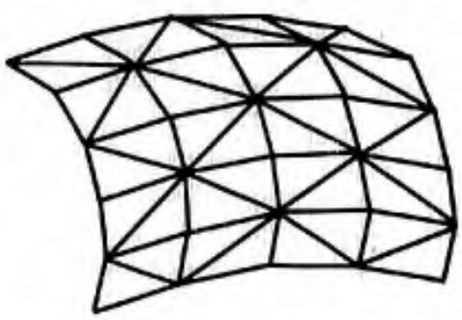

Figure 35b Doubly curved shell.

Figure 35 Idealization process – shells.

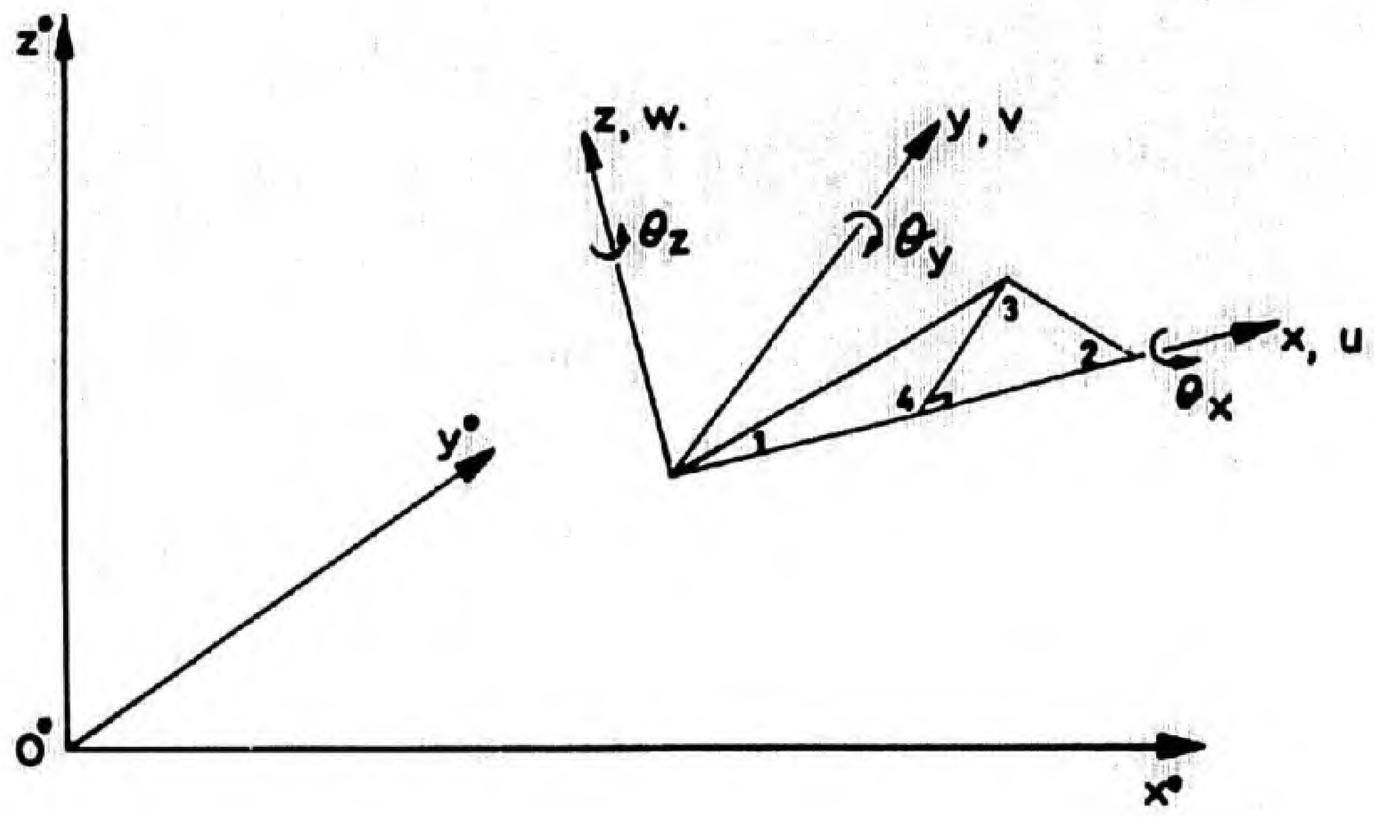

Fig. 36 Transformation to global co-ordinates

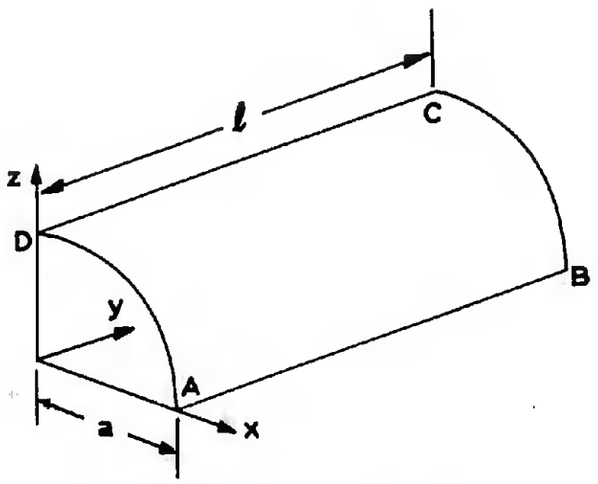

l = 7·7 ins.
a = 1·925 ins.

Fig. 37a. Details of a cylindrical shell.

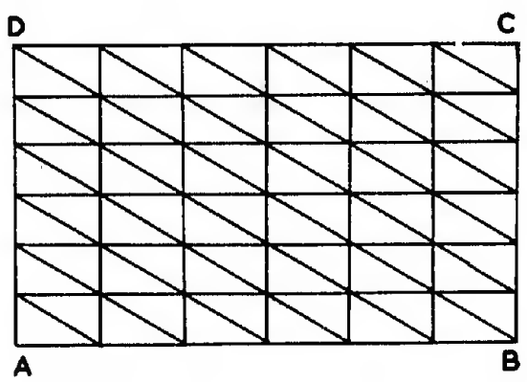

Fig. 37 b. Idealisation of a cylindrical shell.

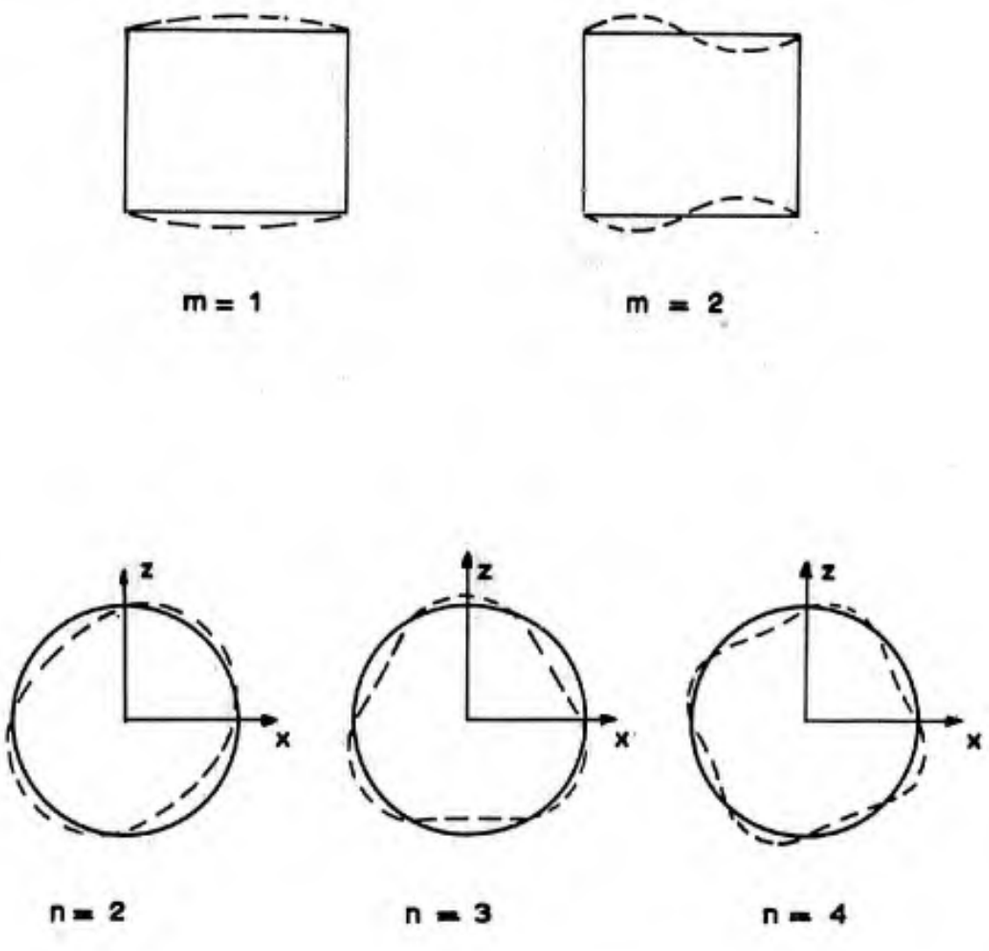

Fig. 38. Modes of vibration of a cylindrical shell.

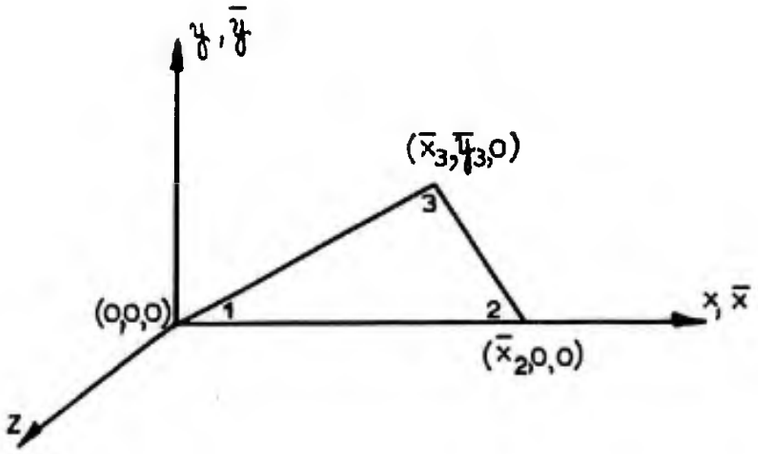

Figure 39a. Before incremental displacement.

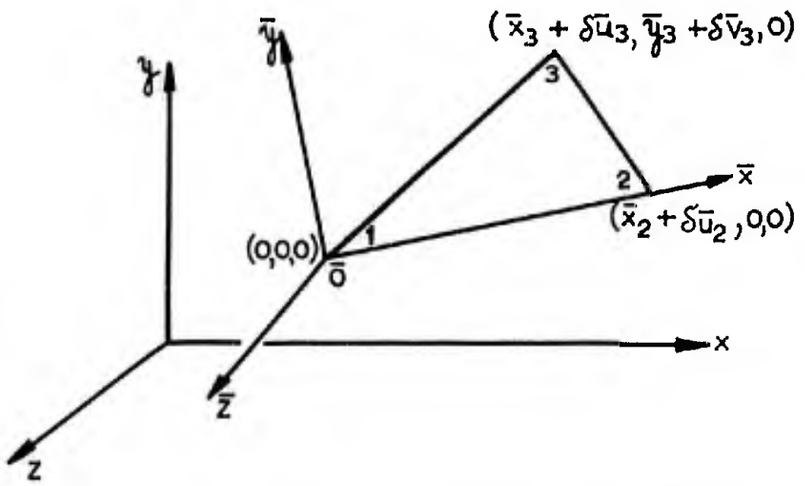

Figure 39b After incremental displacement.

Figure 39 Geometry of triangular element before and after incremental displacement.

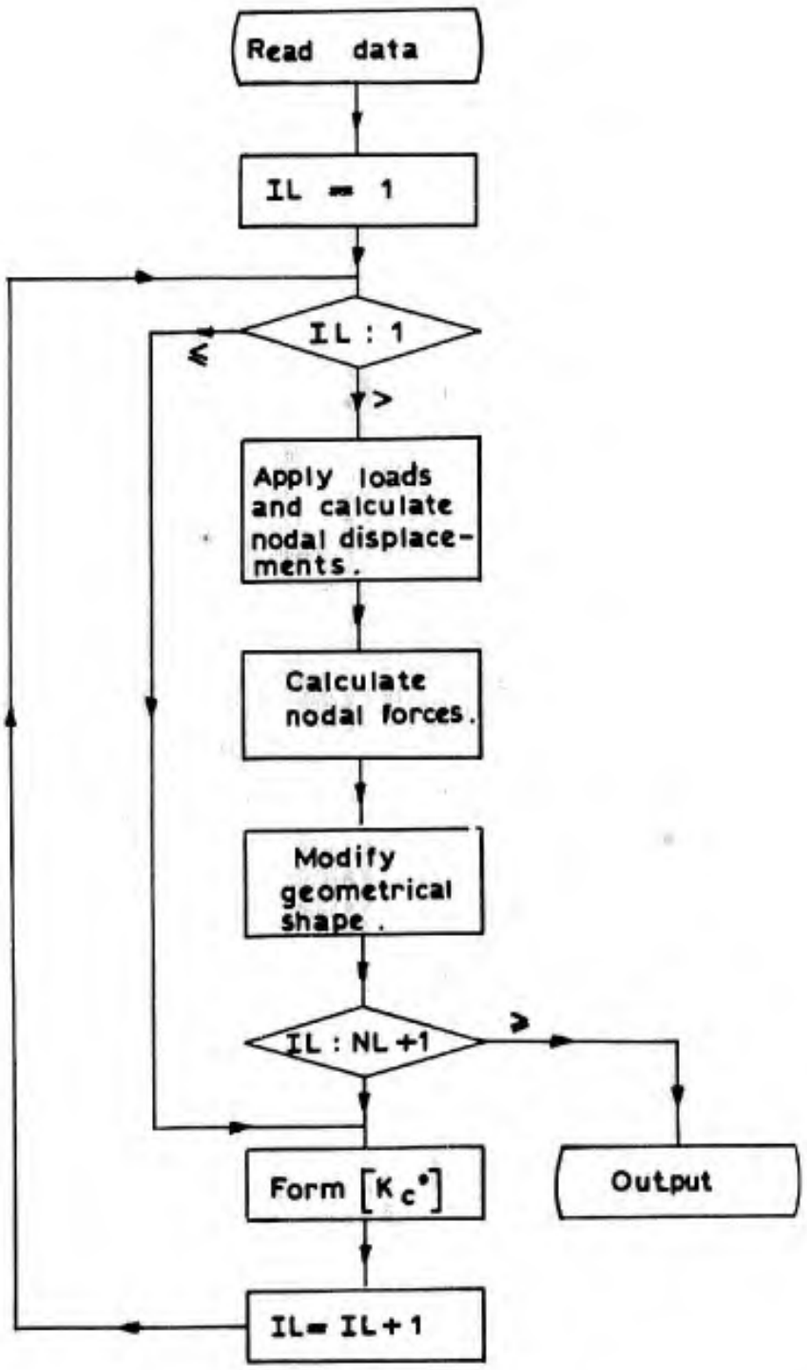

Fig. 40. Flow diagram for large deflection analysis using a step-by-step procedure.

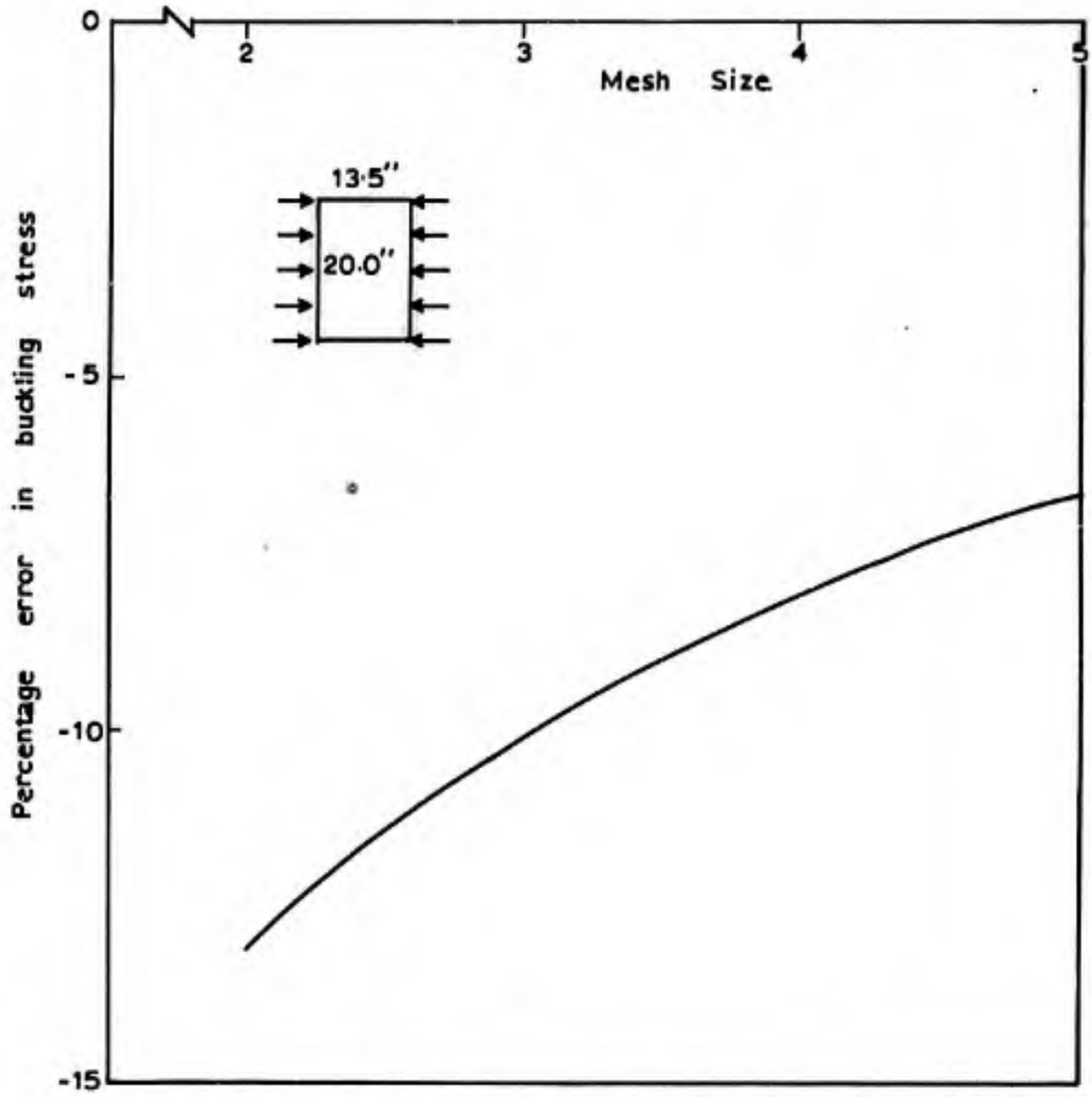

Figure 41 Buckling of a simply supported rectangular plate in compression.

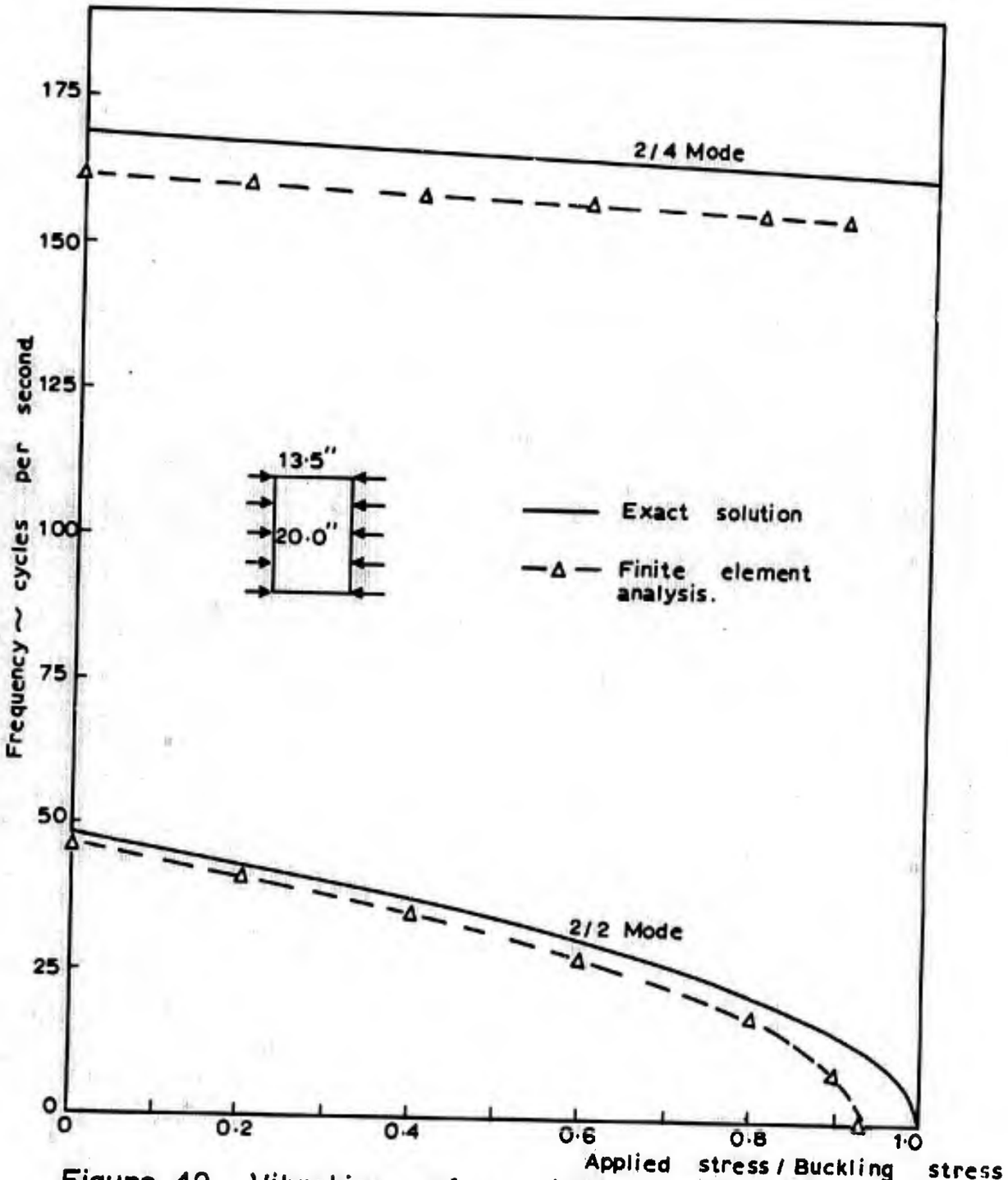

Figure 42. Vibration of a simply supported rectangular plate in compression.

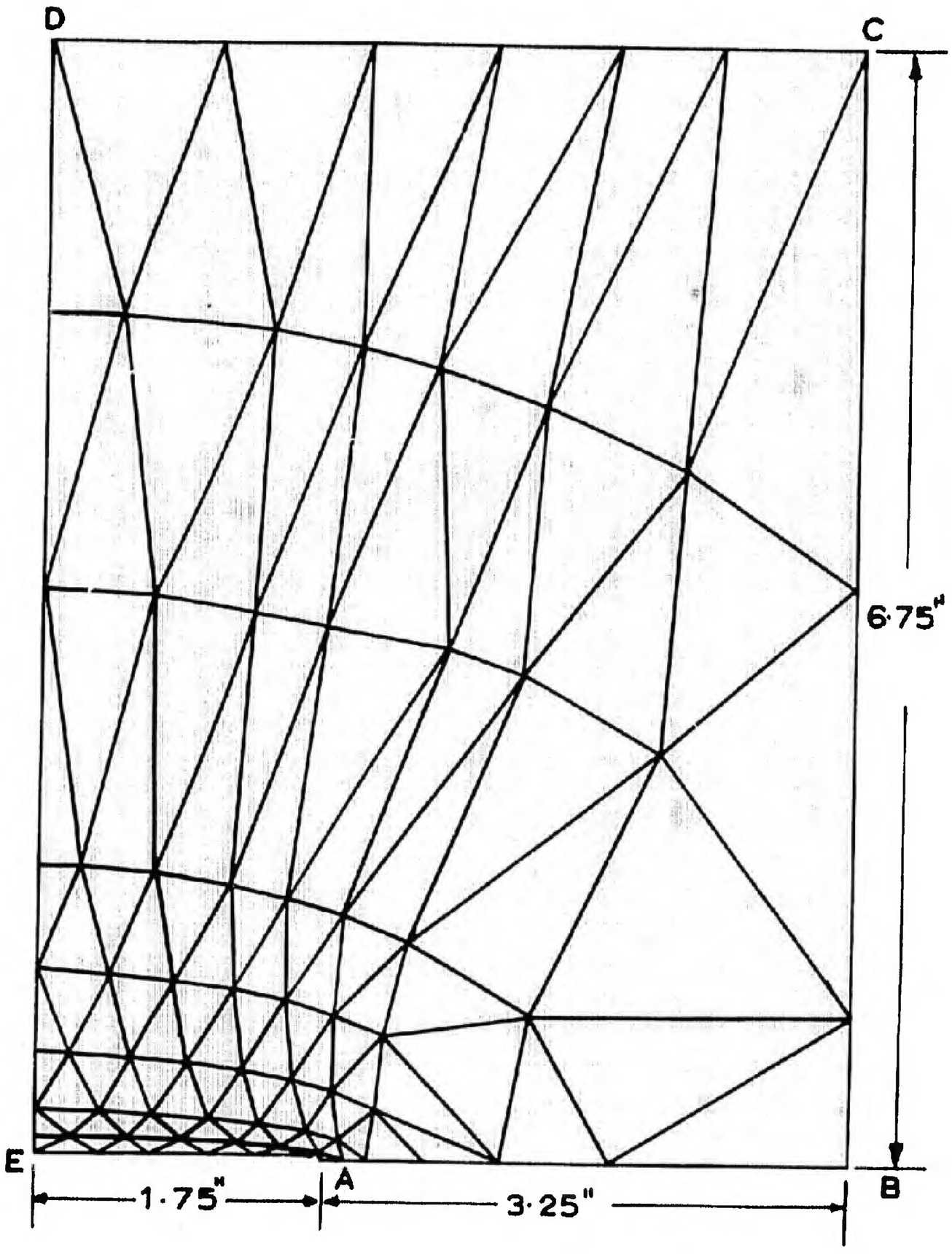

Fig. 43. Idealisation of a rectangular plate containing a central crack.

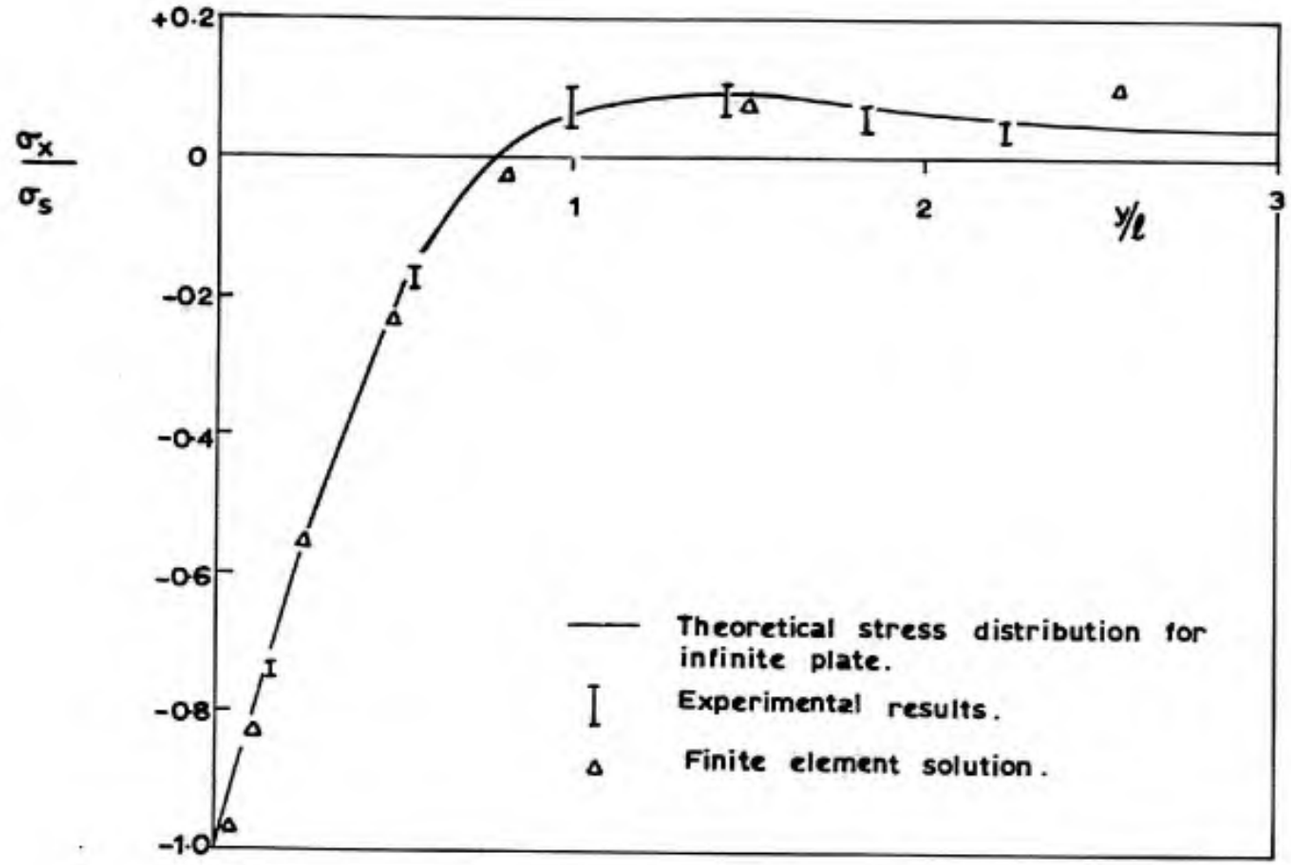

Figure 44 Theoretical and experimental stress distribution curves along the plate centre line normal to the crack.

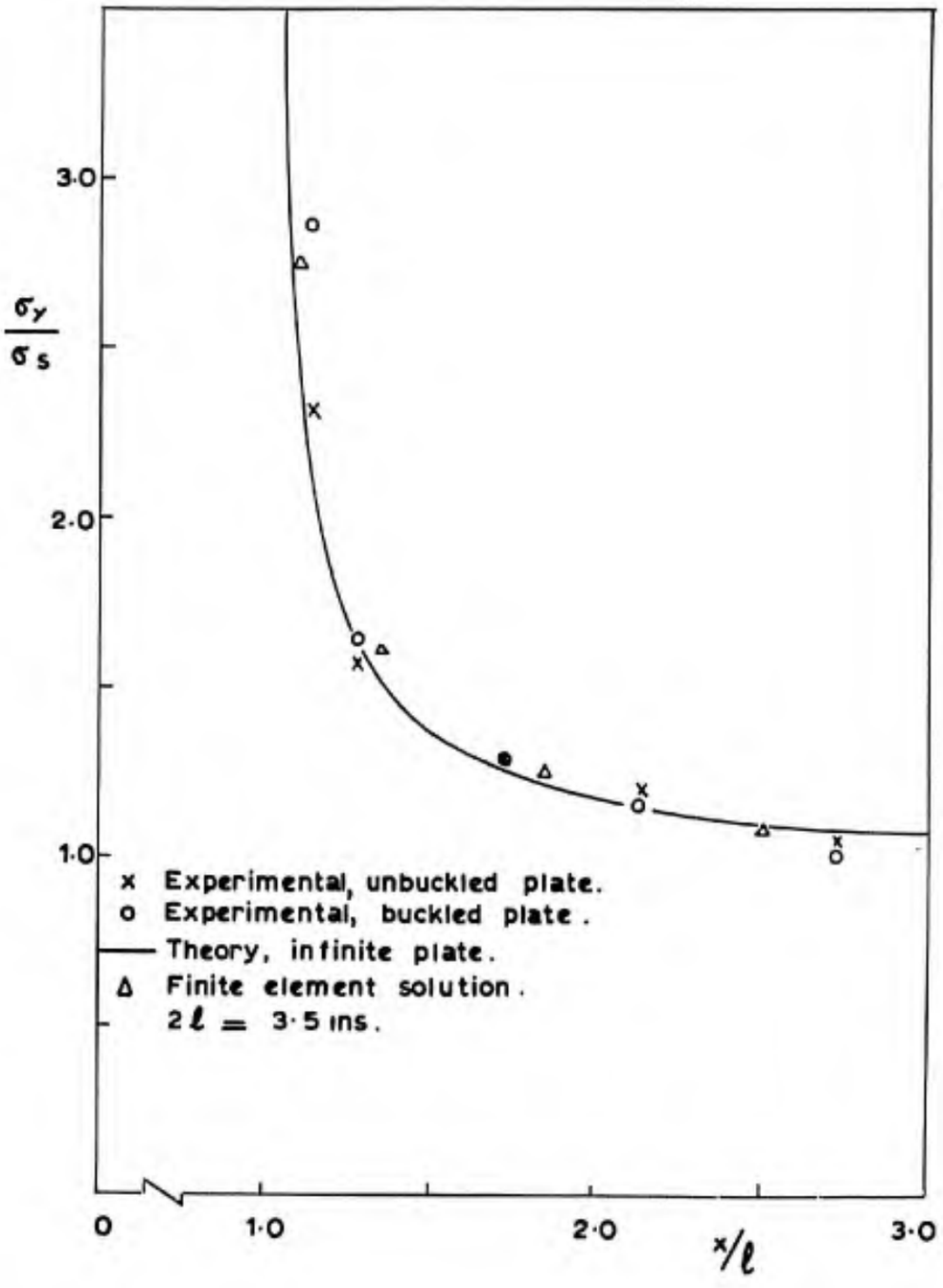

Fig. 45. Theoretical and experimental stress distributions along the plate centreline.

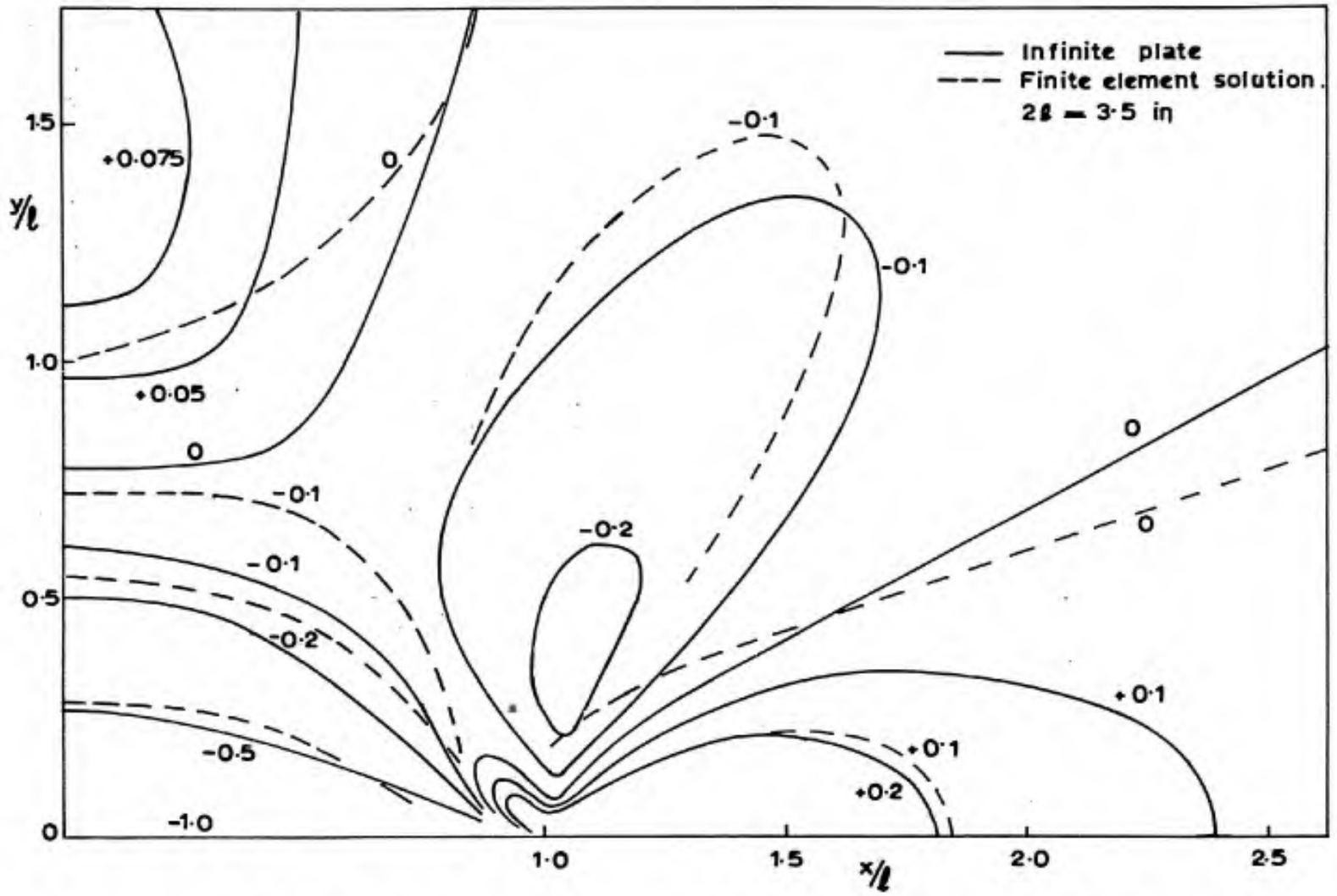

Fig. 46. Transverse direct stress distribution σ_x / σ_s.

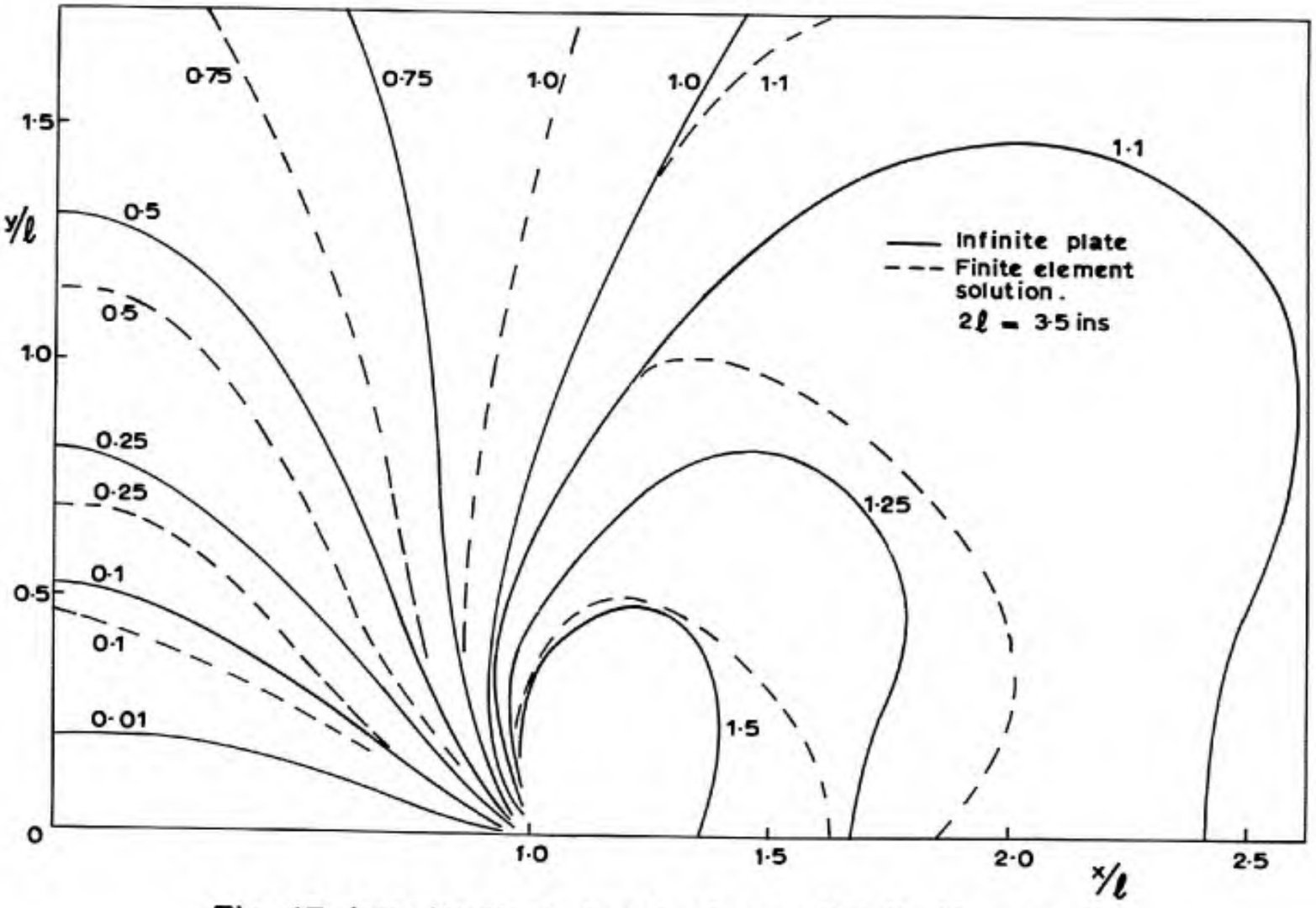

Fig. 47. Longitudinal direct stress distribution σ_y/σ_s.

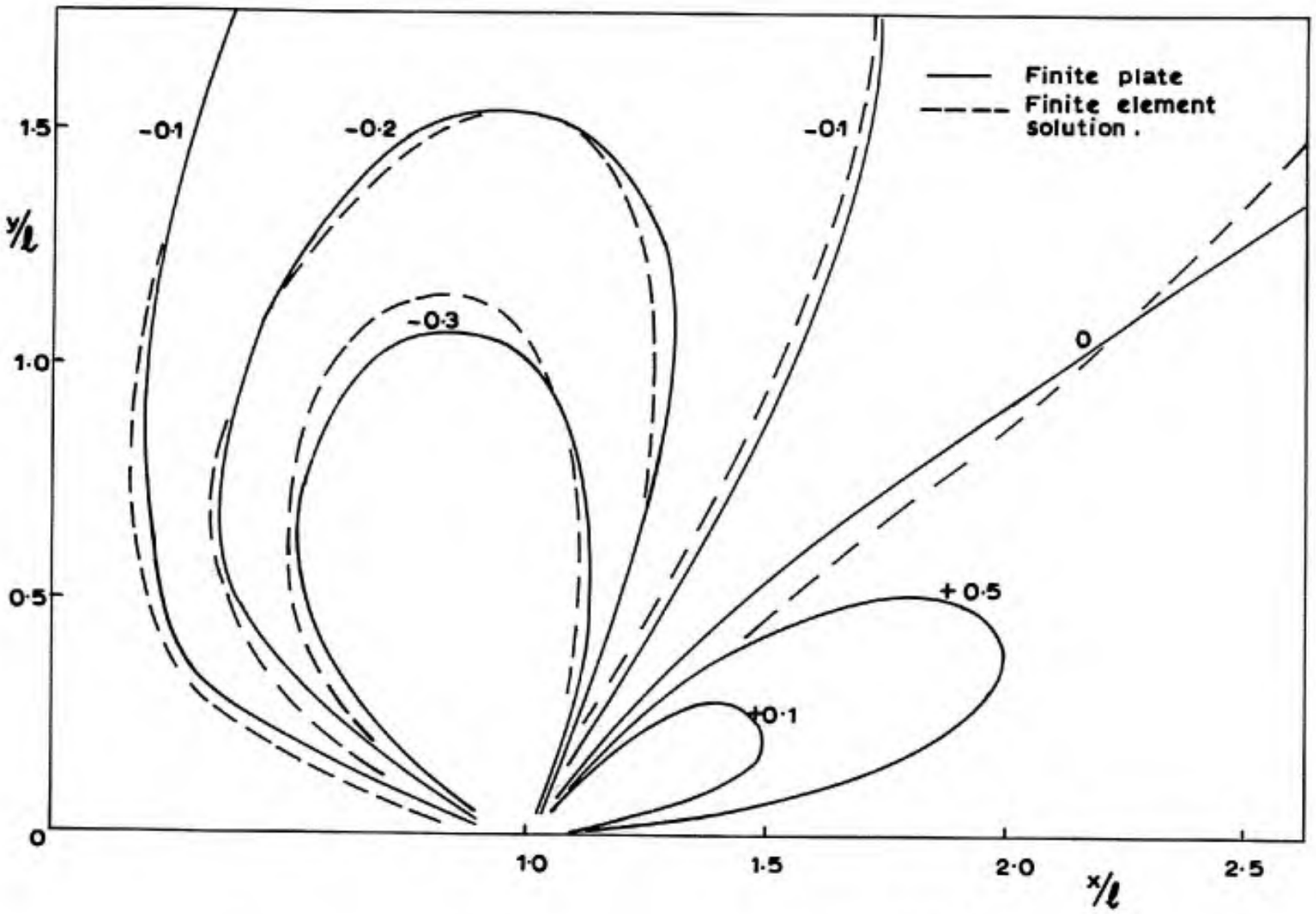

Fig. 48. Shear stress distribution τ_{xy}/σ_s.

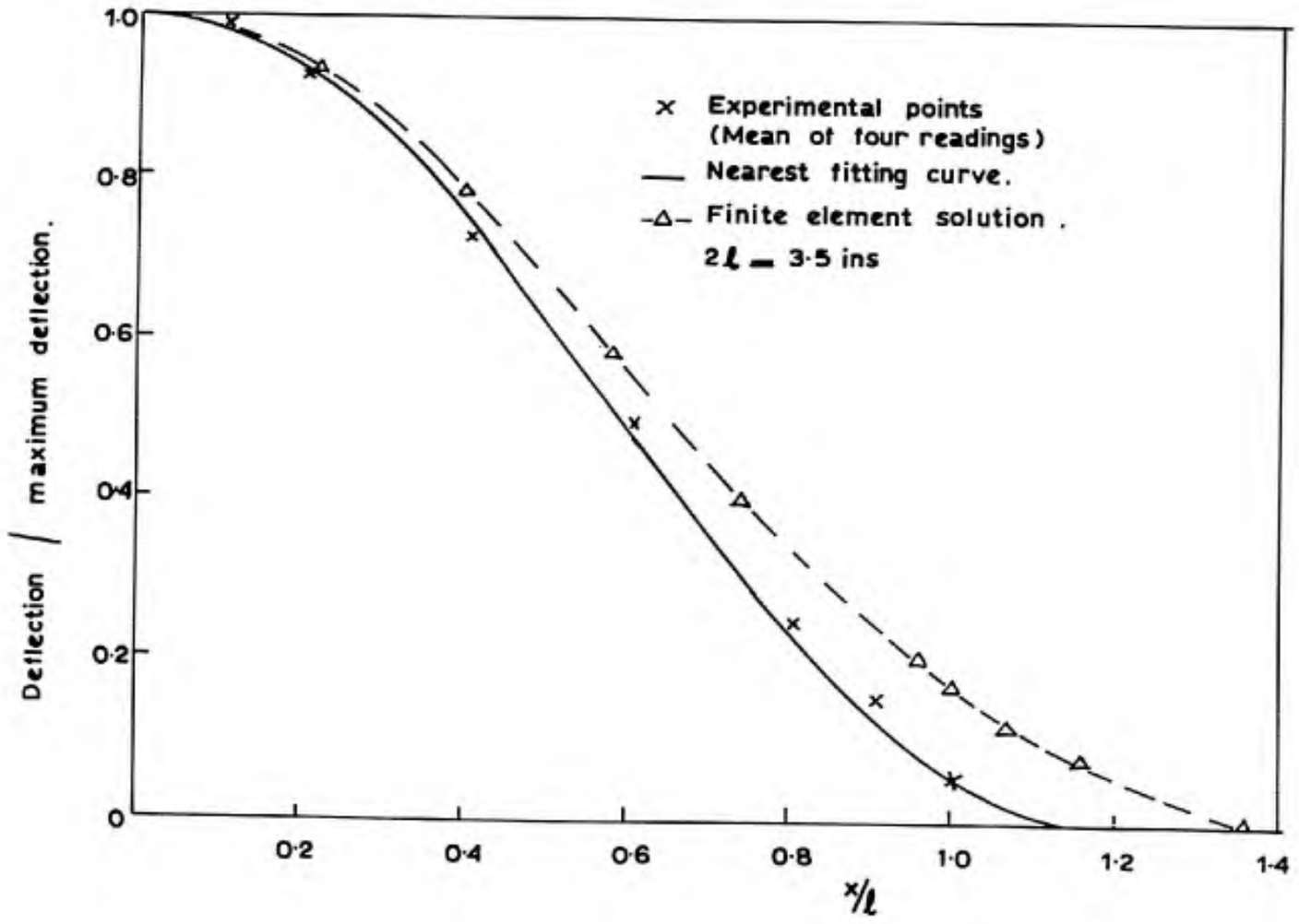

Figure 49 Static deflections of a buckled plate along the line of the crack.

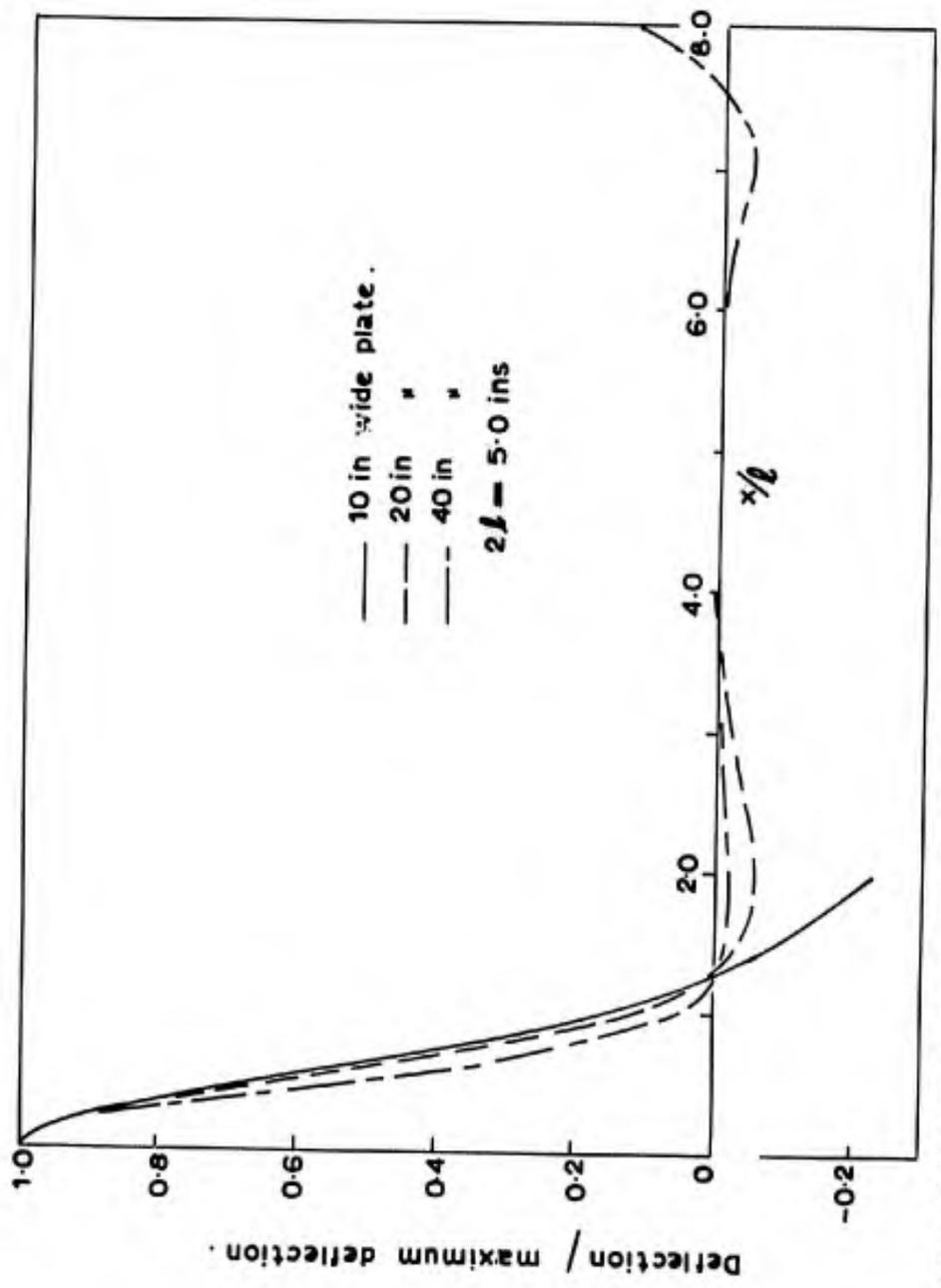

Fig. 50. Comparison of buckling modes along the line of the crack.

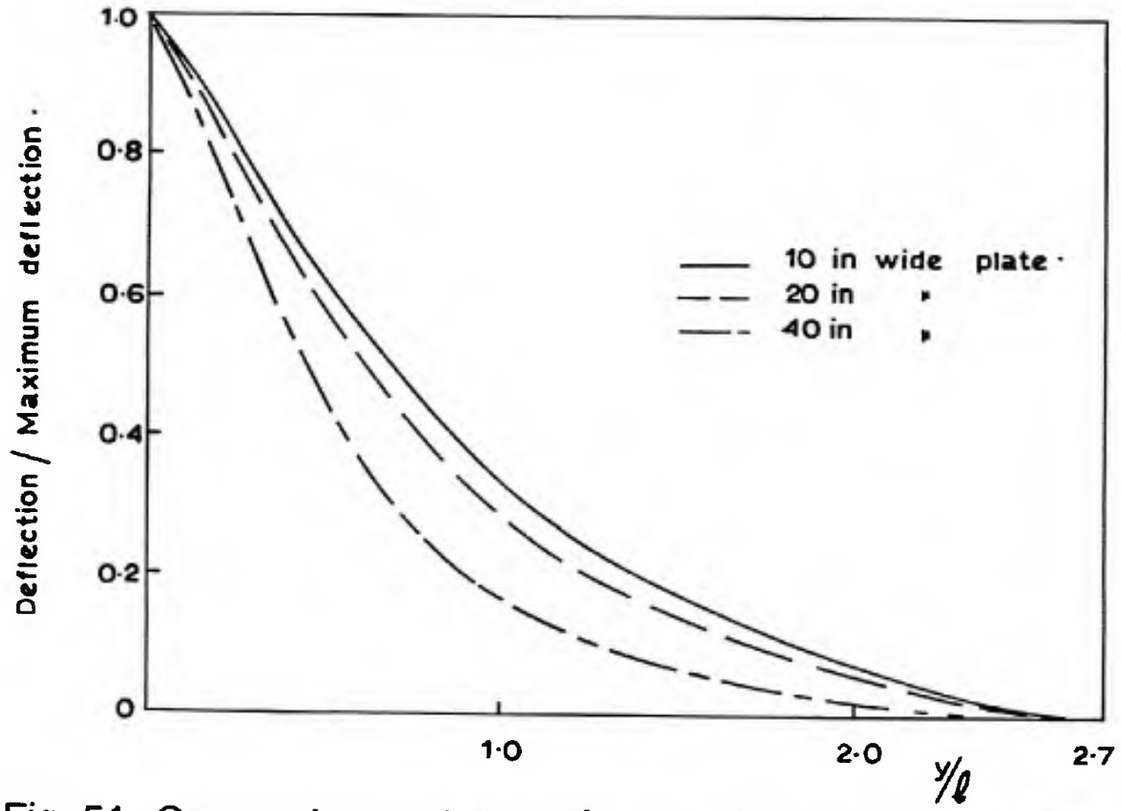

Fig. 51. Comparison of buckling modes normal to the crack.

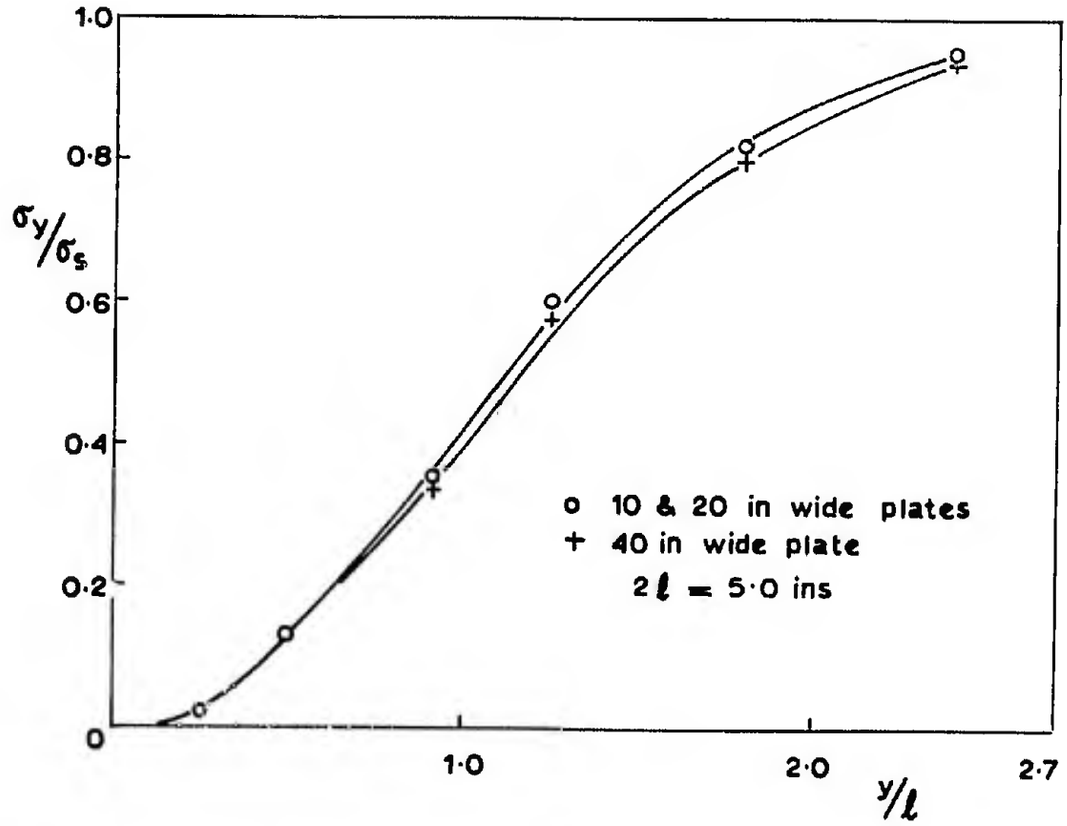

Fig. 52. Distribution of longitudinal direct stress along the plate centreline normal to the crack.

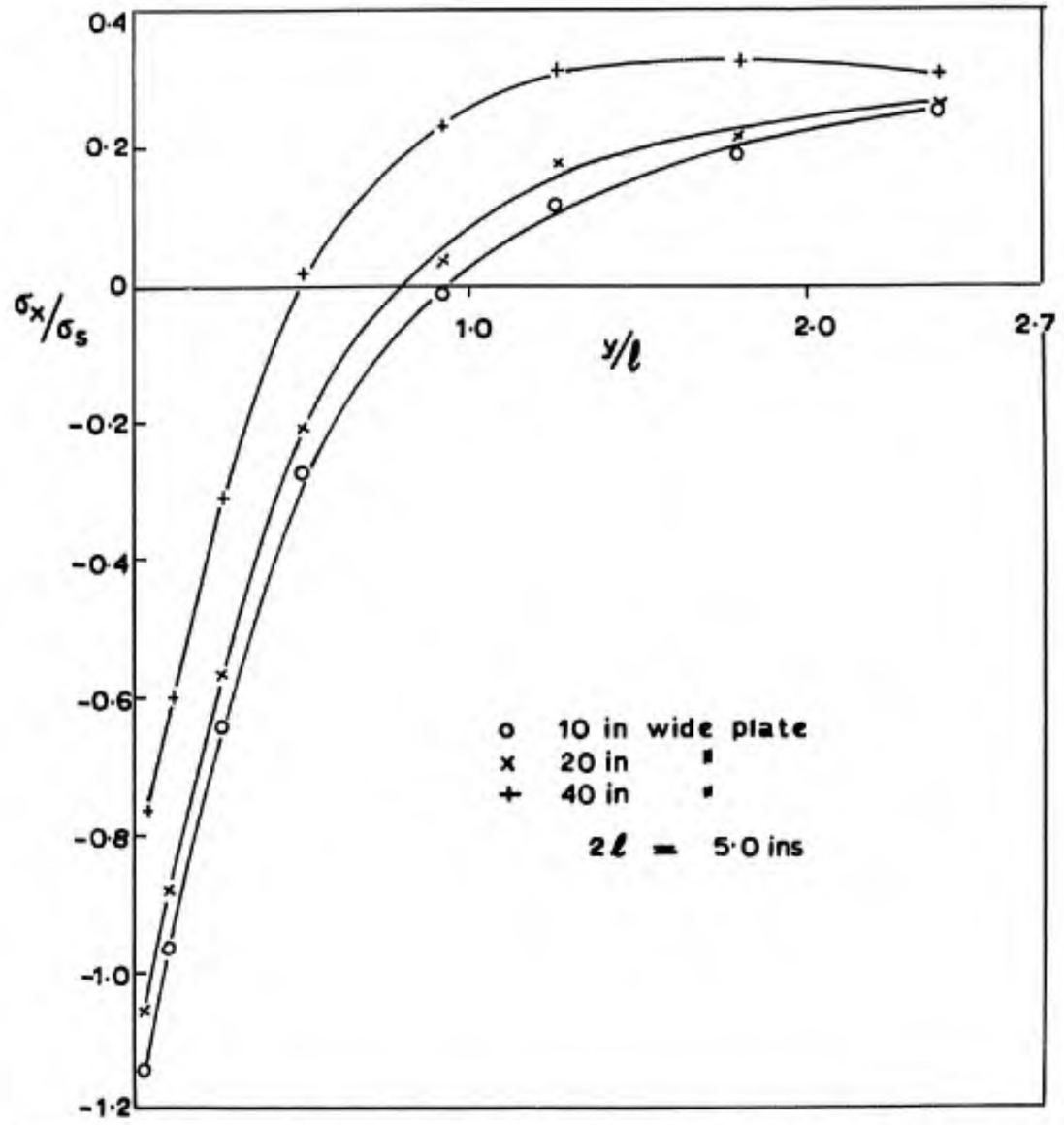

Fig. 53. Distribution of transverse direct stress along the plate centreline normal to the crack.

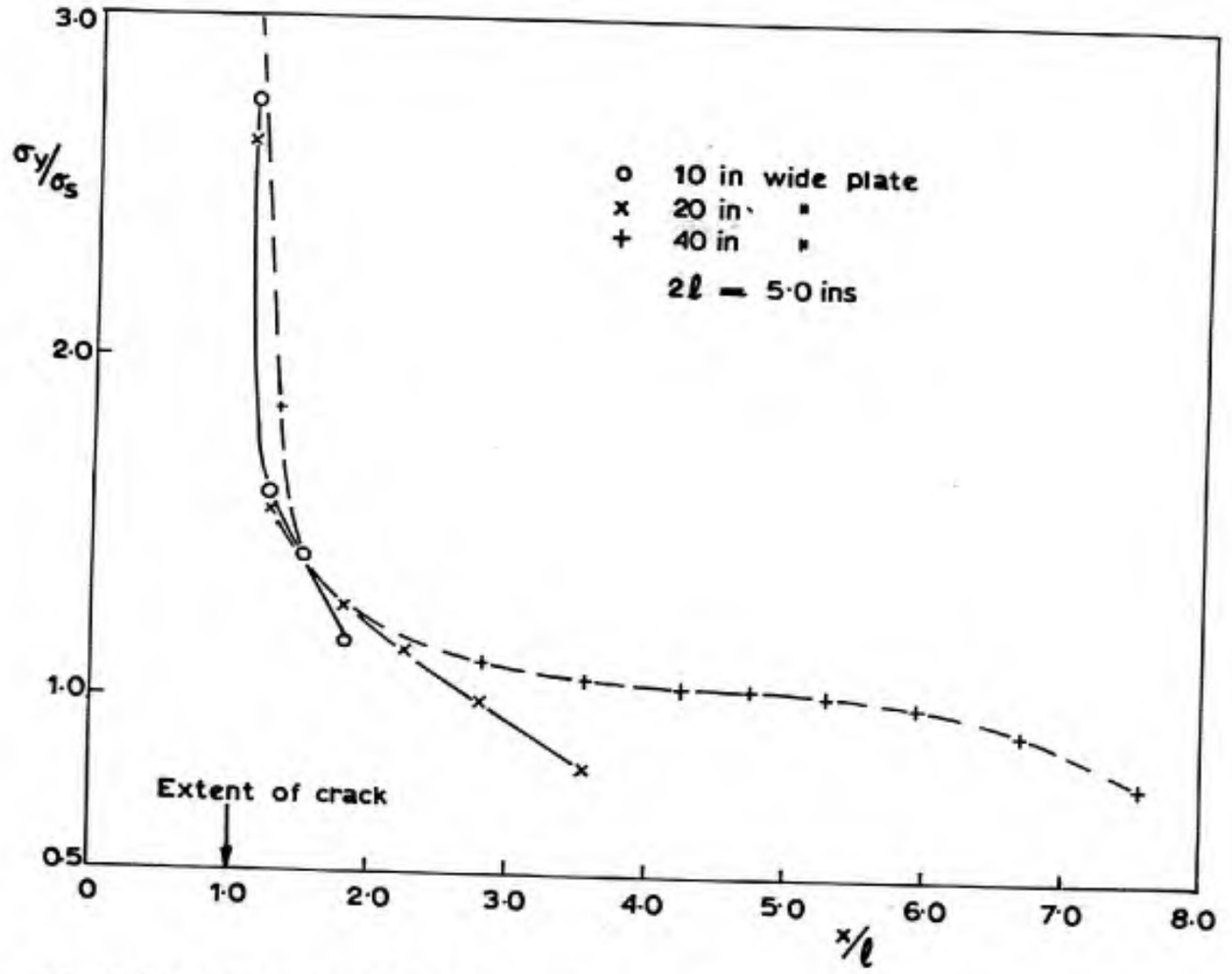

Fig. 54 Distribution of longitudinal direct stress along the plate centre line in the direction of the crack

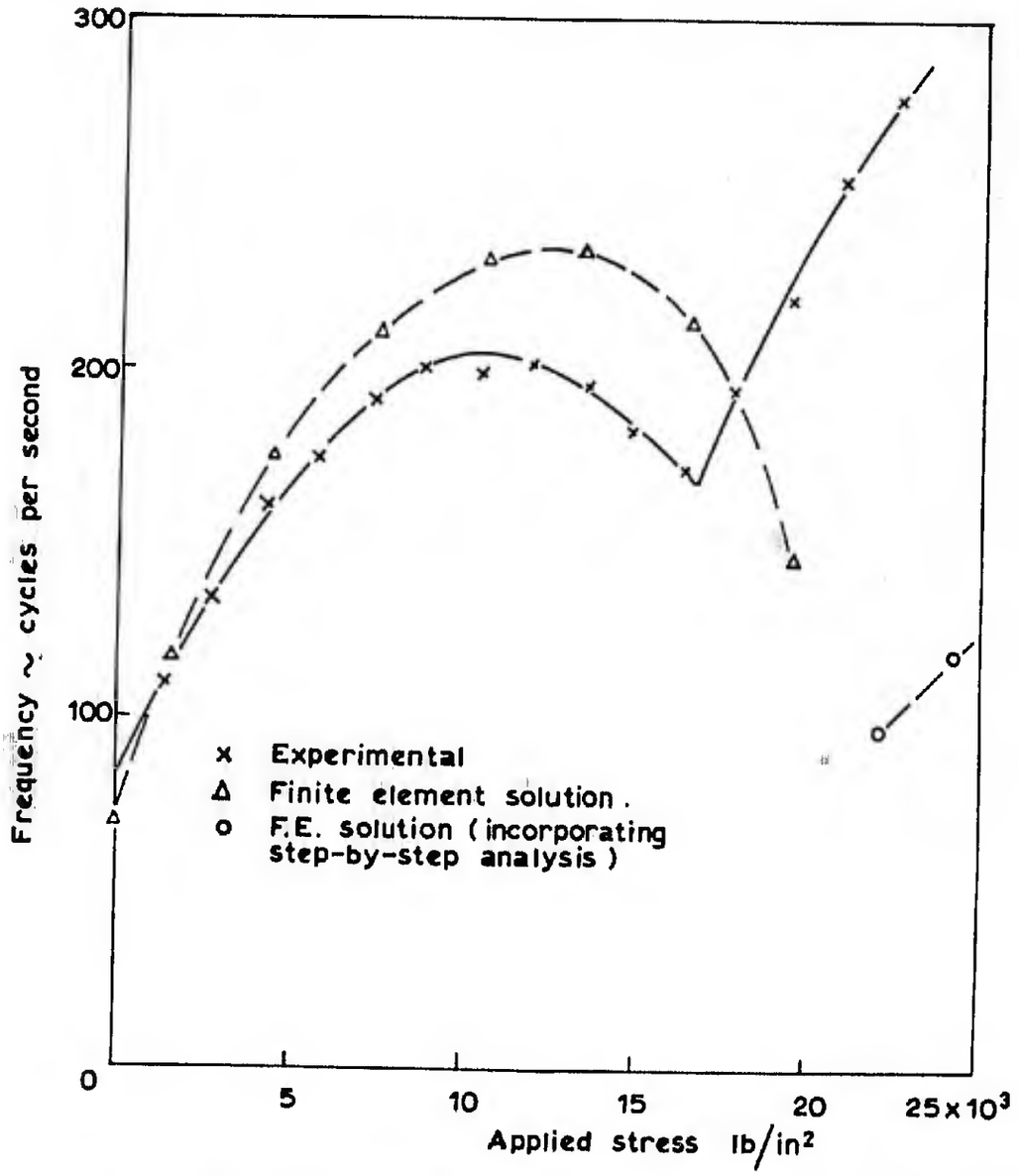

Fig. 55. Variation of frequency of fundamental mode of vibration with applied stress.

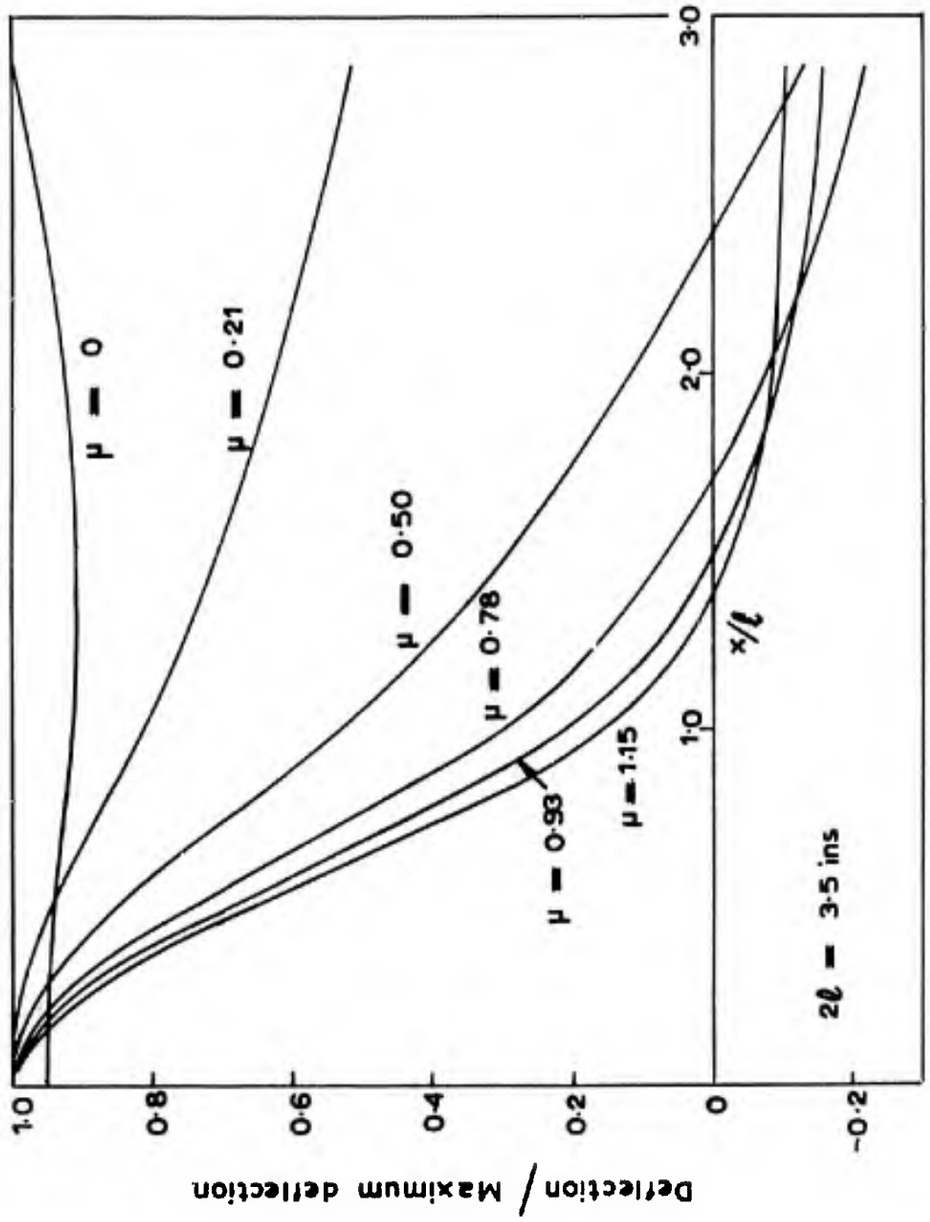

Fig. 56. Effect of applied load on dynamic mode shape along the line of the crack.

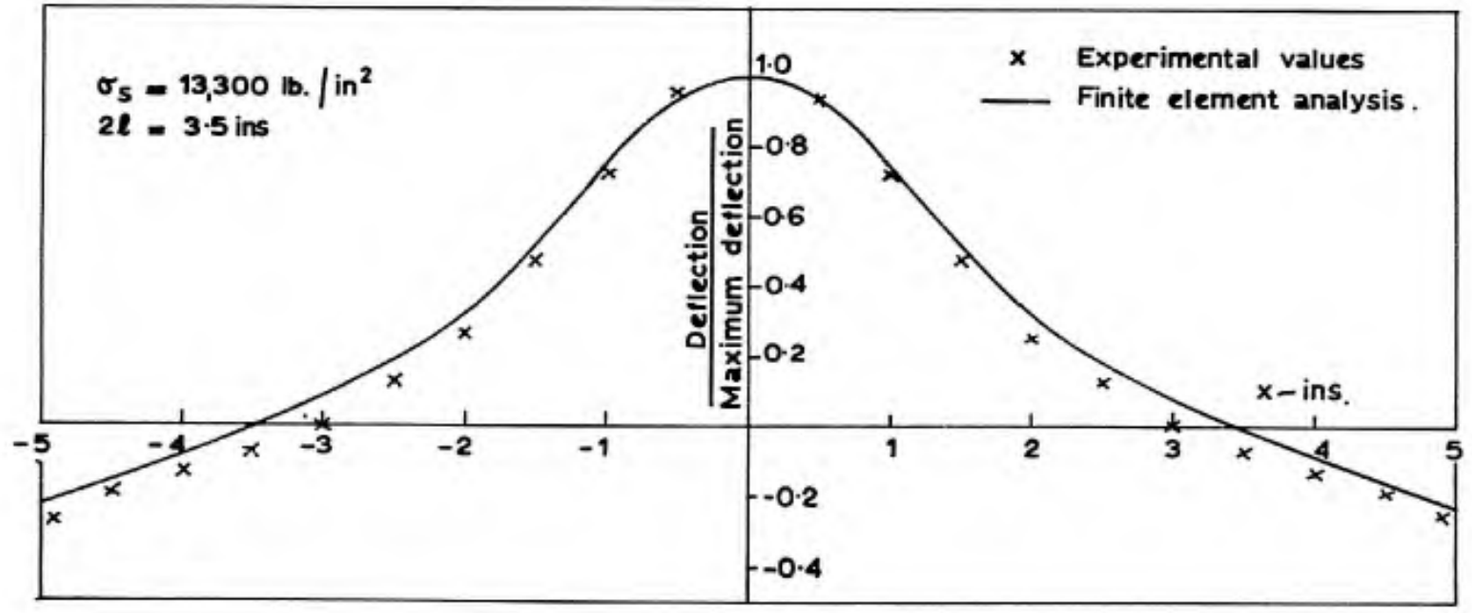

Figure 57. Dynamic deflections of a cracked plate along the line of the crack.

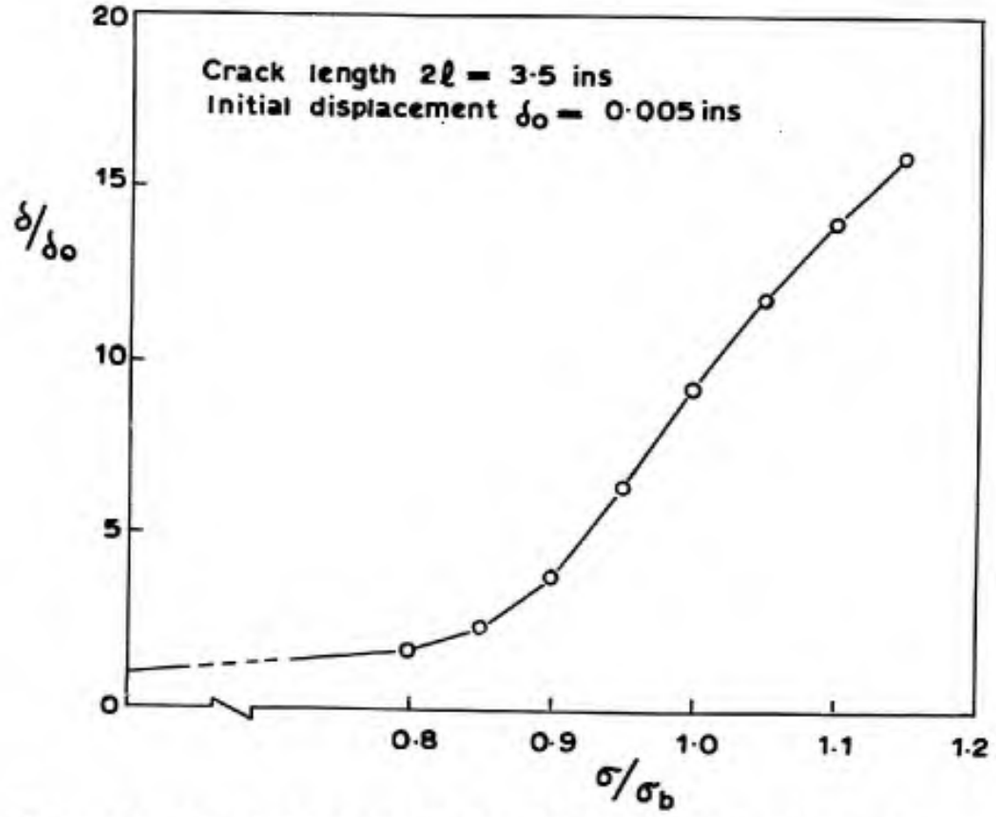

Fig. 58 Variation of the static deflection of the mid point of the crack with applied load.

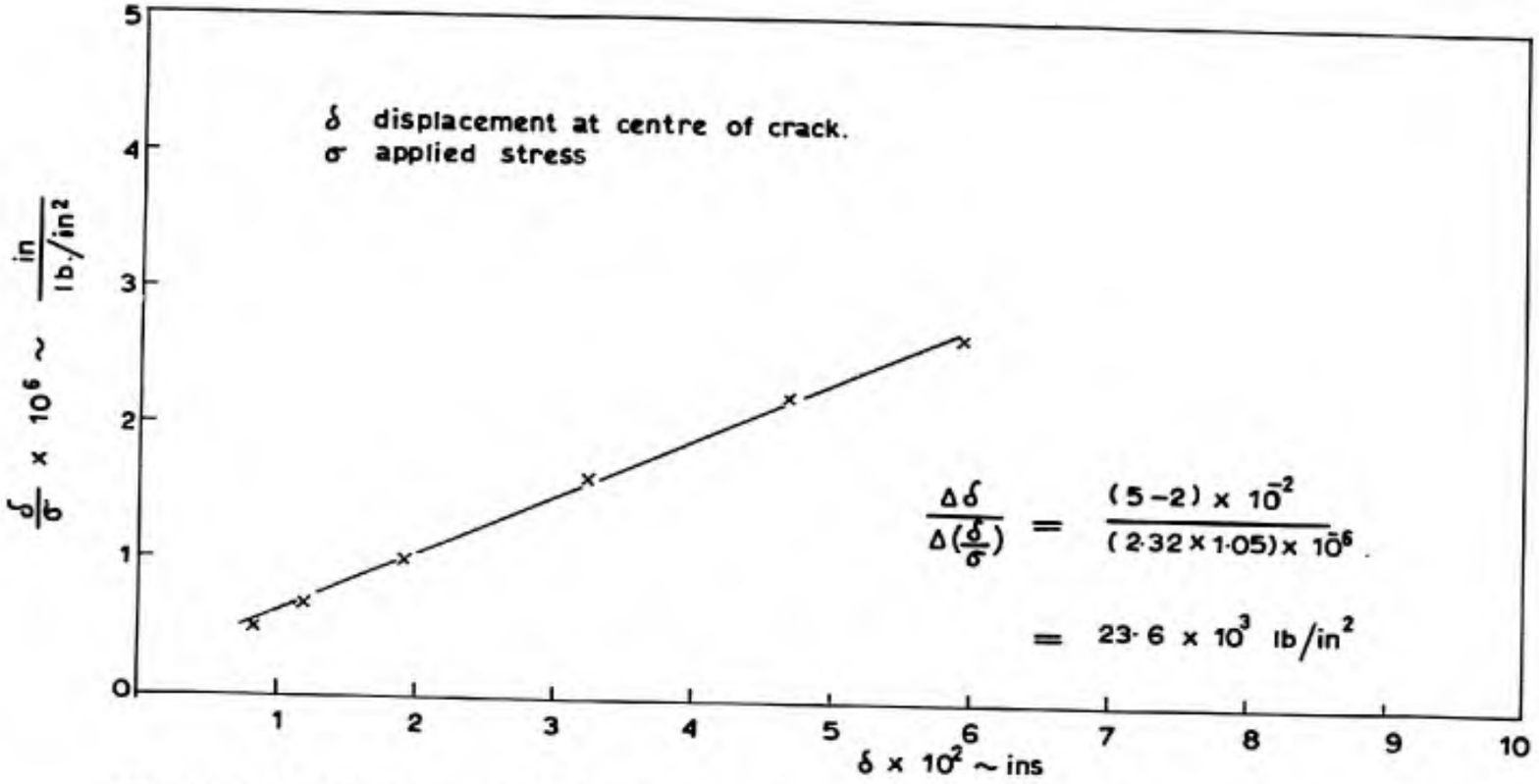

Fig. 59. Buckling analysis using a Southwell plot.

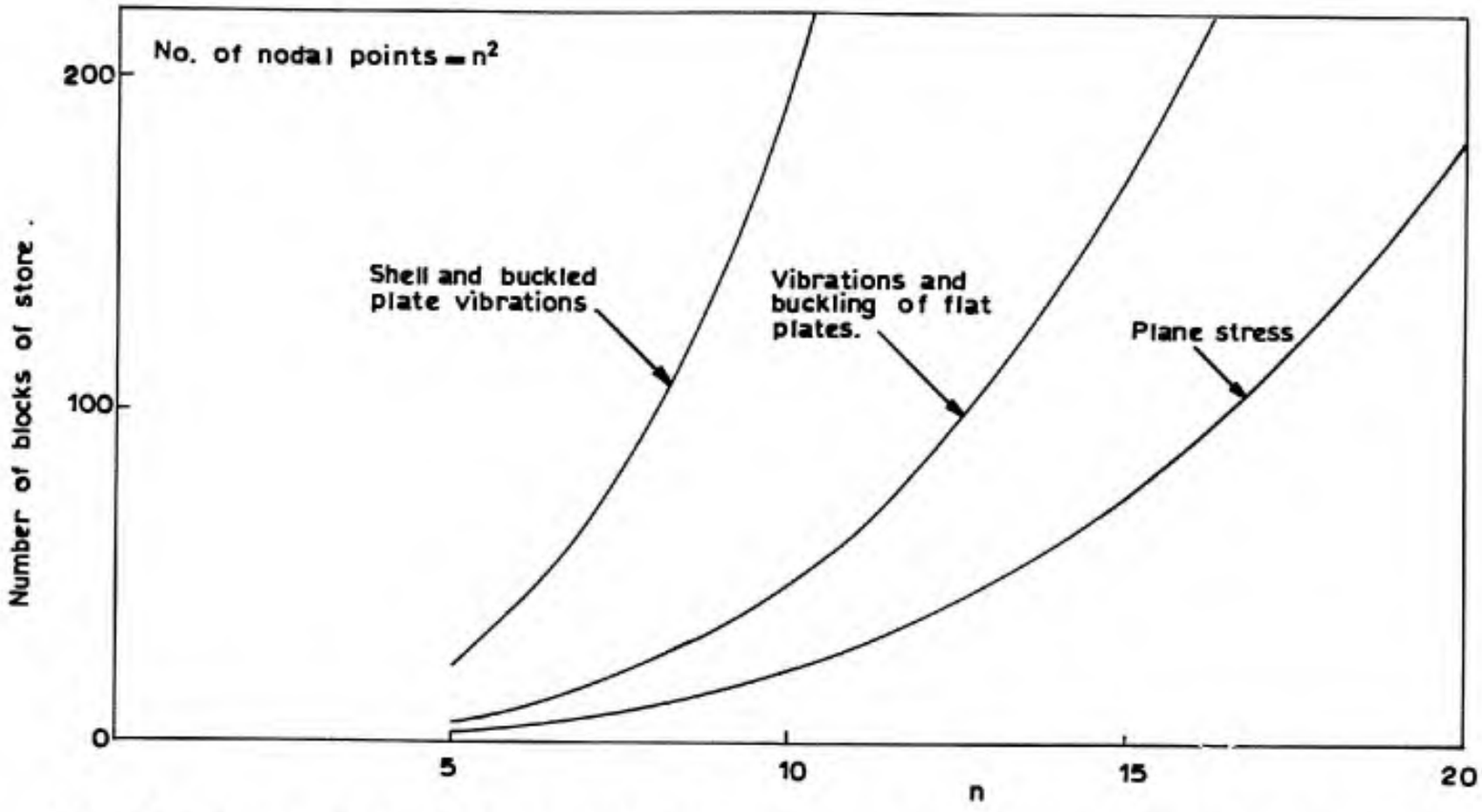

Fig. 60 Computer storage requirements for stiffness or inertia matrix.

UNCLASSIFIED

Security Classification

DOCUMENT CONTROL DATA - R&D

(Security classification of title, body of abstract and indexing annotation must be entered when the overall report is classified)

1. ORIGINATING ACTIVITY (Corporate author) Institute of Sound and Vibration Research Univeristy of Southampton, Southampton England	2a. REPORT SECURITY CLASSIFICATION UNCLASSIFIED 2b. GROUP

3. REPORT TITLE

FINITE ELEMENT VIBRATION ANALYSIS OF CRACKED PLATES IN TENSION

4. DESCRIPTIVE NOTES (Type of report and inclusive dates)

Summary Report 1 January 1965-31 March 1967

5. AUTHOR(S) (Last name, first name, initial)

PETYT, MAURICE

6. REPORT DATE	7a. TOTAL NO. OF PAGES	7b. NO. OF REFS
January 1968	161	36

8a. CONTRACT OR GRANT NO.	9a. ORIGINATOR'S REPORT NUMBER(S)
AF 61(052)-862	Report No. 27
b. PROJECT NO. 7351	
c. Task No. 735106	9b. OTHER REPORT NO(S) (Any other numbers that may be assigned this report)
d.	AFML-TR-67-396

10. AVAILABILITY/LIMITATION NOTICES

This document has been approved for public release and sale; its distribution is unlimited.

11. SUPPLEMENTARY NOTES	12. SPONSORING MILITARY ACTIVITY
	Metals and Ceramics Division (MAMD) Air Force Materials Laboratory, Wright-Patterson AFB, Ohio, 45433

13. ABSTRACT

A finite element method of analysis is developed to determine the vibration characteristics of an aircraft fuselage panel, containing a fatigue crack. Experimental observations show that as the length of the crack increases, the frequency of vibration reaches a minimum when the free edge of the crack buckles. The variation in this phenomena with increasing plate width is studied both experimentally and theoretically.

The analysis is developed in a systematic manner, and calculations are performed, at each stage, on problems with known solutions, in order to determine the accuracy of the method. The problems considered include the vibrations of flat plates of varying planform, the vibrations of a cylindrical shell, the buckling of a rectangular plate, and the vibrations of a rectangular plate in compression.

The method is finally applied to the problem of a cracked plate in tension and the results compared with experimental measurements. The post buckling behaviour is calculated using a step-by-step analysis to permit linearisation of the governing equations. By considering the calculated stress distributions, the variation in buckling stress with crack length and plate width is explained.

Distribution of this abstract is unlimited.

DD FORM 1 JAN 64 1473

UNCLASSIFIED

Security Classification

14. KEY WORDS	LINK A		LINK B		LINK C	
	ROLE	WT	ROLE	WT	ROLE	WT
Finite Element Method Vibration Frequency Mode Shape Fatigue Cracked Plate Plate Buckling						

INSTRUCTIONS

1. ORIGINATING ACTIVITY: Enter the name and address of the contractor, subcontractor, grantee, Department of Defense activity or other organization *(corporate author)* issuing the report.

2a. REPORT SECURITY CLASSIFICATION: Enter the overall security classification of the report. Indicate whether "Restricted Data" is included. Marking is to be in accordance with appropriate security regulations.

2b. GROUP: Automatic downgrading is specified in DoD Directive 5200.10 and Armed Forces Industrial Manual. Enter the group number. Also, when applicable, show that optional markings have been used for Group 3 and Group 4 as authorized.

3. REPORT TITLE: Enter the complete report title in all capital letters. Titles in all cases should be unclassified. If a meaningful title cannot be selected without classification, show title classification in all capitals in parenthesis immediately following the title.

4. DESCRIPTIVE NOTES: If appropriate, enter the type of report, e.g., interim, progress, summary, annual, or final. Give the inclusive dates when a specific reporting period is covered.

5. AUTHOR(S): Enter the name(s) of author(s) as shown on or in the report. Enter last name, first name, middle initial. If military, show rank and branch of service. The name of the principal author is an absolute minimum requirement.

6. REPORT DATE: Enter the date of the report as day, month, year; or month, year. If more than one date appears on the report, use date of publication.

7a. TOTAL NUMBER OF PAGES: The total page count should follow normal pagination procedures, i.e., enter the number of pages containing information.

7b. NUMBER OF REFERENCES: Enter the total number of references cited in the report.

8a. CONTRACT OR GRANT NUMBER: If appropriate, enter the applicable number of the contract or grant under which the report was written.

8b, 8c, & 8d. PROJECT NUMBER: Enter the appropriate military department identification, such as project number, subproject number, system numbers, task number, etc.

9a. ORIGINATOR'S REPORT NUMBER(S): Enter the official report number by which the document will be identified and controlled by the originating activity. This number must be unique to this report.

9b. OTHER REPORT NUMBER(S): If the report has been assigned any other report numbers *(either by the originator or by the sponsor)*, also enter this number(s).

10. AVAILABILITY/LIMITATION NOTICES: Enter any limitations on further dissemination of the report, other than those imposed by security classification, using standard statements such as:

(1) "Qualified requesters may obtain copies of this report from DDC."

(2) "Foreign announcement and dissemination of this report by DDC is not authorized."

(3) "U. S. Government agencies may obtain copies of this report directly from DDC. Other qualified DDC users shall request through _____."

(4) "U. S. military agencies may obtain copies of this report directly from DDC. Other qualified users shall request through _____."

(5) "All distribution of this report is controlled. Qualified DDC users shall request through _____."

If the report has been furnished to the Office of Technical Services, Department of Commerce, for sale to the public, indicate this fact and enter the price, if known.

11. SUPPLEMENTARY NOTES: Use for additional explanatory notes.

12. SPONSORING MILITARY ACTIVITY: Enter the name of the departmental project office or laboratory sponsoring *(paying for)* the research and development. Include address.

13. ABSTRACT: Enter an abstract giving a brief and factual summary of the document indicative of the report, even though it may also appear elsewhere in the body of the technical report. If additional space is required, a continuation sheet shall be attached.

It is highly desirable that the abstract of classified reports be unclassified. Each paragraph of the abstract shall end with an indication of the military security classification of the information in the paragraph, represented as *(TS)*, *(S)*, *(C)*, or *(U)*.

There is no limitation on the length of the abstract. However, the suggested length is from 150 to 225 words.

14. KEY WORDS: Key words are technically meaningful terms or short phrases that characterize a report and may be used as index entries for cataloging the report. Key words must be selected so that no security classification is required. Identifiers, such as equipment model designation, trade name, military project code name, geographic location, may be used as key words but will be followed by an indication of technical context. The assignment of links, rules, and weights is optional.

GPO 886-551